SYNTHESIS OF NONLINEAR CIRCUITS IN TIME-FREQUENCY DOMAIN

by

Nalan ÖZKURT

DECEMBER, 2003
İZMİR

SYNTHESIS OF NONLINEAR CIRCUITS IN TIME-FREQUENCY DOMAIN

A Thesis Submitted to the
Graduate School of Natural and Applied Sciences of
Dokuz Eylül University
In Partial Fulfillment of the Requirements for
The Degree of Doctor of Philosophy in Electrical and Electronics Engineering,
Electrical and Electronics Program

by

Nalan ÖZKURT

DECEMBER, 2003
İZMİR

Ph.D. THESIS EXAMINATION RESULT FORM

We certify that we have read the thesis, entitled **"SYNTHESIS OF NONLINEAR CIRCUITS in TIME-FREQUENCY DOMAIN"** completed by **NALAN ÖZKURT** under supervision of **PROF.DR MUSTAFA GÜNDÜZALP** and that in our opinion it is fully adequate, in scope and in quality, as a thesis for the degree of Doctor of Philosophy.

Mustafa Gündüzalp

Supervisor

Prof. Dr. Cüneyt Güzeliş

Jury Member

Ömer Morgül

Jury Member

Prof. Dr. Coşkun İşçi

Jury Member

T. Cem Göknar

Jury Member

Approved by the

Graduate School of Natural and Applied Sciences

Prof.Dr. Cahit HELVACI

Director

ACKNOWLEDGMENTS

I would like to express my sincere gratitude to Prof.Dr. F. Acar Savacı for his guidance in the construction of the original idea of this dissertation, continuing support in improvement my theoretical background and encouragement in presenting our ideas in scientific society. He always had confidence in me even if I doubted myself.

For his guidance and support, I gratefully acknowledge my supervisor Prof.Dr. Mustafa Gündüzalp with whom I have worked since my senior project. I would also like to thank to the members of my Thesis Progress Committee Prof.Dr. Cüneyt Güzeliş and Prof.Dr. Coşkun İşçi for their useful comments and suggestions.

I'm thankful to my husband Dr. Ahmet Özkurt for his love and patience. He have always been with me to help when I feel distressed. I'm also grateful to my family and to my friends. They have always believed in me and gave me the strength to carry on.

Nalan ÖZKURT

ABSTRACT

In this thesis, the modelling and the circuit implementation of nonlinear dynamical systems have been accomplished from the given time-frequency domain specifications. After the synthesis of the signal from the time-frequency domain energy distribution using either wavelet atom or wavelet ridges method, the dynamical wavelet network has been proposed from the synthesized signal. Then, the circuit of the dynamical wavelet network has been implemented using the newly proposed sigmoidal and Mexican Hat mother wavelet circuits. Finally, the wavelet ridges of the wavelet network output have been calculated by the new ridge determination algorithm based on singular value decomposition in order to compare with the given time-frequency domain specifications.

Keywords: Nonlinear dynamical systems, chaos, time-series embedding, time-series modelling, time-frequency distributions, wavelet theory, wavelet network, the circuit implementation of sigmoidal and Mexican hat mother wavelet.

ÖZET

Bu tezde, istenen zaman-frekans düzlemi özelliklerini sağlayan doğrusal olmayan dinamik sistemlerin modellenmesi ve devre gerçeklemeleri yapılmıştır. İstenen zaman-frekans düzlemi enerji dağılımına sahip işaretlerin dalgacık atomu veya dalgacık-tepeleri yöntemleriyle sentezi ile elde edilen işaret kullanılarak dinamik dalgacık ağı tasarlanmıştır. Dinamik dalgacık ağının, sigmoid ve Meksika şapkası temel dalgacıkları için devre tasarımları önerilmiş ve gerçeklenmiştir. Dalgacık ağının çıkış işaretinin dalgacık-tepelerinin yeni önerilen ve tekil değer ayrıştırmasına dayalı dalgacık-tepesi bulma yöntemiyle elde edilmesinden sonra istenen zaman-frekans düzlemi özellikleri ile karşılaştırılmıştır.

Anahtar Sözcükler: Doğrusal olmayan dinamik sistemler, kaos, zaman-serisi gömme, zaman-serisi modelleme, zaman-frekans dağılımları, dalgacık teorisi, dalgacık ağı, sigmoid ve Meksika şapkası temel dalgacıkları için devre gerçeklemeleri.

CONTENTS

LIST OF TABLES

LIST OF FIGURES

CHAPTER ONE
INTRODUCTION

The original contributions of this thesis can be stated as specifying the signal in the time-frequency domain and constructing the dynamical circuit which implements these specifications with the proposed wavelet network circuit. The stages of proposed system have been built on the concepts such as nonlinear time-series analysis, time-frequency domain analysis especially the wavelet transform, chaotic dynamics and fractal geometry.

1.1 Time-Series Analysis and Modelling

The time-series identification or modelling process can be defined as the construction of a mathematical model of a dynamical system from observations for prediction, control or simulation purposes to gain deeper insight of complicated phenomena (de Moor, 1988). The model structures may be parametric or nonparametric, time-domain or frequency-domain, linear or nonlinear, stochastic or deterministic etc. Hence, the model selection is an important issue in the model building process (Judd & Mees, 1995).

Although the dynamical behavior of linear networks is fully determined, the behavior of nonlinear dynamic circuits can be extremely complex and unpredictable. Due to the complication of the behaviors, there have been several works which attempt to analyze this kind of dynamics, especially the chaotic behavior. The qualitative theory of nonlinear networks deals with the analysis of behavior of the systems. The classical time-domain and frequency domain methods, such as averaging method, perturbation method, describing function analysis and harmonic balance analysis have been used to identify the solutions of the system (Cunningham, 1958; Minorsky, 1962; Ogata, 1970; Sastry, 1999). Some of the applications of these methods for chaotic dynamics can be found in (Genesio & Tesi, 1992; Yalçın & Savacı, 1996; Savacı, Günel, Özkurt, & Yapalı, 2001). In these works it has been observed that the chaotic signals have shown nonstationary property (i.e. time-varying frequency content). Therefore, it would be more convenient to describe the chaotical signals in time-frequency domain instead of frequency domain alone. With the given specifications in the time-frequency domain, the corresponding time-series can be obtained and the dynamical model of this time-series can be implemented.

The invariants of the dynamics such as strange attractor and Lyapunov exponents (i.e. the rate of exponential divergence of the initially nearby trajectories) (Rasband, 1990) can be obtained from the nonlinear time-series. In the identification of the time-series, the dynamical evaluation of the system is modelled with time-delay embedding (Takens, 1985) and the system evolution function is approximated by some arbitrary set of basis functions for the modelling or identification of the nonlinear dynamical systems (Conti & Turchetti, 1994; Judd & Mees, 1995, 1996; Allingham, West, & Mees, 1998; Billings & Coca, 1999).

1.2 Time-Frequency Analysis of Nonlinear Dynamical Systems

Due to the nonstationarity of the most of the signals from nature, the study of nonstationary signals in many different fields of science and engineering is very important. Since the time-domain methods and frequency domain methods individually do not provide adequate information about the dynamics of such signals, the time-frequency domain methods have received considerable attention (Cohen, 1989), (Hess-Nielsen & Wickerhauser, 1989). The wavelet transform is particularly suitable for the analysis of transient signals and time-varying systems since it is localized in both time and frequency. The wavelet method follows the rapid variations of the instantaneous frequencies by adapting the width of the window according to the frequency (Mallat, 1999; Chui, 1992).

Because of its multi-resolution property, the wavelet analysis has found a wide interest in various areas such as in mechanics (Newland, 1993), in data compression (Vetterli &

Kovacevic, 1995), in molecular dynamics (Askar, Cetin, & Rabitz, 1996), in geophysics (Foufoula-Georgiou & Kumar, 1994), in biomedical engineering (Akay, 1997; Carmona, Hwang, & Frostig, 1995; Rosso, Blanco, Yordanova, Kolev, Figliola, Schürmann, & Basar, 2001), in electromagnetics (Barmada & Raugi, 2000), in circuit theory (Li, Ling, & Zheng, 2002; Zhou, Cai, & Zhang, 1999; Soveiko & Nakhla, 2000), in pattern recognition (Mallet, Coomans, & de Vel, 1997; Pittner & Kamarthi, 1999), in dynamical systems and control (Fedorova & M.G.Zeitlin, 1996; Sureshbabu & Farrel, 1999).

The chaotic waveforms have also been analyzed in the time-frequency domain especially by Wigner distribution (Chen, 1994; L. Galleani & Presti, 1999) and by wavelets (Liang & Page, 1997; Galleani, Presti, & de Stefano, 1998; Staszewski & Worden, 1999; Özkurt & Savacı, 2001; Wong & Chen, 2001; Chandre, Wiggins, & Uzer, 2003) because of the nonstationary nature of the chaotic waveforms. In (L. Galleani & Presti, 1999) the time-frequency domain analysis results have been used to achieve a reconstruction of the chaotic attractor of the Chua's circuit.

The time-frequency representation of the trajectories would be more convenient to get dynamical information about the chaotic system, since the asymptotic quantities (Lyapunov exponents, entropy, fractal dimension) only reflect the asymptotical behavior. This representation can reveal the phase-space structures by obtaining the relevant information from a single trajectory through the extraction of main frequencies along the ridge (i.e., a curve at the time-frequency plane along which the energy is locally maximum). The original signal can be recovered using the skeleton of the transform (Carmona, Hwang, & Torresani, 1999; Quatieri, 2001; Özkurt & Savacı, 2003a, 2003d) which is defined as the values of the wavelet transform coefficients along the ridges. The instantaneous frequencies which have been determined through the ridges can also be used to detect the resonance trappings and to characterize the degree of the chaoticity (Chandre et al., 2003). The time-series can be modelled with the wavelet ridges and the approximation of this model can be implemented by the wavelet network.

1.2.1 Wavelet Network

With the advent of artificial neural networks, the analog computation has received much attention over the last ten years. A methodology for implementing neural network architecture using VLSI circuits has been developed in (Mead, 1989). It has been shown that any continuous multivariate function can be approximated arbitrarily closely by artificial neural networks (Kolmogorov, 1957; Cybenko, 1989; Poggio & Girosi, 1990). The approximate identity neural networks for analog synthesis of nonlinear static and dynamical systems which have been realized with BJT and MOS devices have been proposed in (Conti & Turchetti, 1994). In order to approximate arbitrary nonlinear functions, wavelet network which combines feedforward neural networks and wavelet decompositions using a learning algorithm of backpropagation type has been proposed in (Zhang & Benveniste, 1992).

In the wavelet network, each coefficient shows the similarity between the function and the dilated and scaled version of the mother wavelet. The nonlinear function is decomposed in terms of wavelet basis. The identification of static and dynamical systems using wavelet network has attracted many researchers (Cao, Hong, Fang, & He, 1995; Zhang, 1997; Oussar, Rivals, Personnaz, & Dreyfus, 1998). A method for selecting the wavelet basis for modelling the nonlinear systems has been given (Pati & Krishnaprasad, 1994). Unlike the wavelet network proposed in (Zhang & Benveniste, 1992), the candidate wavelets have been chosen by inspecting the time-frequency plane in (Pati & Krishnaprasad, 1994). It has been shown that a sigmoidal mother wavelet can be obtained by the tangent hyperbolic functions in (Pati & Krishnaprasad, 1994). There have been several attempts to use and to improve the wavelet networks by many researchers such as (Bernard, Mallat, & Slotine, 1998; Clancy & Ozguner, 1994; Yu, Tan, Vandewalle, & Deprettere, 1996).

1.3 The Overview of the Proposed System

In this thesis, a method for the synthesis of the signals with predefined time-frequency domain characteristics has been proposed in the time-frequency domain and then the circuit implementation of the model obtained from time-series has been implemented. The proposed method includes four main stages: Signal synthesis, the system modelling from the produced time-series, circuit synthesis and verification are shown in Figure 1.1.

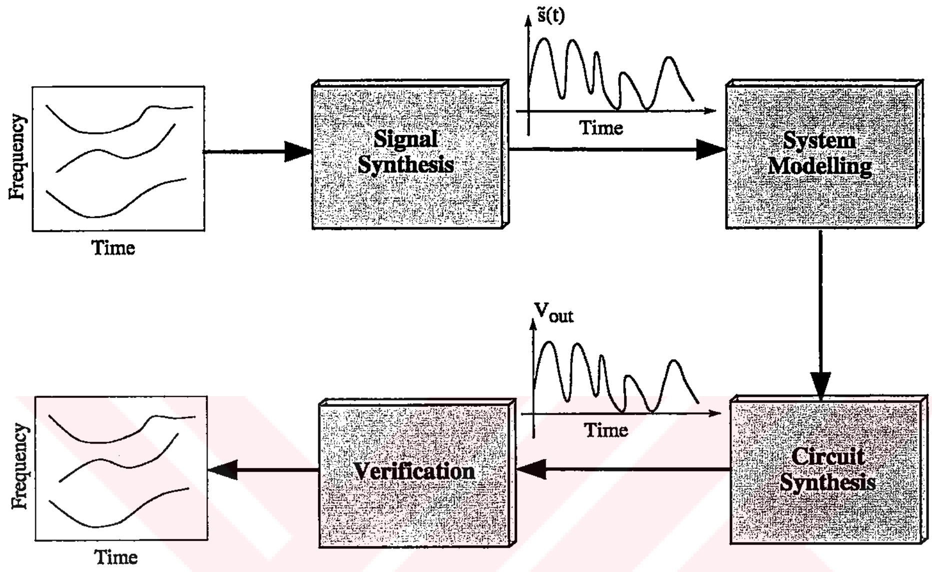

Figure 1.1: The block diagram of the system

There are several studies on the signal synthesis from time-frequency domain properties of which in (Shah, El-Jaroudi, Loughlin, & Chaparro, 2000) the signal is recovered from the desired positive time-frequency distribution and in (Hlawatsch & Kozek, 1995) the autocorrelation function is optimized to obtain the desired time-frequency spectrum. Since the wavelet domain methods are more suitable for the circuit implementation two wavelet domain methods have been chosen for the signal synthesis in this thesis: wavelet atom method proposed in (Özkurt, Gündüzalp, & Savacı, 2001) and the wavelet ridges method (Carmona & Hwang, 1997; Carmona et al., 1999) as is explained in (Savacı & Özkurt, 2003).

After the synthesis of the signal, the system modelling block determines the parameters of the wavelet network which produces the given time series by using time-delay embedding theorem (Takens, 1985) and the wavelet network training algorithm proposed in (Zhang, 1997).

The fundamental components of circuit synthesis stage of the proposed nonlinear circuit given in Figure 1.1 are the wavelons of the wavelet network. The circuit implementations of wavelet transform usually rely on the filterbank implementations of wavelet transform (Mallat, 1999; Vetterli & Herley, 1992). Some of the implementations can be found in (Fridman & Manolakos, 1997; Chakrabarti & Mumford, 1999; Chakrabarti, Vishwanath, & Owens, 1996). The switched capacitor circuits have also been used in the implementation of the wavelet transform in (Lin, Pati, Edwards, & Shamma, 1996). The circuit implementation of the wavelet network for static system approximation has been accomplished in (Özkurt, Savacı, & Gündüzalp, 2002b) by using the sigmoidal wavelet function proposed in (Pati & Krishnaprasad, 1994). Also, the circuit implementation for the Mexican Hat mother wavelet has been proposed in (Özkurt, Savacı, & Gündüzalp, 2003a). The circuit of the dynamical wavelet network has been implemented using the static wavelet network with Mexican hat mother wavelet as a main block (Özkurt et al., 2003a) and also using the delay blocks which have been realized by voltage controlled switches and capacitors (Özkurt, Savacı, & Gündüzalp, 2003b).

When the design process has been completed, the synthesis results have been tested to determine whether the proposed circuit satisfies the given conditions. Therefore, the wavelet ridges of the obtained signal have been determined using the wavelet ridge determination method proposed in (Özkurt & Savacı, 2003b) to compare with the desired wavelet ridges.

1.4 Outline of the Thesis

The building blocks of the proposed method have been explained by giving the necessary theoretical background information in the following chapters of the thesis. The time-frequency domain methods and the wavelet analysis of the signals arising from the generalized Chua's circuit (Özkurt & Savacı, 2001) have been introduced in Chapter II.

After giving the basic definitions, the wavelet atom (Özkurt et al., 2001) and wavelet ridge signal synthesis methods (Savacı & Özkurt, 2003) have been explained and some exemplar signals have been synthesized with both methods in Chapter III.

The definition and construction of the wavelet network and the identification of nonlinear static and dynamical systems have been introduced in Chapter IV. The static systems have been modelled by wavelet networks in Matlab by using the Mexican hat and sigmoidal mother wavelets . Additionally, the identification of the period-1 limit cycle and the spiral attractor of the Chua's circuit have been accomplished by the wavelet network with Mexican hat mother wavelet .

The circuit realizations of the both sigmoidal (Özkurt et al., 2002b, 2002c) and the Mexican hat mother wavelets (Özkurt et al., 2003a) have been given in Chapter V and then the circuits of the static modelling examples given in Chapter IV have been simulated in Spice. A circuit structure for the dynamical wavelet network has been proposed (Özkurt et al., 2003b) and the simulations of the the period-1 limit cycle and the spiral attractor of the Chua's circuit have been done in Spice.

In Chapter VI, the SVD-based ridge determination method (Özkurt & Savacı, 2003c, 2003b) which will be used to verify the results of the synthesis have been explained. Then, the ridges of the monocomponent and multicomponent signals have been determined and compared with the existing methods (Todorovska, 2001). Also, the periodicity and the degree of the chaoticity of the signals arising from the Chua's circuit have been investigated by considering the number and shapes of the wavelet ridges (Özkurt & Savacı, 2003b).

In the case of noisy signals before the determination of the wavelet ridges the noise reduction has been applied. The SVD-based noise reduction method proposed in (Özkurt & Savacı, 2003a, 2003d) has been given in Chapter VI.

The synthesis of the circuits producing monocomponent periodic and multicomponent aperiodic signals have been accomplished in Chapter VII by using the proposed method (Savacı & Özkurt, 2003).

CHAPTER TWO

TIME-FREQUENCY DISTRIBUTIONS

Most of the signals from the nature have nonstationary characteristics. For a deterministic signal, the signal is said to be stationary if the signal can be expressed as the discrete sum of the sinusoids as

$$s(t) = \sum_{k \in \mathbb{N}} A_k sin(2\pi\, f_k\, t + \Phi_k) \tag{2.1}$$

for real signals and

$$s(t) = \sum_{k \in \mathbb{N}} A_k exp\,(j(2\pi\, f_k\, t + \Phi_k)) \tag{2.2}$$

for complex signals (Aguer, Flandrin, Goncalves, & Lemoine, 1996).

Before the definition of stationarity for the random signals, the mean and the correlation of a random process should be defined. For a discrete random process the mean is

$$m[n] = E\{s[n]\} = \int_{-\infty}^{\infty} s[n] f_{s[n]}(s_n)\, ds_n \tag{2.3}$$

where for any fixed value of n, $f_{s[n]}(s_n)$ represents the probability density function of the random variable $s[n]$. The correlation between any two samples of a random process is defined as

$$R_s[n_1, n_0] = E\{s[n_1] * s[n_0]\}. \tag{2.4}$$

A random process is said to be stationary if the mean is a constant and the correlation is a function only of the spacing between the samples

$$R_s[n_1, n_0] = R_s(n_1 - n_0) \tag{2.5}$$

otherwise, the process is called nonstationary. The properties of a stationary signal are statistically invariant over the time. In nonstationary case, transient events appear that cannot be predicted statistically, like spikes or breakdowns.

When the signal is stationary, the spectral content of the signal does not vary with time. Therefore, frequency content of the signal $s(t) \in L^2(0, 2\pi)$ is precisely defined by representing the signal by Fourier series as

$$s(t) = \sum_{n=-\infty}^{\infty} c_n e^{jnt} \tag{2.6}$$

where the constants c_n are the Fourier coefficients and defined by

$$c_n = \frac{1}{2\pi} \int_0^{2\pi} s(t) e^{-jnt} dt. \tag{2.7}$$

The function is decomposed into infinitely many orthogonal components and the coefficients are the inner product of the function with the orthogonal basis elements in this representation. In other words, a time-domain signal is represented in frequency-domain. However, while transforming the time-domain signal into its frequency-domain equivalent, the time information is lost. If the signal is nonstationary the time instant where a frequency component is localized or discontinuity takes place could not be known. In order to find the change of the frequency information with time, a windowing process is developed. Denis Gabor adapted Fourier transform into Short Time Fourier Transform (STFT) which maps a signal into time-frequency domain. There have been many studies in time-frequency representations since his study. Therefore, the time-frequency domain techniques will be explained in the next sections.

2.1 Time-Frequency Distributions

Two types of approach are present to obtain the time-frequency distributions: the atomic decomposition and the energy distributions. These time-frequency distributions will be explained in the sequel. The examples given in this chapter have been implemented with "Time-Frequency Toolbox for use with Matlab" (Aguer et al., 1996).

2.2 Atomic Decompositions

The Short-Time Fourier transform and the wavelet transform are in this class of distributions and they are also known as linear time-frequency representations.

2.2.1 Short-Time Fourier Transform (STFT)

The main principle is to suppress the signal out of the time window and obtain the Fourier transform of the remaining part and continue the operation for the rest of the signal as

$$F_s(u,\omega;h) = \int_{-\infty}^{\infty} s(t)\, h(t-u)e^{-j\omega t}dt \tag{2.8}$$

where $h(\cdot)$ is the chosen window function (Mallat, 1999). If $s(t) \in L^2(\mathbb{R})$ the original signal can be recovered form STFT coefficients (Mallat, 1999)

$$s(t) = \frac{1}{2\pi}\int_{-\infty}^{\infty}\int_{-\infty}^{\infty} F_s(u,\omega;h)\, h(t-u)e^{j\omega t}\, d\omega\, du \tag{2.9}$$

and

$$\int_{-\infty}^{\infty} |s(t)|^2 dt = \frac{1}{2\pi} \int_{-\infty}^{\infty} \int_{-\infty}^{\infty} |F_s(u, \omega; h)|^2 \, d\omega \, du. \tag{2.10}$$

Thus, the signal can be composed as the weighted sum of elementary waveforms

$$h_{u,\omega} = h(t-u)e^{j\omega u} \tag{2.11}$$

which can be interpreted as "building blocks" or "atoms".

The chosen window function defines the time and frequency resolution of the transform. There is a trade-off between the time and frequency resolutions because of the Heisenberg's uncertainty principle which states that the infinite time and frequency resolutions can not be obtained simultaneously. First we choose time window as $h(t) = \delta(t)$ which provides perfect time resolution. The time-frequency plane is shown in Figure 2.1. As it can be seen from the figure, although the time resolution is perfect, the frequency resolution of the transform is poor. The window $\hat{H}(\omega) = \delta(\omega)$ makes the frequency resolution perfect but the time resolution poor as can be seen in Figure 2.2. Thus, it is important to choose a window which provides a trade-off between the time and frequency resolutions.

The Discrete STFT: The STFT can be sampled in time-frequency plane to reduce the redundancy of STFT. Let's consider the discrete signals of period N. The window $h[n]$ is chosen to be a symmetric discrete signal of period N with unit norm $\|h\| = 1$. The discrete STFT atoms are defined by

$$h_{m,l}[n] = h[n-m] \, exp(\frac{-j\,2\pi ln}{N}) \tag{2.12}$$

and the discrete STFT of a signal $s(n)$ with period N is

$$F_s[m, l; h] = \sum_{n=0}^{N-1} s[n] \, h[n-m] \, exp(\frac{-j\,2\pi ln}{N}). \tag{2.13}$$

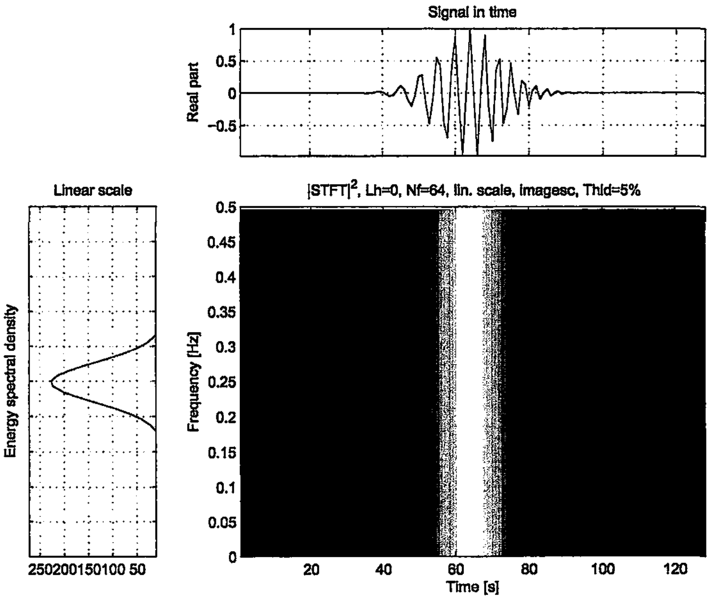

Figure 2.1: Perfect time resolution in STFT

If s is a signal of period N then

$$f[n] = \frac{1}{N} \sum_{m=0}^{N-1} \sum_{l=0}^{N-1} F_s[m, l; h]\; h[n-m]\; exp(\frac{j\, 2\pi l n}{N}) \tag{2.14}$$

and

$$\sum_{n=0}^{N-1} |f[n]|^2 = \frac{1}{N} \sum_{m=0}^{N-1} \sum_{l=0}^{N-1} |F_s[m, l; h]|^2 \tag{2.15}$$

as defined in (Mallat, 1999). The reconstruction formula can be obtained by applying the Parseval and Plancherel formulas of the discrete Fourier transforms.

2.2.2 Time-Scale Analysis and the Wavelet Transform

While working in reflection seismology, Morlet realized that it is more suitable to send shorter pulses for high frequencies and longer pulses for low frequencies rather than sending pulses of equal durations. Then, he obtained these pulses by scaling a single function

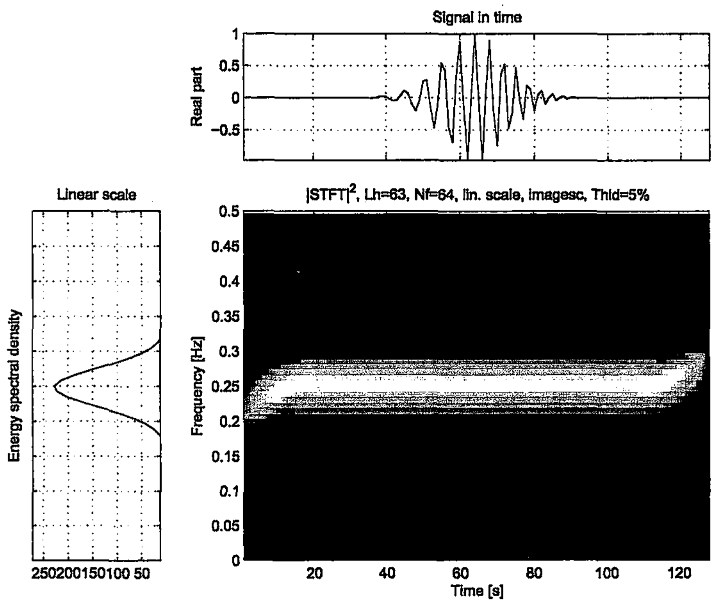

Figure 2.2: Perfect frequency resolution in STFT

called wavelet. A theoretical physicist Grossman recognized that the approach of Morlet is similar to his approach on coherent quantum states and they formulated the continuous wavelet transform together. Although the theory is not new to the mathematicians working on the harmonic analysis and to computer vision researchers working on the multiscale analysis, after Grosman and Morlet's work (Mallat, 1999) the wavelet theory have been used in different areas of science .

In continuous wavelet transform (CWT), the signal is projected on a family of zero-mean functions called wavelets, deduced from an elementary function mother wavelet by translations and dilations

$$W_s(a, b; \Psi) \triangleq \int_{-\infty}^{\infty} s(t)\ \Psi^*_{a,b}(t)\ dt \tag{2.16}$$

where a and b are the dilation (scale) and translation coefficients, respectively; the scaled and translated wavelet is obtained as

$$\Psi_{a,b}(t) \triangleq \frac{1}{\sqrt{a}}\Psi\left(\frac{t-b}{a}\right), \quad a \in \mathbb{R}^{+}, \quad b \in \mathbb{R} \tag{2.17}$$

where $\Psi(\cdot)$ is the mother wavelet and * denotes the complex conjugate . The mother wavelet must satisfy the admissibility condition which implies zero mean as

$$c_{\psi} = \int_{0}^{\infty} |\Psi(\omega)|^{2}\frac{d\omega}{|\omega|} < \infty. \tag{2.18}$$

as given in (Mallat, 1999). Any basic mother wavelet $\Psi(x)$ must necessarily satisfy

$$\int_{\infty}^{\infty} \Psi(x)\, dx = 0 \tag{2.19}$$

therefore its graph is a small wave which gives the name wavelet.

Theorem 2.1 *(Mallat, 1999) Let $\Psi \in L^{2}(\mathbb{R})$ be a real function satisfying the admissibility condition in (2.18). Any $s \in L^{2}(\mathbb{R})$ satisfies*

$$s(t) = \frac{1}{c_{\Psi}}\int_{0}^{\infty}\int_{-\infty}^{\infty} W_{s}(a,b;\Psi)\frac{1}{\sqrt{a}}\Psi\left(\frac{t-b}{a}\right)\, db\frac{da}{a^{2}} \tag{2.20}$$

and

$$\int_{-\infty}^{\infty} |s(t)|^{2}dt = \frac{1}{c_{\Psi}}\int_{0}^{\infty}\int_{-\infty}^{\infty} |W_{s}(a,b;\Psi)|^{2}\, db\frac{da}{a^{2}}. \tag{2.21}$$

Wavelet coefficients are the wavelet domain representation of the function with respect to mother wavelet and represent the degree of correlation with a fixed scale and translated mother wavelet.

Wavelet algorithms process data at different scales and resolutions. The scale plays an important role in wavelet analysis. If we look at the signal with a large window we see gross features, but if we look at with a small window, we notice small features. Therefore, all aspects of the signal are observed with the wavelet analysis.

The energy of the translated and dilated wavelet atoms is localized in time-frequency domain. The central time of a wavelet atom $\Psi_{a,b}$ can be obtained as (Mallat, 1999)

$$\bar{t}_{a,b} \triangleq \frac{\int_{-\infty}^{\infty} t|\Psi_{a,b}(t)|^2 dt}{\int_{-\infty}^{\infty} |\Psi_{a,b}(t)|^2 dt} \tag{2.22}$$

and the variance in time is determined as

$$\sigma_{t;a,b}^2 \triangleq \frac{\int_{-\infty}^{\infty} (t-\bar{t}_{a,b})^2 |\Psi_{a,b}(t)|^2 dt}{\int_{-\infty}^{\infty} |\Psi_{a,b}(t)|^2 dt} \quad . \tag{2.23}$$

Similarly, the center frequency and the variance can be defined as

$$\bar{\omega}_{a,b} \triangleq \frac{\int_{-\infty}^{\infty} \omega|\hat{\Psi}_{a,b}(\omega)|^2 d\omega}{\int_{-\infty}^{\infty} |\hat{\Psi}_{a,b}(\omega)|^2 d\omega} \tag{2.24}$$

where $\hat{\Psi}_{a,b}(\omega)$ is the Fourier transform of the wavelet and the variance is defined as

$$\sigma_{\omega;a,b}^2 \triangleq \frac{\int_{-\infty}^{\infty} (\omega-\bar{\omega}_{a,b})^2 |\hat{\Psi}_{a,b}(\omega)|^2 d\omega}{\int_{-\infty}^{\infty} |\hat{\Psi}_{a,b}(\omega)|^2 d\omega} \quad . \tag{2.25}$$

Let t_0 and ω_0 to be the central time and central frequency of the mother wavelet, and the corresponding variances are $\sigma_{t,0}^2$ and $\sigma_{\omega,0}^2$, respectively. The central time, frequency and the variances of the wavelet atom $\Psi_{a,b}$ are obtained as

$$\begin{array}{ll} \bar{t}_{a,b} = t_0 + b & \bar{\omega}_{a,b} = \frac{\omega_0}{a} \\ \sigma_{t;a,b}^2 = a^2 \sigma_{t,0}^2 & \sigma_{\omega;a,b}^2 = \frac{\sigma_{\omega,0}^2}{a^2}. \end{array} \tag{2.26}$$

Thus, the energy distribution of the wavelet atom $\Psi_{a,b}(t)$ is localized in the cell

$$\left(\bar{t}_{a,b} \pm \sigma_{t;a,b}\right) \times \left(\bar{\omega}_{a,b} \pm \sigma_{\omega;a,b}\right) = \left(t_0 + b \pm a\sigma_{t,0}\right) \times \left(\frac{\omega_0}{a} \pm \frac{\sigma_{\omega,0}}{a}\right) \tag{2.27}$$

in the time-frequency domain (Mallat, 1999; Chui, 1992). An important property of the time-frequency window is that it narrows in higher frequencies and widens in low frequencies, the area of window is constant and equal to $4\sigma_{t,0}\sigma_{\omega,0}$ as can be observed in Figure 2.3.

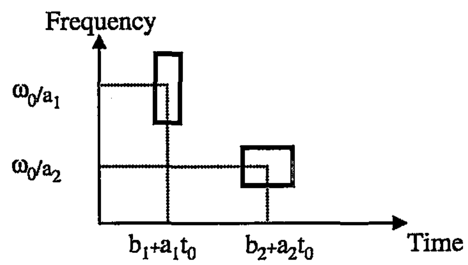

Figure 2.3: The time-frequency window of wavelets for $a_1 < a_2$ and $b_1 < b_2$

The simplest example of the wavelet function is Haar function

$$\Psi_H(t) = \begin{cases} 1 & for \quad 0 \le t < \frac{1}{2} \\ -1 & for \quad \frac{1}{2} \le t < 1 \\ 0 & \quad elsewhere \end{cases} \tag{2.28}$$

The Haar wavelet is compactly supported, i.e., it vanishes outside of a fixed interval, but its disadvantage is that it cannot be continuously differentiable. This limits the operation.

For the numerical computations the discrete samples of the continuous wavelet transform are considered and the scaled and translated wavelets are defined at the dyadic grid as

$$\Psi_{mn}(t) = a_0^{-m/2}\Psi(a_0^{-m}t - nb_0) \quad m, n \in \mathbb{Z} \tag{2.29}$$

where $a_0, b_0 \in \mathbb{R}$ are the dilation and translation coefficients, respectively. Then the numerical approximation of the total energy gives

$$E_T \approx \frac{k}{c_\psi} \sum_{m=-\infty}^{\infty} \sum_{n=-\infty}^{\infty} |c_{mn}|^2 \tag{2.30}$$

with $k \triangleq b_0 \ln a_0$ and WT coefficients as

$$c_{mn} \triangleq W_s(a_m, b_n; \Psi). \tag{2.31}$$

where $a_m \triangleq a_0^{-m}$, $b_n \triangleq nb_0$.

2.2.2.1 Real and Analytical Wavelets

The wavelet transform measures the time evolution of the frequency transients. When a complex analytical wavelet is used, the amplitude and phase components can be separated.

Definition 2.1 *The analytical mono-component signal $Z_s(t)$ associated with the real signal $s(t)$ is a complex function of time defined as*

$$Z_s(t) \triangleq s(t) + j\tilde{s}(t) \ = A(t)\, exp\,(\, j\phi(t)) \tag{2.32}$$

where the function $\tilde{s}(t)$ is the Hilbert transform of $s(t)$ which is defined as

$$\tilde{s}(t) = \frac{1}{\pi} P.V. \int_{-\infty}^{\infty} \frac{s(\tau)}{t-\tau}\, d\tau = \frac{1}{\pi} \lim_{R \to \infty} \int_{-\infty}^{\infty} \frac{s(\tau)}{t-\tau}\, d\tau \tag{2.33}$$

where P.V. means that the integral is taken in the sense of the Cauchy principal value (Delprat, Escudie, Guillemain, Kronland-Martinet, Tchamitchian, & Torresani, 1992).

Therefore, the spectrum of the analytical signal does not have energy distribution in the negative frequencies.

An analytical wavelet can be constructed with a frequency modulation of a real symmetric window function $A_\Psi(t)$ as

$$\Psi(t) = A_\Psi(t)\, e^{j\omega_0 t} \tag{2.34}$$

and its Fouirer transform is

$$\hat{\Psi}(\omega) = \hat{A}_{\Psi}(\omega - \omega_0). \tag{2.35}$$

If $\hat{A}_{\Psi}(\omega) = 0$ for $|\omega| > \omega_0$, then $\hat{\Psi}(\omega) = 0$ for $\omega < 0$ which means the wavelet is analytical (Mallat, 1999) .

2.2.2.2 Orthogonal Wavelets

A mother wavelet $\Psi(t) \in L^2(\mathbb{R})$ is called as orthogonal wavelet if the family $\{\Psi_{m,n}\}$ is an orthonormal basis of $L^2(\mathbb{R})$ and the orthonormality can be expressed as

$$\langle \Psi_{i,k}, \Psi_{l,m} \rangle = \delta_{i,l}\delta_{k,m} \tag{2.36}$$

where $\langle \cdot, \cdot \rangle$ represents the inner product and

$$\delta_{i,k} = \begin{cases} 1 & for \quad i = k \\ 0 & for \quad i \neq k \end{cases} \tag{2.37}$$

2.2.2.3 The Scaling Function

When the wavelet transform coefficients of a signal are known only for the scales $a < a_0$, i.e. for high frequencies, then a complement of the information containing the low frequency components should be present in order to recover the signal. This function is called as scaling function and it is defined in (Mallat, 1999) as

$$|\hat{\Phi}(\omega)|^2 \triangleq \int_1^{\infty} |\hat{\Psi}(a\omega)| \frac{da}{a}. \tag{2.38}$$

The scaling function also can be interpreted as the impulse response of a low-pass filter as

$$Ls(a,b) = \langle s(t), \frac{1}{\sqrt{a}} \Phi(\frac{t-b}{a}) \rangle = s(t) * \overline{\Phi}_a(b) \tag{2.39}$$

where $\Phi_a(t) = \frac{1}{\sqrt{a}}\Phi(\frac{t-b}{a})$ and $\overline{\Phi}_a(t) = \Phi_a^*(-t)$.

2.3 The Energy Distributions Obtained from Atomic Decompositions

The signals can be represented by the time-frequency atoms or elementary components as in STFT or WT. The energy distribution of the signal in time-frequency domain are represented by the "Spectrogram" and "Scalogram" which are defined by using the STFT and WT coefficients.

2.3.1 The Spectrogram

It is obtained by the square of the modulus of the STFT as

$$S_s(t,\omega;h) = |F_s(t,\omega;\Psi)|^2 . \tag{2.40}$$

The total energy in the time-frequency plane is represented as

$$E_s \triangleq \int_{-\infty}^{\infty}\int_{-\infty}^{\infty} S_s(t,\omega;h)\, dt\, d\omega \tag{2.41}$$

where the energy of the window is unity.

The spectrogram

- preserves the time and frequency shift

$$y(t) = x(t-t_0) \quad \Rightarrow \quad S_y(t,\omega;h) = S_x(t-t_0,\omega;h), \tag{2.42}$$

$$y(t) = x(t)e^{j\,2\pi\omega_0 t} \quad \Rightarrow \quad S_y(t,\omega;h) = S_x(t,\omega-\omega_0;h), \tag{2.43}$$

- the time-frequency resolution is poor caused by STFT
- the spectrogram of the sum of the signals also consists of interference terms

$$\begin{aligned} &y(t) = x_1(t) + x_2(t) \quad \Rightarrow \\ &S_y(t,\omega;h) = S_{x_1}(t,\omega;h) + S_{x_2}(t,\omega;h) + 2\Re\{S_{x_1,x_2}(t,\omega;h)\}, \end{aligned} \tag{2.44}$$

where

$$S_{x_1,x_2}(t,\omega;h) \triangleq F_{x_1}(t,\omega;h)F_{x_1}(t,\omega;h) \tag{2.45}$$

and called as cross spectrogram (Aguer et al., 1996).

2.3.2 The Scalogram

The time-frequency energy distribution scalogram is obtained as the square modulus of the CWT as given in (Aguer et al., 1996)

$$S_s(a,b;\Psi) \triangleq |W_s(a,b;\Psi)|^2 . \tag{2.46}$$

The normalized scalogram is also defined as

$$P_s(a,b;\Psi) \triangleq \frac{1}{a^2} |W_s(a,b;\Psi)|^2 . \tag{2.47}$$

The scalogram preserves the total energy

$$E_s \triangleq \int_{-\infty}^{\infty} \int_{-\infty}^{\infty} P_s(a,b;\Psi) \, \frac{da \, db}{a^2} . \tag{2.48}$$

The time-frequency resolution is limited via uncertainty principle. The signals with overlapped components cause the interference terms. If the components of the signals are sufficiently far apart in time-frequency plane, their cross scalogram will be zero. The signal with four components which are constant frequency modulated Gaussian waves, i.e. Gaussian atoms, and its scalogram are shown in Figure 2.4-a and -b, respectively.

2.4 Cohen's Class Time-Frequency Distributions

The basic idea in the time-frequency distributions is to define a joint distribution function that will describe the energy density or intensity of a signal simultaneously in time and

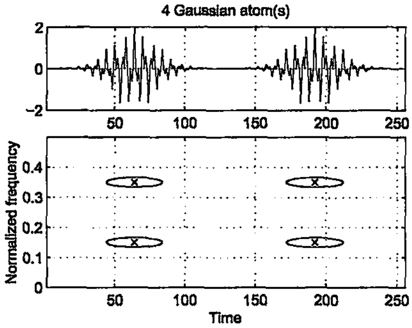

(a)

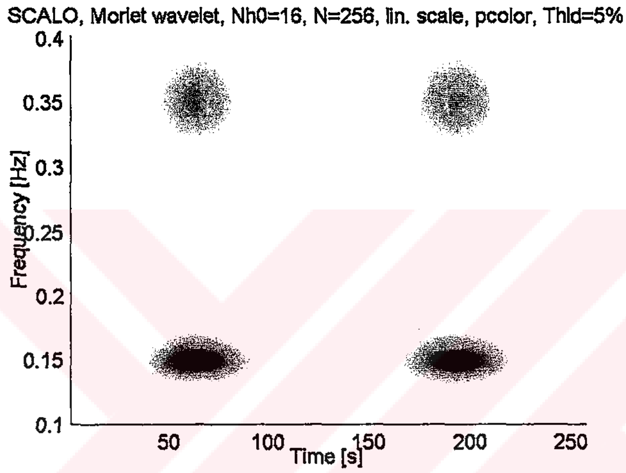

(b)

Figure 2.4: (a) The signal and expected time-frequency domain view and (b) scalogram of four Gaussian atoms

frequency. Ideally, it can be thought as a multidimensional density function. Therefore, the frequency of a signal at a particular time instant can be calculated using the given density function and vice versa. Additionally, if we have that distribution, then we can construct a signal with desired properties. Assume that $|s(t)|^2$ and $|\hat{S}(\omega)|^2$ are the density functions. The mean and variances are defined in the sequel: The mean over time is

$$t_m \triangleq \frac{1}{E_s}\int_{-\infty}^{\infty} t|s(t)|^2 dt \tag{2.49}$$

where E_s is the energy of the signal and it is defined as

$$E_s = \int_{-\infty}^{\infty} |s(t)|^2 dt = \frac{1}{2\pi}\int_{-\infty}^{\infty} |\hat{S}(\omega)|^2 d\omega \tag{2.50}$$

and the mean in frequency is

$$\omega_m \triangleq \frac{1}{2\pi E_s}\int_{-\infty}^{\infty} \omega|\hat{S}(\omega)|^2 d\omega. \tag{2.51}$$

The time spreading or the variance in time is defined as

$$\sigma_t^2 \triangleq \frac{1}{E_s}\int_{-\infty}^{\infty} (t-t_m)^2|s(t)|^2 dt \tag{2.52}$$

and variance in frequency is

$$\sigma_\omega^2 \triangleq \frac{1}{2\pi E_s}\int_{-\infty}^{\infty} (\omega-\omega_m)^2|\hat{S}(\omega)|^2 d\omega. \tag{2.53}$$

Then, signal can be characterized in time-frequency plane by its mean position (t_m, ω_m) and its area is proportional to time-bandwidth product $\sigma_t^2 \times \sigma_\omega^2$. For all signals

$$\sigma_t^2 \times \sigma_\omega^2 \geq \frac{1}{4} \tag{2.54}$$

according to the Heisenberg's uncertainty principle (Mallat, 1999). Thus, a signal can not have simultaneously an arbitrarily small support in time and in frequency.

For a joint distribution $\rho_s(t,\omega)$, the total energy should be

$$E_s = \int_{-\infty}^{\infty}\int_{-\infty}^{\infty} \rho_s(t,\omega)dt\, d\omega \tag{2.55}$$

and the distribution should satisfy the marginal properties as

$$\int_{-\infty}^{\infty} \rho_s(t,\omega)d\omega = |s(t)|^2 \tag{2.56}$$

For a joint distribution $\rho_s(t,\omega)$, the total energy should be

$$E_s = \int_{-\infty}^{\infty}\int_{-\infty}^{\infty} \rho_s(t,\omega)dt\, d\omega \tag{2.55}$$

and the distribution should satisfy the marginal properties as

$$\int_{-\infty}^{\infty} \rho_s(t,\omega)d\omega = |s(t)|^2 \tag{2.56}$$

and

$$\int_{-\infty}^{\infty} \rho_s(t,\omega)dt = |\hat{S}(\omega)|^2. \tag{2.57}$$

The time-frequency distribution theory searches the functions which satisfy the given conditions and also investigates the limitations of the obtained transforms. To gain additional desired properties, some constraints are added to the previous basic properties. The time and frequency covariance principles are the most important ones. These properties guaranty that, if the signal is delayed in time and modulated, its time-frequency distribution is translated of the same quantities in time-frequency plane. The Cohen's Class distributions satisfy these properties and they have the following form

$$C_s(t,\omega;f) = \int_{-\infty}^{\infty}\int_{-\infty}^{\infty}\int_{-\infty}^{\infty} e^{j\,2\pi\xi\,(u-t)} f(\xi,\tau)\, s(u+\tau/2)\, s^*(u-\tau/2)e^{j\,2\pi\omega\tau} d\xi\, du\, d\tau \tag{2.58}$$

where $f(\xi,\tau)$ is a two-dimensional function called as kernel or parametrization function. Different distributions can be obtained by selecting different kernel functions and the spectrogram is a member of the Cohen's class.

2.4.1 The Wigner-Ville Distribution

Selecting the kernel function as Gaussian function the Wigner-Ville Distribution (WVD) is obtained as

$$W_s(t,\omega) = \int_{-\infty}^{\infty} s(u+\tau/2)\, s^*(u-\tau/2)\, e^{j\,2\pi\omega\tau} d\tau \tag{2.59}$$

or in frequency-domain

$$W_s(t,\omega) = \frac{1}{2\pi}\int_{-\infty}^{\infty} \hat{S}(\omega+\xi/2)\, \hat{S}^*(\omega-\xi/2)\, e^{j\,2\pi\xi t} d\xi \tag{2.60}$$

and $W_s(t,\omega) \in \mathbb{R}\ \forall t,\omega$.

The Wigner-Ville distribution

- conserves total energy

$$E_s = \int_{-\infty}^{\infty}\int_{-\infty}^{\infty} W_s(t,\omega)\, d\omega\, dt, \tag{2.61}$$

- satisfies marginal properties

$$\int_{-\infty}^{\infty} W_s(t,\omega)\, d\omega = |s(t)|^2 \qquad \int_{-\infty}^{\infty} W_s(t,\omega)\, dt = 2\pi|\hat{S}(\omega)|^2, \tag{2.62}$$

- satisfies translation covariance

$$y(t) = x(t-t_0) \quad \Rightarrow \quad W_y(t,\omega) = W_x(t-t_0,\omega), \tag{2.63}$$

$$y(t) = x(t)e^{j\,2\pi\omega_0 t} \quad \Rightarrow \quad W_y(t,\omega) = W_x(t,\omega-\omega_0), \tag{2.64}$$

- satisfies dilation covariance

$$y(t) = \sqrt{k}\, x(kt) \quad \Rightarrow \quad W_y(t,\omega) = W_x(kt, \frac{\omega}{k}), \tag{2.65}$$

- is compatible with filterings

$$y(t) = \int_{-\infty}^{\infty} h(t-u)x(u)du \Rightarrow W_y(t,\omega) = \int_{-\infty}^{\infty} W_h(t-u,\omega)W_x(u,\omega)\, du, \tag{2.66}$$

- is compatible with modulations

$$y(t) = m(t)\,x(t) \quad \Rightarrow \quad W_y(t,\omega) = \int_{-\infty}^{\infty} W_m(t,\omega-\xi)\,W_x(t,\xi)\,d\xi, \tag{2.67}$$

- has wide sense support conservation

$$x(t) = 0 \quad for \quad |t| > T \quad \Rightarrow \quad W_y(t,\omega) = 0 \quad for \quad |t| > T, \tag{2.68}$$

$$\hat{X}(\omega) = 0 \quad for \quad |\omega| > B \quad \Rightarrow \quad W_y(t,\omega) = 0 \quad for \quad |\omega| > B, \tag{2.69}$$

- satisfies unitarity of Moyal's Formula

$$2\pi \left| \int_{-\infty}^{\infty} x(t) y^*(t) dt \right|^2 = \int_{-\infty}^{\infty}\int_{-\infty}^{\infty} W_x(t,\omega)\,W_y(t,\omega)\,dt\,d\omega, \tag{2.70}$$

- the instantaneous frequency can be defined as

$$\phi'(t) = \frac{\int_{-\infty}^{\infty} \omega\, W_s(t,\omega) d\omega}{\int_{-\infty}^{\infty} W_s(t,\omega) d\omega}. \tag{2.71}$$

where the analytical signal associated with $s(t)$ is $Z_s(t) = A(t)e^{j\phi(t)}$,

- has perfect localization on linear chirp signals (Figure 2.5)

$$s(t) = e^{j\,2\pi\omega_s t}, \quad \omega_s = \omega_0 + 2\beta t \quad \Rightarrow \quad W_s(t,\omega) = \delta(\omega - (\omega_0 + \beta t)), \tag{2.72}$$

- has interference terms because of the quadratic properties

$$y(t) = x_1(t) + x_2(t) \Rightarrow W_y(t,\omega) = W_{x_1}(t,\omega) + W_{x_2}(t,\omega) + 2\Re\{W_{x_1,x_2}(t,\omega)\} \tag{2.73}$$

where

$$W_{x_1,x_2}(t,\omega) \triangleq \int_{-\infty}^{\infty} x_1(u+\tau/2)\,x_2^*(u-\tau/2)\,e^{j\,2\pi\omega\tau} d\tau \tag{2.74}$$

and called as cross-WVD. An example of the interference terms created by the WVD for the signal introduced in Figure 2.4-a is shown in Figure 2.6. This type of interferences may be removed by averaging the distribution with suitable kernels which yield positive time-frequency distribution. However resolution is reduced. The Pseudo-WVD and Smoothed Pseudo-WVD of the same signal are shown in Figure 2.7 and 2.8, respectively.

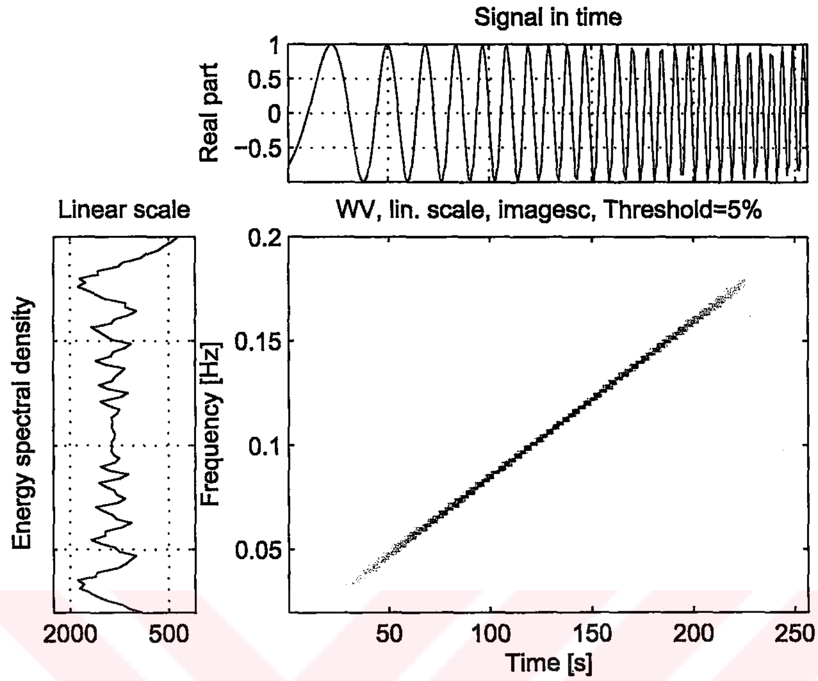

Figure 2.5: The Wigner Ville distribution of a chirp signal

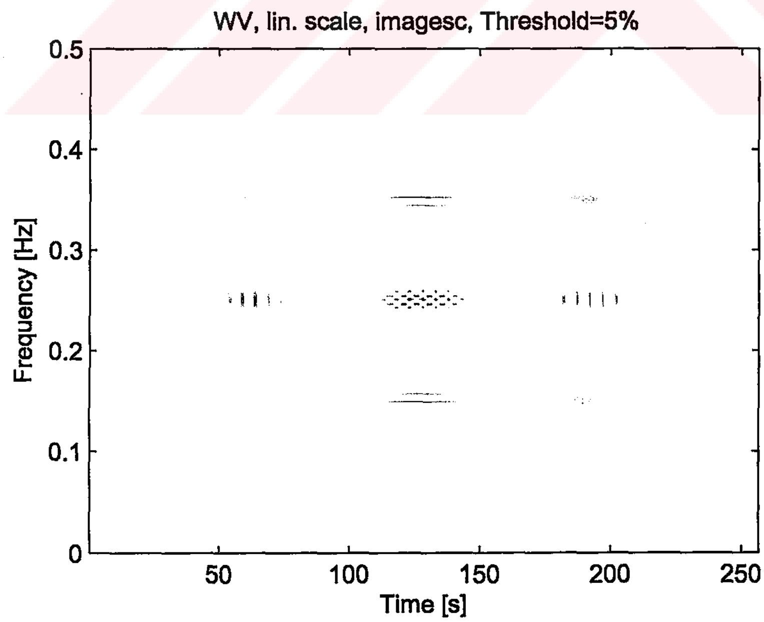

Figure 2.6: The WVD of four Gaussian atoms

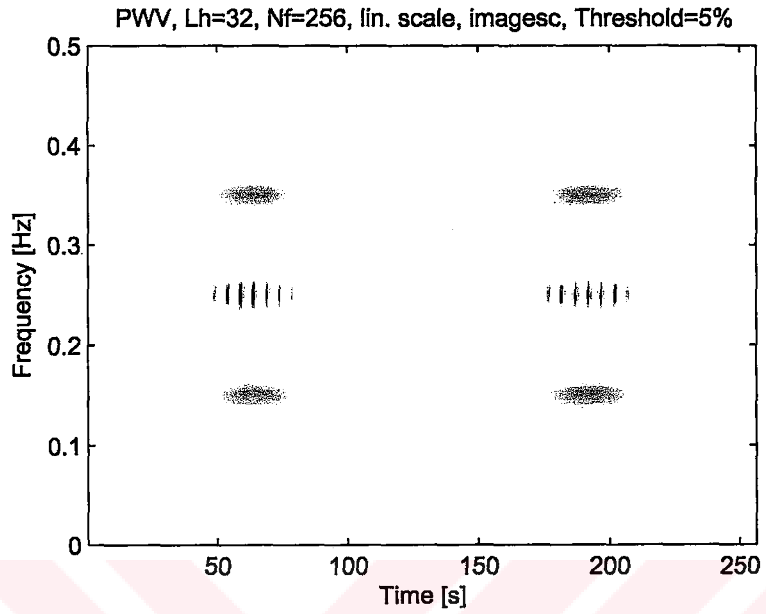

Figure 2.7: The Pseudo-WVD of four Gaussian atoms

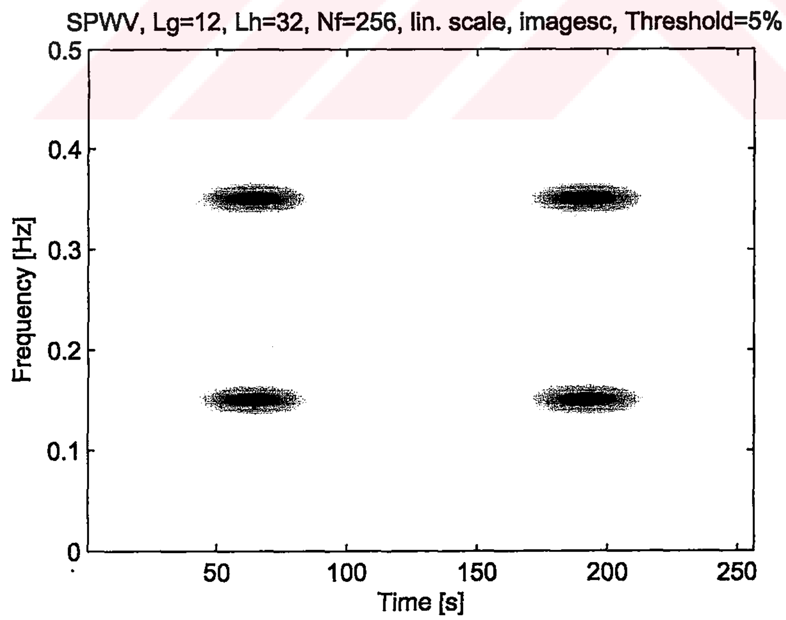

Figure 2.8: The Smoothed Pseudo-WVD of four Gaussian atoms

2.5 Wavelet Analysis of Chaotic Signals

The wavelet analysis of the generalized Chua's circuit exhibiting period-K limit cycle and n-scroll attractor have been accomplished in this section. Specifically, the wavelet transform has been chosen since it provides the local information about the magnitude and phase of the signal both in time and in frequency with multiresolution property.

The wavelet transform has been demonstrated by choosing the following standard complex Morlet mother wavelet

$$\psi(t) = \frac{1}{\sqrt{2\pi}} \cdot e^{j\omega_0 t} e^{-t^2/2} \tag{2.75}$$

where ω_0 defines the center frequency of the wavelet.

From the modulus of the wavelet transform, the time intervals where the dominant frequency components are located can be observed. The phase of the wavelet transform demonstrates structured gray-level spectrum branches when the frequency of the harmonic of the original signal f_0 is locked with the frequency of the "wavelet atom". Starting from the maximum scale, or the minimum frequency, the branches split until the width of the branch is equal to the period of the harmonic $1/f_0$. If the bandwidth of the branch of the phase pattern changes with time (as in Figure 2.10), this implies that the frequency content of the signal is a function of time.

2.5.1 The Generalized Chua's Circuit

The dynamics of the generalized Chua's circuit (Chua, Komuro, & Matsumoto, 1999) is described by the following set of differential equations

$$\begin{aligned} \dot{x} &= \alpha\,(y - h(x))\,, \\ \dot{y} &= x - y + z, \\ \dot{z} &= -\beta\, y. \end{aligned} \tag{2.76}$$

where α and β are the parameters defined by the circuit components and the piecewise linear characteristic is given in (Yalçın, Suykens, & Vandewalle, 2000) as

$$h(x) = m_{2q-1}x + \frac{1}{2}\sum_{i=1}^{2q-1}(m_{i-1} - m_i)\left(|x + c_i| - |x - c_i|\right) \quad q \in \mathbb{N},\ m_i, c_i \in \mathbb{R}. \tag{2.77}$$

For $\alpha = 8.0000, 8.3993$ and 8.44457 period-1, period-2 and period-4 limit cycles have been observed and the phase spaces are shown in Figure 2.9 a-c and the time-domain waveforms are shown in Figure 2.9d-f, respectively. For $\alpha = 9$ and $\beta = 14.286$, the observations have been made in (Suykens, Huang, & Chua, 1997; Suykens & Vandewalle, 1993) are summarized in the Table 2.1. The phase spaces of 2-, 3- and 5-scroll attractors are shown in Figure 2.10 a-c and the time-domain waveforms are shown in Figure 2.10 d-f, respectively.

Table 2.1 Parameters for the n-scroll attractors

q	m	c	Number of Scrolls
1	$\frac{1}{7}[-1\ 2]^T$	1	2
2	$\frac{1}{7}[0.9\ \ -3\ 3.5\ \ -2.4]^T$	$[1\ 2.15\ 4]^T$	3
3	$\frac{1}{7}[0.9\ \ -3\ 3.5\ \ -2.7\ 4\ \ -2.4]^T$	$[1\ 2.15\ 3.6\ 6.2\ 9]^T$	5

2.5.2 Evaluation of the Wavelet Analysis

The analysis procedure includes the numerical determination of the solutions of the differential equations and the application of the continuous wavelet transform to one of the state variables. In this section, the results of the wavelet transform have been demonstrated for period-K limit cycles and n-scroll attractors.

The period-1 limit cycle includes a dominant fundamental harmonic at f_1 and additional harmonics. In the modulus of the continuous wavelet transform of the period-1 as shown in Figure 2.9-g, the fundamental harmonic f_1 can be clearly seen and the other harmonics can not be identified since it is much more smaller in magnitude. However, two harmonics can be identified from the phase patterns given in Figure 2.9-j as it is observed that the branches in the patterns split into two parts along the scale axis just before these harmonics. In modulus pattern of the period-2 limit cycle (Figure 2.9-h), the fundamental harmonic and the subharmonic in $f_1/2$ can be easily observed while the other harmonics can be hardly seen. However, in the phase pattern (Figure 2.9-l), all these harmonics can be observed since the phase branches split into two parts at four different frequencies.

The modulus of the wavelet transform for 2-, 3- and 5-scroll attractors are shown in Figure 2.10 g-i, and the phase of the wavelet transform coefficients are shown in Figure 2.10 j-l, respectively. Because of the broadband spectrum property of chaotic signals, the modulus and phase patterns of the n-scroll attractors have more complex patterns. In the modulus of the wavelet transform, the lighter areas indicate the fundamental harmonics of the corresponding scroll along with the time interval in which the scroll has occurred. The branches in the phase spectrum of the n-scroll attractors split several times, showing that the presence of multiple harmonics. The splitting of branches does not have regularity such as the regularity in the period-K limit cycles. Moreover, the frequencies of the harmonics are not integer multiples of each other, which can be observed from the distributed locations of the splitting. This property can also be seen in quasi-periodic signals of which the modulus and phase patterns of WT are given in Figure 2.11.

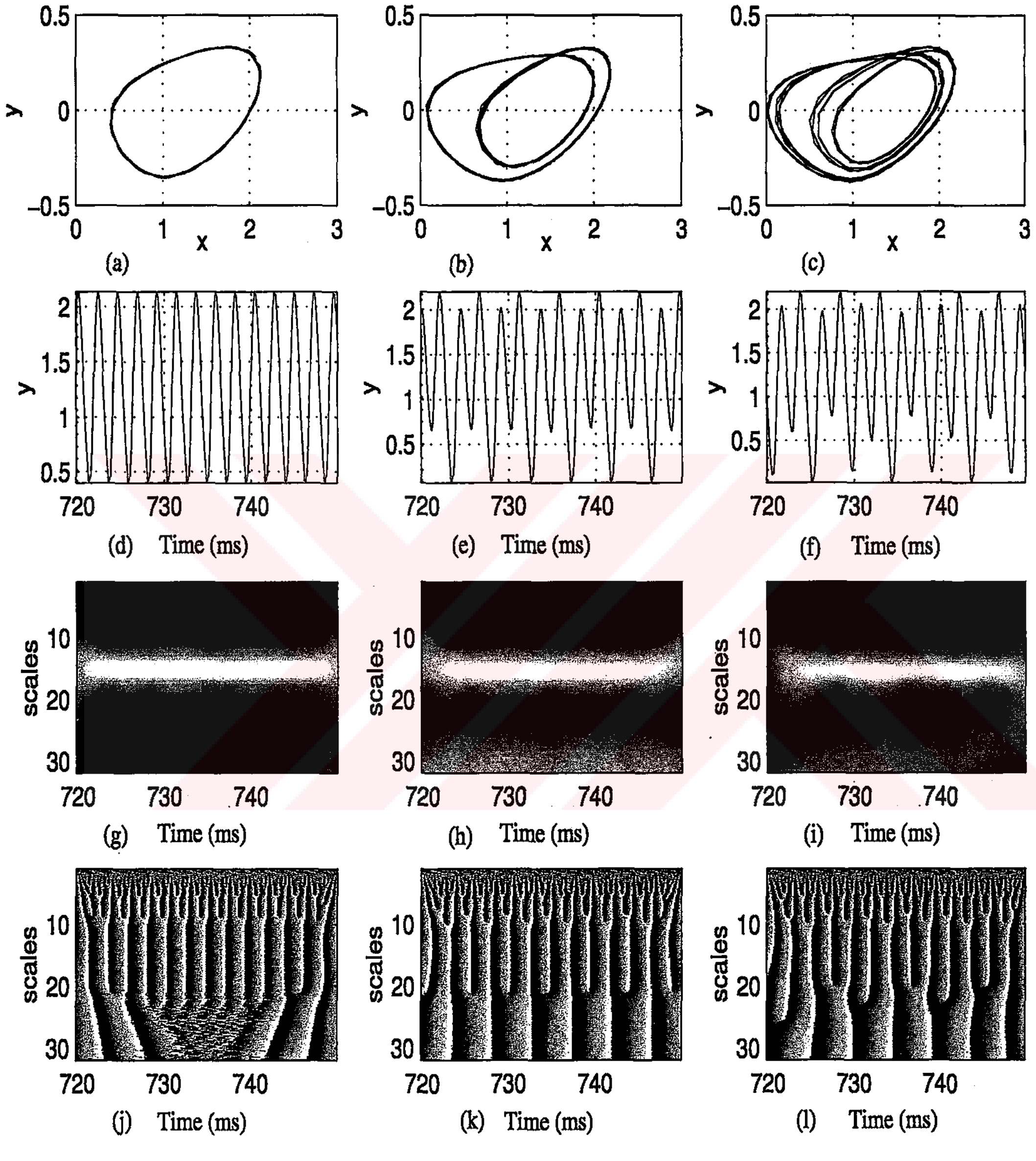

Figure 2.9: The phase space, time waveform, modulus and the phase of the wavelet transform of Period-K limit cycles

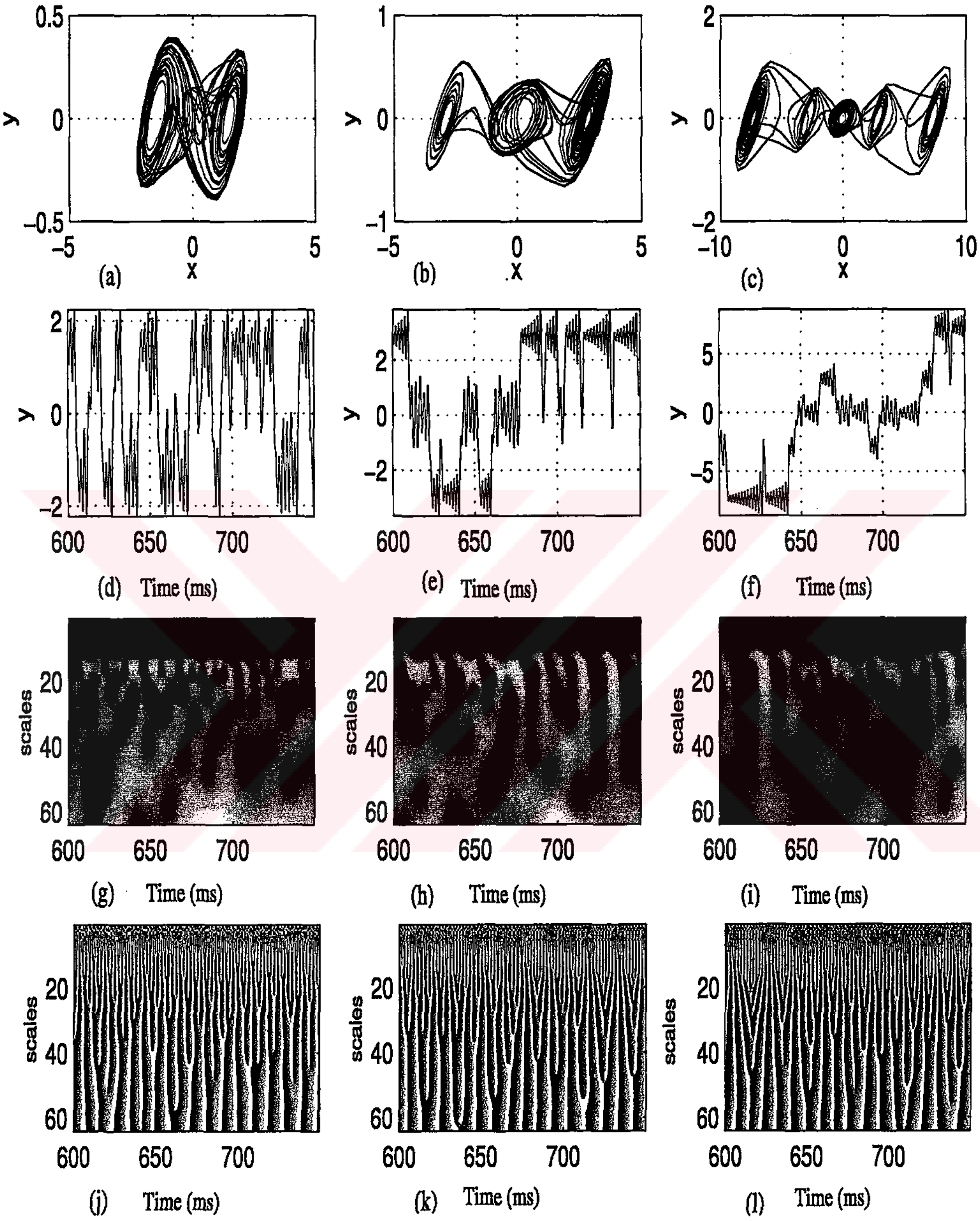

Figure 2.10: The phase space, time waveform, modulus and the phase of the wavelet transform of n-scroll attractors

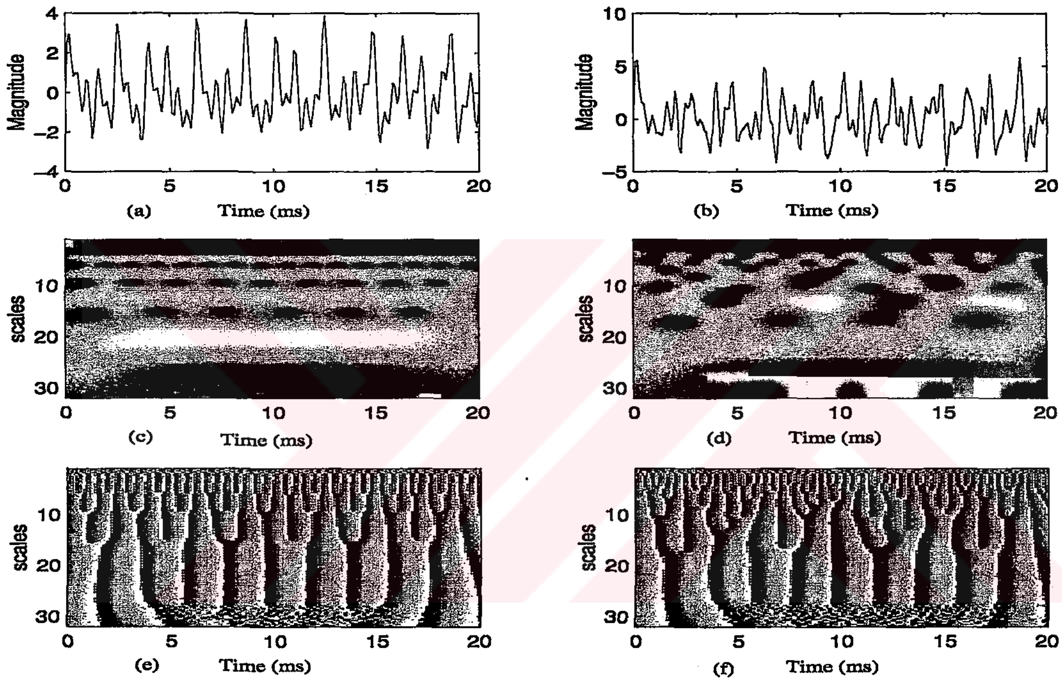

Figure 2.11: The time waveform, modulus and the phase of the wavelet transform of quasiperiodic signals

CHAPTER THREE
SIGNAL SYNTHESIS USING WAVELET METHODS

The signal synthesis block synthesizes the signal with given time-frequency domain specifications as follows:

$$E(t,f) = \begin{cases} E_1(t,f) & t_0 \le t < t_1 \quad and \quad f_0 \le f < f_1 \\ \vdots & \\ E_n(t,f) & t_{n-1} \le t < t_n \quad and \quad f_{n-1} \le f < f_n \\ 0 & otherwise \end{cases} \tag{3.1}$$

where $E(t,f)$ represents the energy distribution in the time-frequency plane.

Two wavelet domain-based methods can be used in the synthesis of the desired signal: First method uses the localized time-frequency energy distribution of the wavelet atoms (Özkurt et al., 2001) and the second one reconstructs the signal from the ridges of wavelet transform which can be called as transform skeleton method (Carmona et al., 1999; Savacı & Özkurt, 2003).

3.1 Wavelet Atom Method

The wavelet atoms have localized energy in the time-frequency plane defined by the window in Equation 2.27. Therefore, in order to provide a time-frequency domain energy localized in the given region, the suitable candidate wavelet atoms may be selected from the wavelet library. The signal with the desired time-frequency domain characteristics can be constructed by the wavelet series as

$$s(t) = \sum_{i \in I} c_i \Psi_i(t) \tag{3.2}$$

where I is the set of wavelet candidates satisfying the time-frequency energy requirements (Özkurt et al., 2001).

Since the energy of the signal in the wavelet domain can be defined as

$$E_T = c_\psi^{-1} \sum_{m=-\infty}^{\infty} \sum_{n=-\infty}^{\infty} |c_{mn}|^2 \tag{3.3}$$

where WT coefficients are

$$c_{mn} = W_s(a_m, b_n; \Psi) \tag{3.4}$$

where $a_m = a_0^{-m}$ and $b_n = nb_0$ and a_0, b_0 are the dilation and translation step sizes, respectively, the energy of the approximated signal is

$$\tilde{E}_T = c_\psi^{-1} \sum_{i \in I} |c_i|^2 \tag{3.5}$$

and the approximation error can be represented as

$$\|E_T - \tilde{E}_T\| = c_\psi^{-1} \sum_{i \notin I} |c_i|^2 \quad . \tag{3.6}$$

Therefore, the aim is to find the wavelet atoms which will minimize the approximation error.

3.1.1 Selection of the Mother Wavelet

An important issue in the wavelet atom signal synthesis is the selection of the mother wavelet. Three mother wavelet candidates have been used in wavelet atom synthesis of a sinusoidal signal and the obtained time-frequency domain results have been compared. The resulting time-frequency planes for sigmoidal, Mexican hat and Morlet mother wavelet are shown in Figure 3.1, Figure 3.2 and Figure 3.3, respectively. It is observed that the best choice is the sigmoidal mother wavelet, since the time-frequency plane for the other wavelets contain interference terms.

3.1.2 Applications

The wavelet atom signal synthesis method has been implemented in MATLAB and used for the synthesis of some test signals (Özkurt et al., 2001).

Example 3.1 *The mono-component signal with a constant frequency is given as*

$$E(t,f) = \begin{cases} 2 & 1 \le t < 3sec \quad and \quad f = 20Hz \\ 0 & otherwise \end{cases} \tag{3.7}$$

and the signal is synthesized with 40 wavelet atoms and $MSE = 0.0031$. *The time waveform, the target spectrogram and the spectrogram of the synthesized signal are shown in Figure 3.4.*

Example 3.2 *The desired signal have the energy distribution as*

$$E(t,f) = \begin{cases} 1 & 1 \le t < 8sec \quad and \quad 20 \le f < 40Hz \\ 0 & otherwise \end{cases} \tag{3.8}$$

and 2948 wavelet atoms have been used for the approximation. The obtained error is $MSE = 0.1462$. *The time waveform, target and resulting spectrograms are shown in Figure 3.5.*

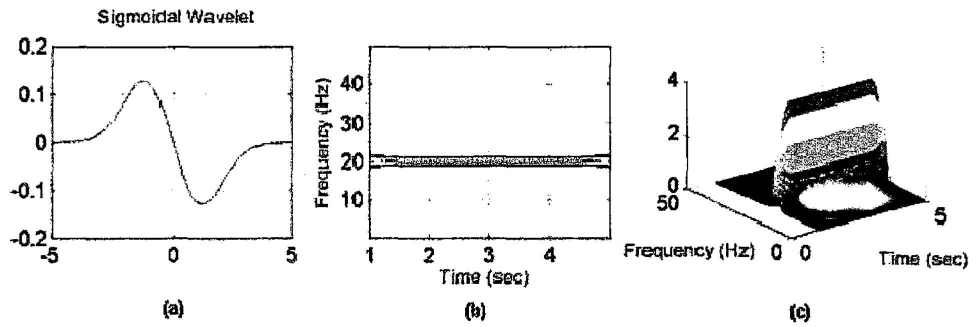

Figure 3.1: (a) The sigmoidal mother wavelet and (b) 2D view and (c) 3D view of time-frequency domain for synthesized sinusoidal signal

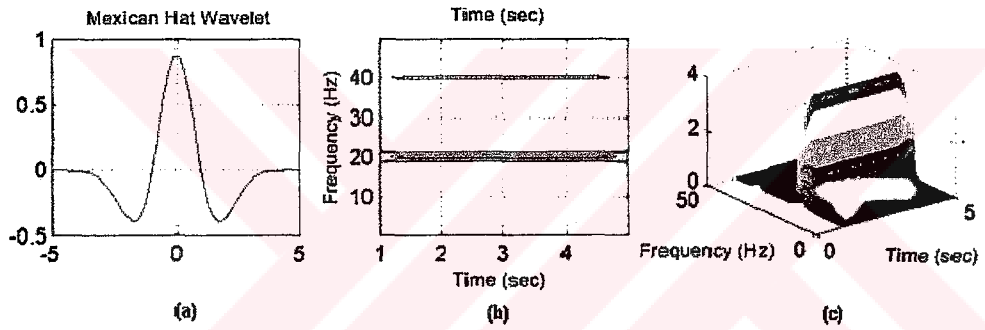

Figure 3.2: (a) The Mexican Hat mother wavelet and (b) 2D view and (c) 3D view of time-frequency domain for synthesized sinusoidal signal

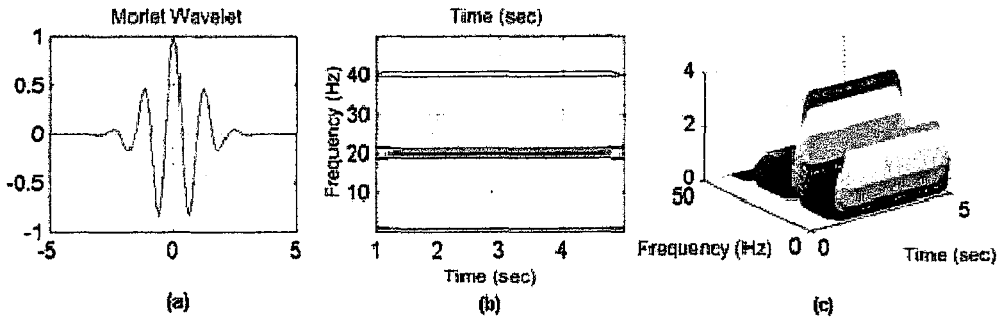

Figure 3.3: (a) The Morlet mother wavelet and (b) 2D view and (c) 3D view of time-frequency domain for synthesized sinusoidal signal

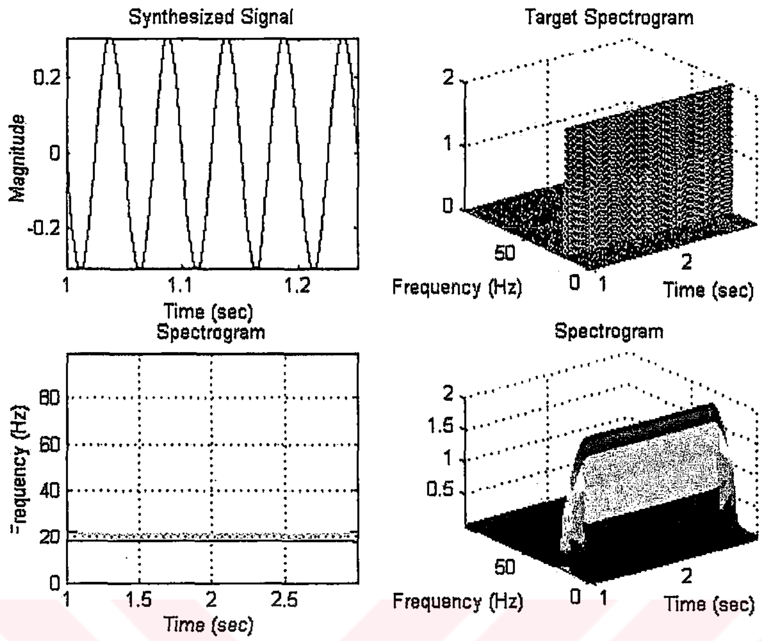

Figure 3.4: The synthesized signal for Example 3.1 with wavelet atom method

Example 3.3 *The signal which has the energy distribution as*

$$E(t,f) = \begin{cases} 2 & 2 \leq t < 6sec \quad and \quad 10 \leq f < 40Hz \quad and \quad f = t^2 + 5 \\ 0 & otherwise \end{cases} \tag{3.9}$$

has been synthesized with 32 *wavelet atoms. The target time-frequency plane, the time waveform, the power spectral density and the spectrogram of the synthesized signal are shown in Figure 3.6.*

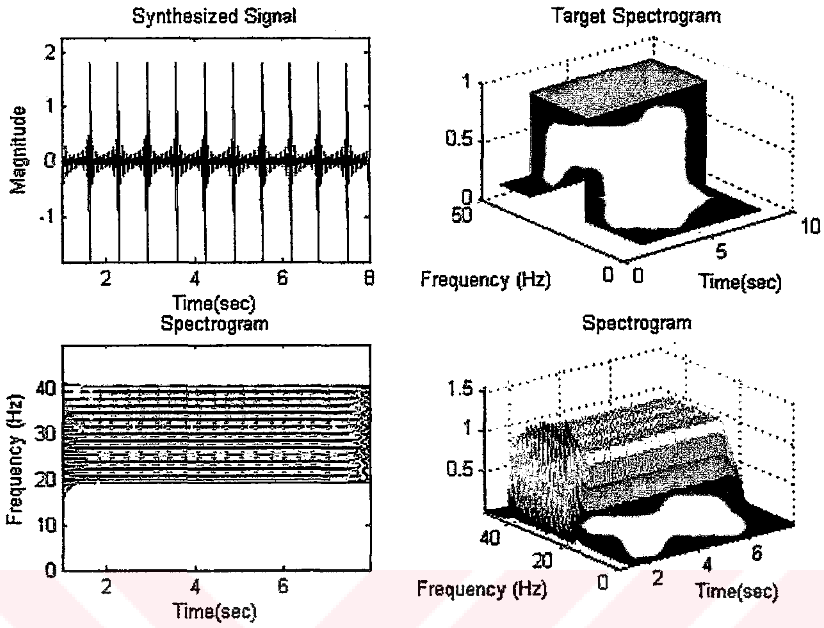

Figure 3.5: The synthesized signal for Example 3.2 with wavelet atom method

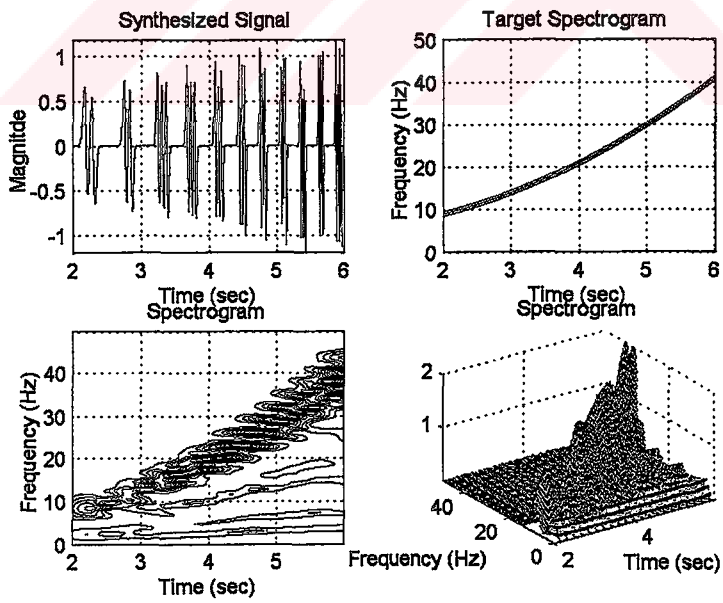

Figure 3.6: The synthesized signal for Example 3.3 with wavelet atom method

3.2 Wavelet Ridges

Another way of giving the time-frequency domain distribution is to specify the ridge of the time-frequency transform (wavelet or Gabor transforms) or the instantaneous frequency of the signal. The instantaneous frequency of a signal is simply defined as the derivative of the phase of the signal, and hence the signals can be modelled by using a frequency modulated signal fitted to the change of the main frequency. In this section, before introducing the signal synthesis using the wavelet ridges, the related definitions will be given as follows:

Definition 3.1 *The analytical mono-component signal $Z_s(t)$ associated with the real signal $s(t)$ is a complex function of time defined as*

$$Z_s(t) \triangleq s(t) + j\tilde{s}(t) = A(t)\, exp\, (\, j\phi(t)) \tag{3.10}$$

where the function $\tilde{s}(t)$ is the Hilbert transform of $s(t)$ which is defined as

$$\tilde{s}(t) = \frac{1}{\pi} P.V. \int_{-\infty}^{\infty} \frac{s(\tau)}{t-\tau} d\tau \tag{3.11}$$

where P.V. means that the integral is taken in the sense of the Cauchy principal value (Delprat et al., 1992)

The instantaneous amplitude $A(t)$ and the instantaneous phase $\phi(t)$ of the signal $s(t)$ are uniquely defined by Equation 3.10 by suppressing the negative frequency components of the signal (Cohen, 1989). For the signal of the form $s(t) = A(t)\, cos(\phi(t))$, the spectrum of $A(t)$ and $(cos(\phi(t)))$ should not overlap for the uniqueness of the analytical signal (Boashash, 1992).

Definition 3.2 *The instantaneous angular frequency is defined as the derivative of the phase*

$$\omega_{inst}(t) \triangleq \frac{d\phi(t)}{dt}. \tag{3.12}$$

Definition 3.3 *Let $s(t) \in L^2(\mathbb{R})$ be a real finite energy signal. The signal is asymptotic iff*

$$\left|\frac{d\phi\left(t\right)}{dt}\right| \gg \left|\frac{1}{A\left(t\right)}\frac{dA\left(t\right)}{dt}\right| \tag{3.13}$$

where $A(t) > 0$ and $\phi(t) \in [0, 2\pi] \quad \forall t$.

The instantaneous frequency of an asymptotic signal has been derived from its wavelet transform by stationary phase method in the sequel as: For the chosen asymptotic mother wavelet in the form of $\Psi(t) = A_\Psi(t)e^{j\phi_\Psi(t)}$, the wavelet transform of the analytical signal $Z_s(t)$ can be found by using Equation 2.16

$$W_{Z_s}(a, b; \Psi) = \frac{1}{a}\int_{-\infty}^{\infty} A(t)A_\Psi(\frac{t-b}{a})\exp(j\Phi_{a,b}(t))\, dt \tag{3.14}$$

where $\Phi_{a,b}(t) \triangleq \phi(t) - \phi_\Psi(\frac{t-b}{a})$ is the argument of the integrand.

Theorem 3.1 *(Mallat, 1999) For any $s(t) \in L^2(\mathbb{R})$*

$$W_s(a, b; \Psi) = \frac{1}{2}W_{Z_s}(a, b; \Psi) \tag{3.15}$$

where $W_{Z_s}(t)$ is the wavelet transform of the analytical signal associated with $s(t)$.

Therefore, the integral wavelet transform of the real signal $s(t)$ is

$$W_s(a, b; \Psi) = \frac{1}{2a}\int_{-\infty}^{\infty} A(t)A_\Psi(\frac{t-b}{a})\exp(j\Phi_{a,b}(t))\, dt \tag{3.16}$$

and since the integrand is asymptotic, the stationary phase theorem given in (Delprat et al., 1992; Todorovska, 2001) can be directly applied. Let $t = t_0$ be the stationary point of the argument of the integrand which satisfies

$$\Phi'_{a,b}(t_0) = \phi'(t_0) - \frac{1}{a}\,\phi'_{\Psi}(\frac{t_0 - b}{a}) = 0 \tag{3.17}$$

$$\Phi''_{a,b}(t_0) = \phi''(t_0) - \frac{1}{a^2}\,\phi''_{\Psi}(\frac{t_0 - b}{a}) \neq 0 \tag{3.18}$$

(Boashash, 1992), and then the wavelet transform in (3.16) can be approximated as in (Todorovska, 2001) by

$$W_s(a,b;\Psi) \approx \frac{1}{2a}\frac{\sqrt{2\pi}e^{(j\pi/4)sgn[\Phi''_{a,b}(t_0)])}}{\sqrt{|\Phi''_{a,b}(t_0)|}}A(t_0)A_{\Psi}(\frac{t_0 - b}{a})e^{j\Phi_{a,b}(t_0)} \tag{3.19}$$

and its simpler form is

$$W_s(a,b;\Psi) \approx \sqrt{\frac{\pi}{2}}\frac{Z_s(t_0)\Psi^*(\frac{t_0-b}{a})}{corr(a,b)} \tag{3.20}$$

where

$$corr(a,b) = a\,\left|\Phi''_{a,b}(t_0)\right|^{1/2} e^{-j(\pi/4)\,sgn[\Phi''_{a,b}(t_0)]}. \tag{3.21}$$

Since at $t_0 = b$, the chosen translated and dilated Morlet mother wavelet in Equation 3.20 has its maximum, then at that time instant $W_s(a,b;\Psi)$ is also locally maximum neglecting the correction term.

Definition 3.4 *The ridge of the wavelet transform of $s(t)$ is the set of points (a,b) which are the stationary points of the argument of the wavelet transform "$\Phi_{a,b}(t)$" in (3.16) (i.e., $t_0(a,b) = b$)*

The ridge can be obtained from Equation 3.17 as

$$a(b) = \frac{\phi'_{\Psi}(0)}{\phi'(b)} \tag{3.22}$$

and then the instantaneous angular frequency along the ridge becomes

$$\omega_{inst}(t)|_{t=b} = \phi'(b) = \frac{\phi'_{\Psi}(0)}{a(b)} \quad . \tag{3.23}$$

The multi-component signal with the instantaneous amplitudes $A_l(t) \in C^1$ and the instantaneous phases $\phi_l \in C^2$ can be described by

$$s(t) = \sum_{l=1}^{L} A_l(t)\, e^{j\phi_l(t)} \tag{3.24}$$

where L is the number of the components. The wavelet transform of the multicomponent signal $s(t)$ has been given in (Carmona et al., 1999) as

$$W_s(a, b; \Psi) = \frac{1}{2}\sum_{l=1}^{L} A_l(b)e^{j\phi_l(b)}\hat{\Psi}^*(a\phi'_l(b)) + r(a, b) \tag{3.25}$$
$$where \quad r(a, b) \sim O(|A'_l|, |\phi''_l|) \quad .$$

If the Fourier transform of the mother wavelet "$\hat{\Psi}(\omega)$" is localized near a certain angular frequency $\omega = \omega_0$, the scalogram is localized around L ridges

$$a^l = a^l(b) = \frac{\omega_0}{\phi'_l(b)}, \quad l = 1, ..., L. \tag{3.26}$$

The representation above is valid at $t = b$ if the instantaneous frequencies of the components of the signal are separable (Mallat, 1999) (i.e., the normalized difference between the instantaneous frequencies is greater than the normalized bandwidth of the mother wavelet as

$$\frac{|\phi_k'(b) - \phi_l'(b)|}{\phi_k'(b)} \geq \frac{\Delta\omega}{\omega_0} \qquad \forall\, k, l = 1, 2, \ldots, L \tag{3.27}$$

where $|\hat{A}_\Psi(\omega)| \ll 1$ for $\omega > \Delta\omega$ and $\hat{A}_\Psi(\omega)$ is the Fourier spectrum of the modulus of the mother wavelet).

3.2.1 Determination of the Ridges

The ridge determination algorithms, i.e., stationary phase method (Delprat et al., 1992; Todorovska, 2001), simple method (Delprat et al., 1992; Todorovska, 2001) and Carmona method for noisy mono-component signals (Carmona & Hwang, 1997) and noisy multi-component signals (Carmona et al., 1999), will be explained in this section.

3.2.1.1 The Stationary Phase Method

For determination of the ridge from the phase of the wavelet transform coefficients, the stationary phase method can be used. The time derivative of the phase of the wavelet transform is as follows

$$\left.\frac{\partial \Phi_{a,b}}{\partial b}\right|_{a(b)} = \frac{1}{a}\phi_\Psi'(0) \tag{3.28}$$

and using this relation the points on the ridge can be determined (Delprat et al., 1992). Extracting the ridge from the modulus of the signal is more robust than the stationary phase method especially in the presence of noise, because the extraction from the modulus does not involve the differentiation of the phase.

3.2.1.2 The Simple Method

Since the modulus of the wavelet transform in Equation 3.20 is maximum along the ridge, then the simplest way of determination of the ridge of the wavelet transform is to find the scales at which the scalogram is maximum satisfying

$$\left.\frac{\partial P_s(a,b;\Psi)}{\partial a}\right|_{a=a(b)} = 0$$
$$\left.\frac{\partial^2 P_s(a,b;\Psi)}{\partial a^2}\right|_{a=a(b)} < 0. \tag{3.29}$$

This method works well when the the signal is not contaminated with noise (Delprat et al., 1992; Todorovska, 2001).

However, in the noisy situations the ridges can not be determined successfully. Therefore, a new method has been developed by Carmona et.al in (Carmona & Hwang, 1997).

3.2.1.3 Carmona Method

In this method, the ridge extraction problem has been transformed into an optimization problem. A direct search method searches for a ridge $a(b) = \varphi(b)$ which minimizes the following penalty function

$$F(\varphi(b)) = -\int P_s(a,b;\Psi)db + \int \left[\lambda_1 \varphi'(b)^2 + \lambda_2 \varphi''(b)^2\right] db \tag{3.30}$$

where the first term maximizes energy density along the ridge and the second term includes the first and second derivatives of the ridge function $\varphi(b)$ to assure the smoothness of the ridge. This optimization problem can be solved by simulated annealing algorithm which prevents trapping in local extrema caused by strong noise components (Carmona & Hwang, 1997; Todorovska, 2001).

For the multicomponent signals in Equation 3.24, Carmona et.al have developed a new ridge detection algorithm based on Markov Chain Monte Carlo method which is called as crazy climbers (Carmona et al., 1999).

3.2.2 Signal Synthesis by Wavelet Ridges

The reconstruction of the signal from the wavelet ridges for mono-component and multi-component signals have been given in (Carmona & Hwang, 1997) and (Carmona et al., 1999), respectively.

The real part of the signal $s(t)$ given in Equation (3.24) can be constructed from the skeleton of the transform using the approximate formula Equation (3.25) as

$$s_r(b) = 2\,\Re\left\{\sum_{l=1}^{L} W_s(a^l(b), b; \Psi)\right\} \tag{3.31}$$

where L is the number of the ridges. The reconstruction using the transform skeleton is a simple scheme and it produces good approximations. This approach produces successful results; however it requires the knowledge of the transform at each point of the ridge (Carmona et al., 1999). Therefore, each point along the ridge should be given for synthesis, or the gaps along the ridges should be completed using interpolation or curve fitting techniques.

3.2.3 Applications

A signal synthesis program which uses the transform skeleton method has been written in MATLAB (Savacı & Özkurt, 2003). When the time and frequency range is given, the pure sinusoidal signal, a linear or hyperbolic chirp can be synthesized. Also, the points in the ridge can be given interactively by the user and the ridges have been calculated by the linear interpolation. In order to illustrate the performance of the operation, the wavelet transform of the synthesized signal has been calculated.

Example 3.4 *The signal which have the energy distribution as*

$$E(t,f) = \begin{cases} 1 & 1 \leq t < 1.2sec \quad and \quad f = 20Hz \\ 0 & \quad otherwise \end{cases} \tag{3.32}$$

has been synthesized as shown in Figure 3.7.

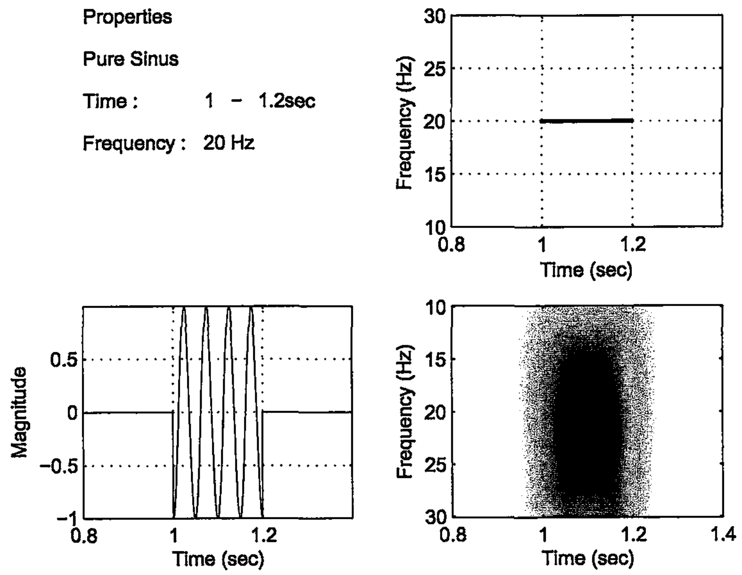

Figure 3.7: The synthesized signal for Example 3.4 with wavelet ridges method

Example 3.5 *The signal which have the energy distribution as*

$$E(t,f) = \begin{cases} 1 & 1 \leq t < 5sec \quad and \quad 5 \leq f < 15Hz \\ 0 & otherwise \end{cases} \tag{3.33}$$

has been synthesized as shown in Figure 3.8.

Example 3.6 *The signal which have the energy distribution as*

$$E(t,f) = \begin{cases} A(t) & 1 \leq t < 4sec \quad and \quad 10 \leq f < 35Hz \\ 0 & otherwise \end{cases} \tag{3.34}$$

where $A(t)$ is given by the ridge points in the time-frequency plane by the user. The gaps along the ridge points are interpolated linearly by the program. The target time-frequency plane, the synthesized signal in time-domain and the wavelet transform of the obtained signal is shown in Figure 3.9.

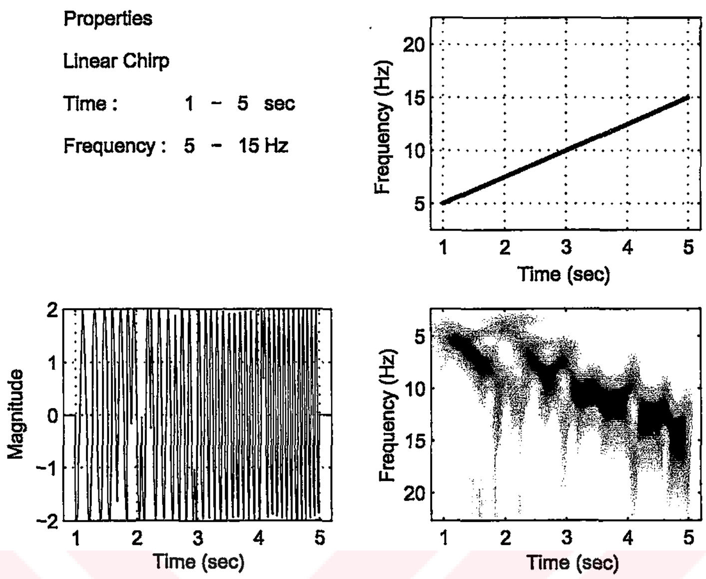

Figure 3.8: The synthesized signal for Example 3.5 with wavelet ridges method

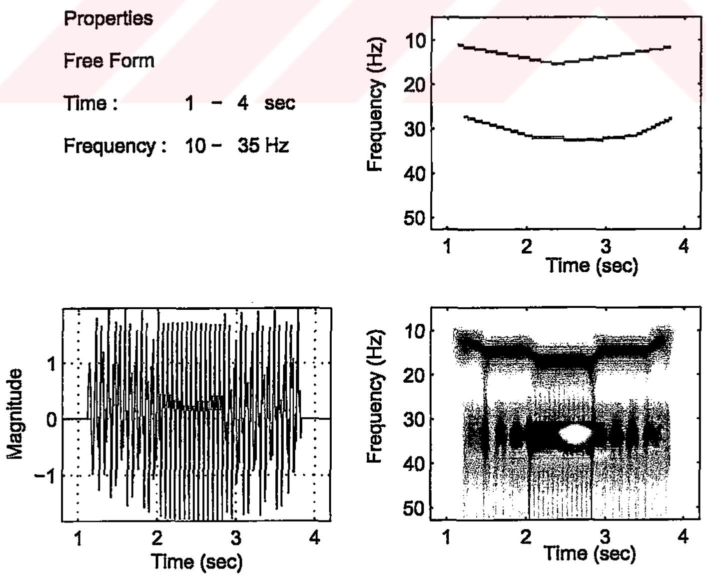

Figure 3.9: The synthesized signal for Example 3.6 with wavelet ridges method

CHAPTER FOUR

SYSTEM MODELLING BY WAVELET NETWORKS

Any finite energy multivariate function can be approximated by wavelets using the multiresolution approximation property of the wavelet decomposition. In order to approximate arbitrary nonlinear functions, wavelet network which combines feedforward neural networks and wavelet decompositions using a learning algorithm of backpropagation type has been proposed in (Zhang & Benveniste, 1992). The identification of static and dynamical systems using wavelet network have attracted many researchers since the wavelet analysis has been successfully applied for analyzing signals both in time and frequency domain with different resolution levels (Cao et al., 1995; Allingham et al., 1998; Oussar et al., 1998; Zhang, 1997).

When the input-output pairs measured from the system to be modelled is given as

$$\{x(t_k), y(t_k) |\, y(t_k) = f(x(t_k)) + \varepsilon_k, \quad k = 1, \ldots, K, \quad f(\cdot) : \mathbb{R}^d \to \mathbb{R}\} \tag{4.1}$$

where ε_k is the measurement error, the problem is to minimize the mean square error between the actual output and the output of the wavelet network

$$e \triangleq \frac{1}{2} E\{\, [\, y - f_w(x)]^2 \} \tag{4.2}$$

where the output of the wavelet network is defined as

$$f_w(x) = \sum_{i=1}^{N} w_i \, \Psi \left(D_i x - b_i \right) + c^T x + \bar{b} \tag{4.3}$$

where N is the number of $d - dimensional$ wavelons, w_i is the wavelet coefficients for each $d - dimensional$ wavelon, $D_i = diag(d^i_{11}, \ldots, d^i_{mm}) \in \mathbb{R}^{d \times d}$ where $d^i_{jj} = 1/a_{ij}$ and a_{ij} is the dilation coefficient, $\Psi(\cdot) : \mathbb{R}^d \to \mathbb{R}$ is the mother wavelet function, $b_i \in \mathbb{R}^d$ is the translation coefficient vector, $c \in \mathbb{R}^d$ represents the coefficient of the linear term and $\bar{b}$ is the bias term to approximate the functions with nonzero mean. The block diagram of the wavelet network is shown in Figure 4.1. The optimum parameter set and the number of wavelons are to be determined for the construction of the wavelet network. The selection of suitable wavelons has been implemented by the "Stepwise Selection by Orthogonalization" algorithm proposed in (Zhang, 1997).

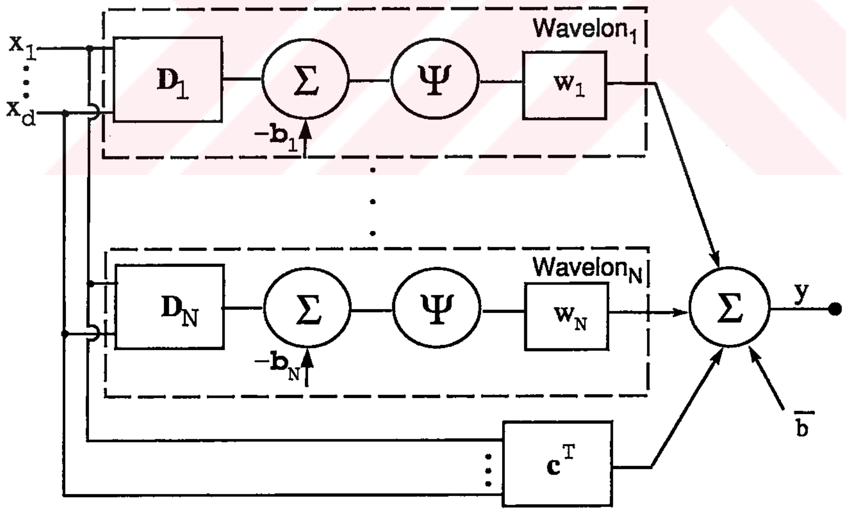

Figure 4.1: The block diagram of the static wavelet network

4.1 The Construction of the Wavelet Network

The wavelet network has been constructed with set of wavelons $I \subseteq W$ which minimizes the mean squared error defined in Equation 4.2 where W is the library of the wavelon candidates $W = \{\Psi_i : i = 1, ..., L\}$. The output of the wavelet network is then defined as

$$f_w(x) = \sum_{i \in I} w_i \Psi_i + c^T x + \bar{b} \tag{4.4}$$

where w_i is the coefficients of the scaled and translated wavelets which will be calculated by the wavelet selection algorithms explained in the following sections. When the training data is given the wavelons whose support do not contain any data point are eliminated and the regression techniques are used for further elimination then the wavelet network is constructed with the remaining wavelons.

4.1.1 Selection of Wavelons

The wavelons are chosen by the regression technique called "Stepwise Selection by Orthogonalization Algorithm" (Zhang, 1997). At each step the algorithm determines the wavelon which reduces the distance between the space spanned by the previously selected wavelons and the output space, and adds the new wavelon to I. This process continues until the number of wavelons is reached.

Let $v_i = [\Psi_i(x_1) \quad \dots \quad \Psi_i(x_N)]^T$ where $\{x_j, y_j | y_j = f(x_j), \quad j = 1, ..., N\}$. The wavelet candidates Ψ_i's are normalized, thus $v_i^T v_i = 1$ and the output observation set is $y = [y_1 \dots y_N]^T$. At the i^{th} stage, assume that $i-1$ wavelets $v_{l1}, ..., v_{li-1}$ has been selected. The v_j which minimizes the distance has been calculated

$$\min_{v_j} d(span(v_{l1}, ..., v_{li-1}, v_j), y) \tag{4.5}$$

Assume that the previously selected wavelets are orthonormalized and renamed as $\omega_{l1}, ..., \omega_{li-1}$. For each j

$$p_j = v_j - \left(\left(v_j^T \omega_{l1}\right) \omega_{l1} + ... + \left(v_j^T \omega_{li-1}\right) \omega_{li-1}\right) \tag{4.6}$$

and its normalized version

$$q_j = \left(p_j^T p_j\right)^{-1/2} p_j \tag{4.7}$$

are computed and searched for

$$\min_{v_j} e\left(v_j\right) = \min_{q_j} e\left(q_j\right) = \left[y - W_j U_j\right]^T \left[y - W_j U_j\right]\right] \tag{4.8}$$

where

$$\begin{gathered} W_j = \left(\omega_{l1}, ..., \omega_{li-1}, q_j\right) \\ U_j = \left(w_{l1}, ..., w_{li-1}, w_j\right)^T = \left(W_j^T W_j\right)^{-1} W_j^T y = W_j^T y. \end{gathered} \tag{4.9}$$

4.1.2 Determination of the Number of the Wavelons

There are several approaches for choosing the number of wavelons such as

- Generalized cross-validation
- Model complexity penalty
- Statistical hypothesis test
- Minimum description length criterion.

The generalized cross-validation is one of the most common methods for determining the number of the wavelons. In this method, separate training and test sets are used and the number of wavelon s which minimizes the performance criterion is chosen

$$\min_{s} GCV = \frac{1}{N} \sum_{k=1}^{N} (y_k - f_w(x_k))^2 + \frac{2s}{N}\sigma_e^2 \tag{4.10}$$

where σ_e^2 is the noise variance. Since the noise variance may not be known in the practical situations it should be estimated from the data points.

4.2 Dynamical System Modelling with Wavelet Network

The purpose of the dynamic modelling block is to build a dynamic model by wavelet networks using the time series obtained from the signal synthesis block. Assume that a random process generating $y(k) \in \mathbb{R}, x(k) \in \mathbb{R}^d, k \in \mathbb{Z}$ and the relationship between them is as following

$$y(k) = F(x(k)) + \varepsilon_k, \qquad F(\cdot) : \mathbb{R}^d \to \mathbb{R} \tag{4.11}$$

where ε_k is a random variable. According to the Taken's time-delay embedding theorem (Takens, 1985), the multidimensional dynamical structure of the system can be retrieved from single scalar variable observed from the system. Let a vector $z \in \mathbb{R}^d$ is constructed from the observations as

$$z(k) = [y(k-T)\, y(k-2T) \ldots y(k-dT)] \tag{4.12}$$

where d is the embedding dimension and T is the embedding delay. The

$$y(k) = \tilde{F}(z(k)) \tag{4.13}$$

follows the dynamical evolution of the original system. Therefore, the next state of the system is predicted form the previous observations.

The important issue in the reconstruction of the embedded vector is to choose the time-delay and the embedding dimension. The criteria which are used in reconstruction will be explained in the sequel:

The time delay should be

- some multiple of the sampling time since only these observations are present,
- long enough to evolve the system
- short enough not to loose the correlation between the samples (Abarbanel, 1996).

Usually, first minimum of average mutual information

$$I(T) = \sum_{s(n),s(n+T)} P(s(n), s(n+T)) \log_2 \left[\frac{P(s(n), s(n+T))}{P(s(n)) \cdot P(s(n+T))} \right] \tag{4.14}$$

is chosen as time delay. The average mutual information is a measure of the information about observation $s(n+T)$ obtained from the observation $s(n)$.

"False Nearest Neighborhood Method" is a method commonly used for the selection of the embedding dimension. Let a state space reconstruction is made as in Equation 4.12 and the nearest neighbor of this vector in phase space is

$$z^{NN}(k) = [y^{NN}(k-T)\, y^{NN}(k-2T) \ldots y^{NN}(k-dT)] \tag{4.15}$$

The distance between these two vectors in d-dimensional space is compared with the distance in $d+1$-dimensional space. The only difference in the vectors are the $d+1^{th}$ elements of the vectors, i.e. $y(k-(d+1)T)$ and $y^{NN}(k-(d+1)T)$. If the additional distance $\left|y(k-(d+1)T) - y^{NN}(k-(d+1)T)\right|$ is large compared to the distance in d-dimensional space $\left|z(k) - z^{NN}(k)\right|$, then the points $z(k)$ and $z^{NN}(k)$ separated from each other in the next dimension which means that they are false neighbors. Therefore, the dimension is increased until the geometric structure of the dynamics is unfolded in phase space.

The evolution of the system is approximated by some arbitrary set of basis functions for the modelling or identification of the nonlinear dynamical systems (Cao et al., 1995; Judd & Mees, 1995, 1996; Allingham et al., 1998). The purpose is to represent Equation 4.13 with the suitable wavelet network. Since the observations can be expressed as a function of past measurements, the past values are used as inputs and the present values are used as output for the wavelet network to train the network. The output of the wavelet network F_w is

$$y(k) = F_w(z(k)) = \sum_{i=1}^{N} w_i \, \Psi_d \, (D_i \, z(k) - b_i) + c^T \, z(k) + \bar{b} \tag{4.16}$$

The block diagram of the dynamical wavelet network is shown in Figure 4.2.

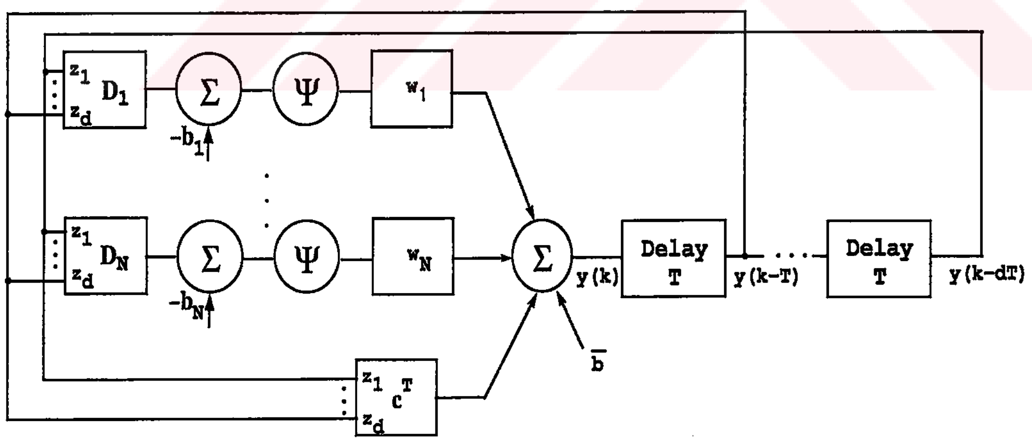

Figure 4.2: The block diagram of the dynamical wavelet network

4.3 Applications

The wavelet network can be used for the modelling of the both static and dynamical systems as it has been introduced in the previous sections. In this section some wavelet network modeling examples have been demonstrated by Wavelet Network program written by Zhang in (Zhang, 1997). Simulations have been done for the Mexican Hat wavelet as the default mother wavelet for the program and also the program has been adapted for the sigmoidal wavelet proposed by (Pati & Krishnaprasad, 1994). The implementations of these two type of approximation circuits will be explained in next chapter.

4.3.1 Static System Modelling with Sigmoidal Mother Wavelet

In (Pati & Krishnaprasad, 1994), a sigmoidal mother wavelet has been proposed satisfying the admissibility condition. It has been obtained by combining three sigmoids as

$$\Psi\left(x\right) = s\left(x+k\right) - 2\,s\left(x\right) + s\left(x-k\right) \tag{4.17}$$

where $s(x) = tanh(qx)$ and q is a constant and $0 < k \leq \infty$. The dilated and translated wavelets form an affine frame for dilation stepsize $a_0 = 2$ and the translation stepsize $0 \leq b_0 \leq 3.5$ where the wavelets can be obtained as

$$\Psi\left(a_i, b_i\right) = a_0^{nd/2}\,\Psi\left(a_0^n\ \left(x - mb_0\right)\right) \tag{4.18}$$

with $m, n \in \mathbb{Z}$ and d is the dimension.

In this study, the sigmoidal mother wavelet parameters have been chosen as $k = 2$, $q = 1$, and the dilation and translation step sizes have been selected as $a_0 = 2$ and $b_0 = 0.01$ where $\Psi : \mathbb{R} \to \mathbb{R}$.

In order to approximate the functions in higher dimensions, the tensor product of the one dimensional wavelet functions are used. For the construction of the tensor product wavelet frame, the multidimensional wavelet $\Psi(\cdot) : \mathbb{R}^d \rightarrow \mathbb{R}$ is defined as the tensor product of the 1-dimensional wavelet functions as

$$\Psi(\mathbf{x}) = \Psi(x_1) \cdot \Psi(x_2) \cdots \Psi(x_d) \tag{4.19}$$

where $\mathbf{x} = [x_1 x_2 \ldots x_d]$ (Meyer, 1992).

Example 4.1 *The target function is given by the* 21 *data points and the approximation is done by* 3 *wavelons. The result of the approximation is shown in Figure 4.3. The obtained mean squared error (MSE) is* 0.004.

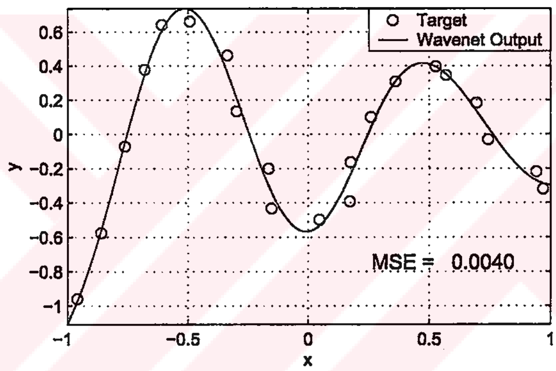

Figure 4.3: Result of approximation for Example 4.1 with sigmoidal mother wavelet.

Example 4.2 *The function to be approximated is given by*

$$y = \begin{cases} -2.186x - 12.864 & -1 < x \leq -0.2 \\ 4.246x & -0.2 < x \leq 0 \\ \exp(-0.5x - 0.5)\sin(3x^2 + 7x) & 0 < x \leq 1 \end{cases} \tag{4.20}$$

6 *wavelons have been used for the approximation and the obtained MSE is* 0.0011 *which is shown in Figure 4.4.*

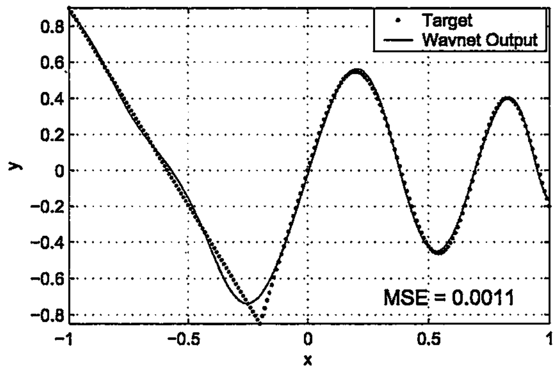

Figure 4.4: Result of approximation for Example 4.2 with sigmoidal mother wavelet.

Example 4.3 *The 2-dimensional function*

$$y = f(x_1, x_2) = \begin{cases} 2\,exp\,(x_1^2 - x_2^2)\,cos(4x_1)\,sin(3x_2) & 0 < x \leq 1 \quad 0 < x \leq 1 \\ 0 & elsewhere. \end{cases} \tag{4.21}$$

has been approximated by ten 2-dimensional wavelons and the $MSE = 0.0714$. *The target and the result of the approximation have been shown in Figure 4.5-a and -b, respectively.*

4.3.2 Static System Modelling with Mexican Hat Mother Wavelet

The test signals approximated by wavelet network with the sigmoidal mother wavelet in Section 4.3.1 have also been modelled with the Mexican Hat mother wavelet. The results have been demonstrated and compared with the results of approximation with sigmoidal mother wavelet. The suitable wavelons have chosen by the step-wise selection by orthogonalization algorithm (Zhang, 1997) and then the network has been trained with back-propagation algorithm for further improvement of the approximation.

Example 4.4 *The same number of the wavelons are used for the approximation of the signal given in Example 4.1 and the obtained MSE is slightly worse than the result for sigmoidal mother wavelet. This can be probably caused by the similarity of the target waveform with the sigmoidal wavelet. The target signal and the output of the wavelet network is shown in Figure 4.6.*

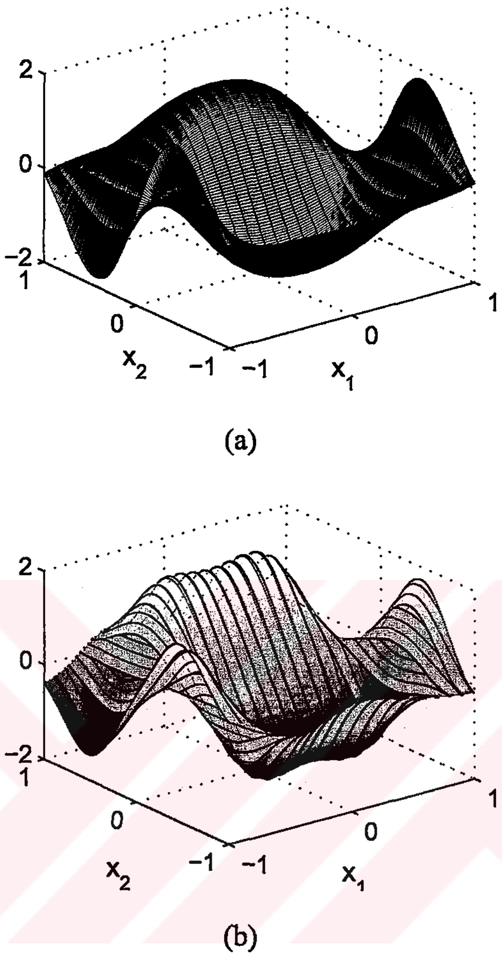

Figure 4.5: (a) The target function, (b) The result of approximation for Example 4.3 with sigmoidal mother wavelet.

Example 4.5 *The approximation of the signal given in Example 4.2 has been made by the Mexican Hat mother wavelet. It has been observed that the wavelet network with Mexican Hat mother wavelet produces better results than the sigmoidal mother wavelet. The target signal and the output of the wavelet network is shown in Figure 4.7.*

Example 4.6 *The* $2-D$ *wavelet network trained for the approximation to the function given in Equation 4.21 contains* 5 *Mexican Hat wavelons. The obtained mean square error is* $MSE = 0.0955759$ *and the result of the approximation is shown in Figure 4.8.*

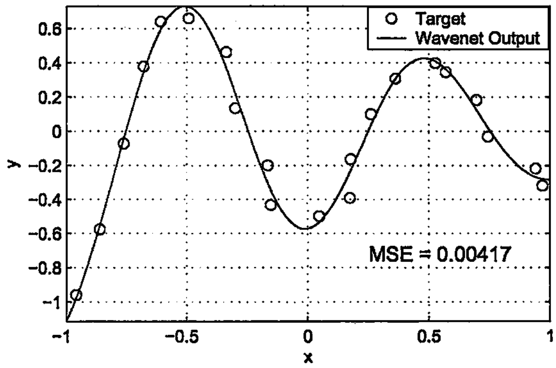

Figure 4.6: Result of approximation for Example 4.4 with Mexican Hat mother wavelet.

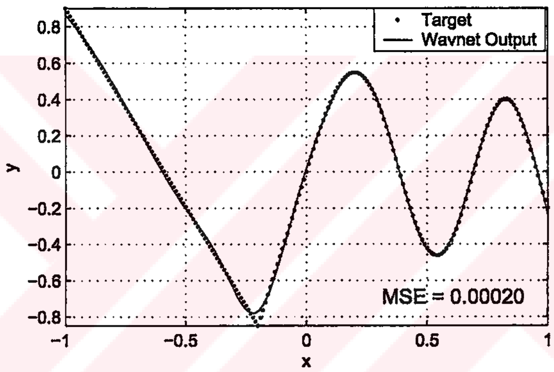

Figure 4.7: Result of approximation for Example 4.5 with Mexican Hat mother wavelet.

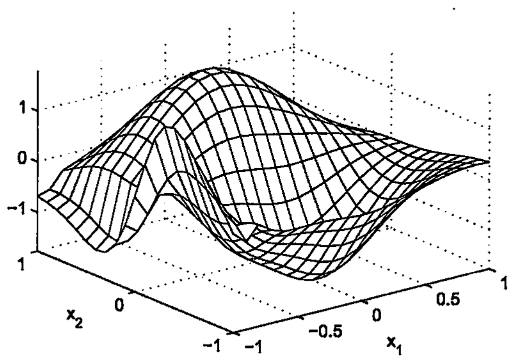

Figure 4.8: Result of approximation for Example 4.6 with Mexican Hat mother wavelet.

4.3.3 Dynamical System Modelling with Wavelet Network

The dynamical system modelling applications have only been introduced for the Mexican Hat mother wavelet because of the better approximation abilities. The Chua's circuit with periodic limit cycle and the spiral attractor have been chosen as the dynamical model examples. The dynamics of the Chua's circuit (Chua et al., 1999) is described by the following differential set of equations

$$\begin{aligned} \dot{x} &= \alpha\,(y - h\,(x))\,, \\ \dot{y} &= x - y + z, \\ \dot{z} &= -\beta\, y. \end{aligned} \tag{4.22}$$

where α and β are the parameters defined by the circuit components and the piecewise linear characteristic is as

$$h(x) = (m_1 - m_0)\,(|x+1| - |x-1|) \tag{4.23}$$

where $m_1 = -1/7, m_0 = -2/7$.

Period-1 Limit Cycle of Chua's Circuit

The time series of the period-1 limit cycle has been obtained by numerically integrating the system equation of the Chua's circuit with sampling period $\tau_s = 0.01 sec$ and by selecting the parameters $\alpha = 8$ and $\beta = 14.2857143$. The time-series has been embedded with embedding dimension $d_e = 3$ and embedding delay $T = \tau_s$. The wavelet network contains three $3 - dimensional$ wavelons. The output of the wavelet network in time-domain and the attractor embedded in the phase space are shown in Figure 4.9.

The observed limit-cycle is stable almost everywhere except on the set with zero measure $B = D - D_A$ where $D = \{x = [x_1, x_2, x_3] | -5 \leq x_i \leq 5 \quad i = 1, 2, 3\}$ and x_1, x_2, x_3 are the time-delay embedded coordinates, $D_A = \{x \in D_{in} | x_1 = x_2 = x_3\}$ and D_{in} represents the set inside the attractor. The basin of attraction of the wavelet network has been

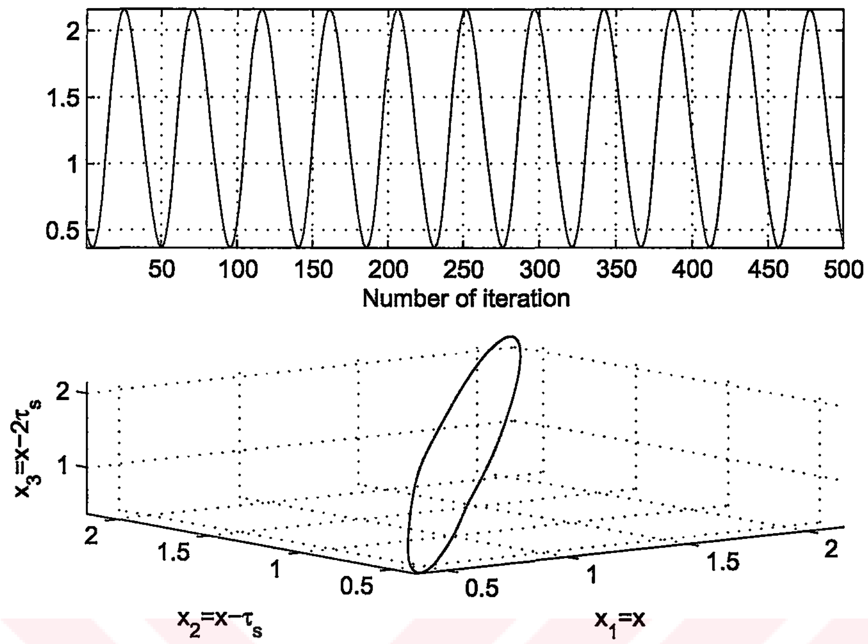

Figure 4.9: The output of the modelled dynamical system for spiral attractor of the Chua's circuit

investigated by comparing the Hausdorrf distances (Barnsley, 1993) of the attractors to the original attractor. An illustration of the basin of the attraction of the wavelet network is shown in Figure 4.10.

Spiral Attractor of Chua's Circuit

The time series of the spiral attractor of Chua's circuit has been obtained for $N = 1000$ samples for $\tau_s = 0.05sec$ and selecting the parameters $\alpha = 8.50000425$ and $\beta = 14.2857143$. The embedding dimension and the embedding delay have been chosen as $d_e = 3$ and $T = \tau_s$, respectively. The wavelet network contains 5 wavelons and the output of the wavelet network in time-domain and in phase space are shown in Figure 4.11.

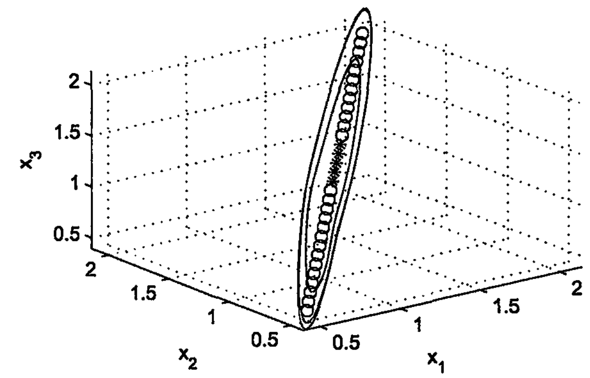

Figure 4.10: The basin of attraction of period-1 limit cycle of the Chua's circuit

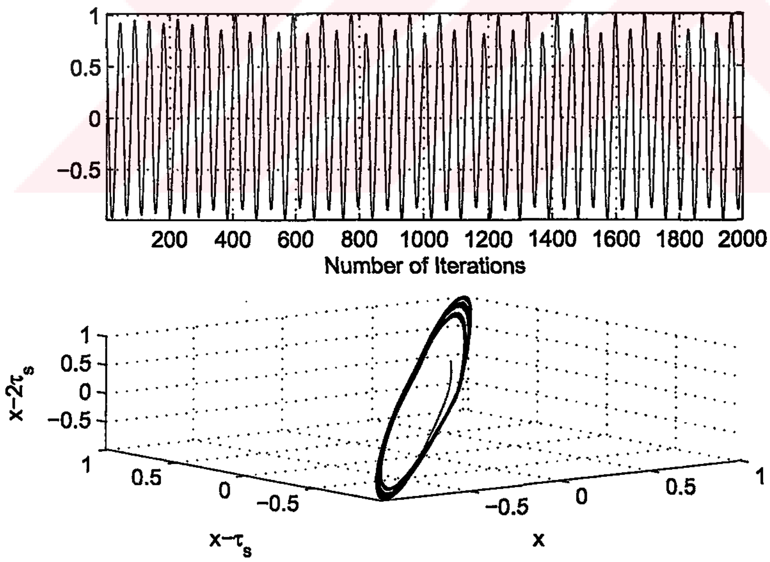

Figure 4.11: The output of the modelled dynamical system for spiral attractor of the Chua's circuit

CHAPTER FIVE
THE CIRCUIT SYNTHESIS

The static and dynamical wavelet networks successfully model the nonlinear systems. The circuit implementation of the wavelet network with sigmoidal mother wavelet (Özkurt, Savacı, & Gündüzalp, 2002a, 2002b, 2002c) and Mexican Hat mother wavelet (Özkurt et al., 2003a) for modelling static systems will be introduced in this chapter. Also, the circuit implementation of the wavelet network for modelling dynamical systems proposed in (Özkurt et al., 2003b) has been explained.

5.1 The Circuit Implementation of Sigmoidal Mother Wavelet

The sigmoidal mother wavelet function, which has been proposed in (Pati & Krishnaprasad, 1994), can be implemented as the sum of three translated hyperbolic tangent functions as

$$\Psi(x) = \tanh(x-2) - 2\tanh(x) + \tanh(x+2). \tag{5.1}$$

The hyperbolic tangent function can be implemented by a dual-transistor pair given in Figure 5.1. With the analysis of the differential transistor pair, the difference of the collector currents can be calculated as

$$i_1 - i_2 = I \tanh\left(\frac{V_1 - V_2}{2V_t}\right). \tag{5.2}$$

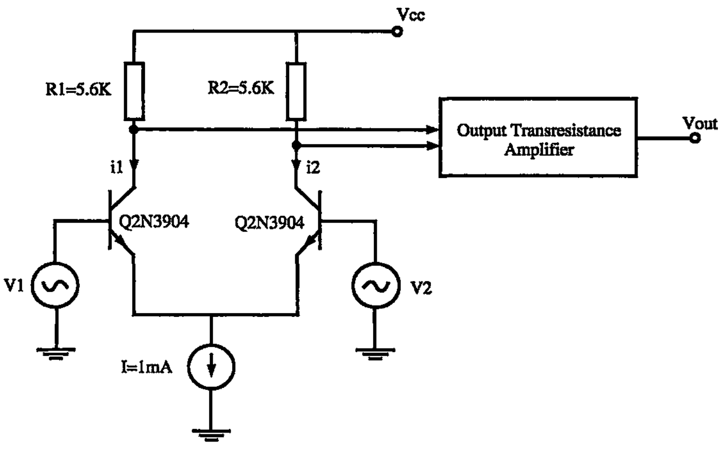

Figure 5.1: The circuit implementation of "tanh" function

By choosing the input $V_2 = 0$ and determining the difference, the output of tangent hyperbolic block (tanh) is determined as

$$V_{out} = A\,tanh(\frac{V_1}{2V_t}) \tag{5.3}$$

where A is the gain of the transresistance amplifier which converts input currents to the output voltage. The block diagram of the wavelet function is shown in Figure 5.2.

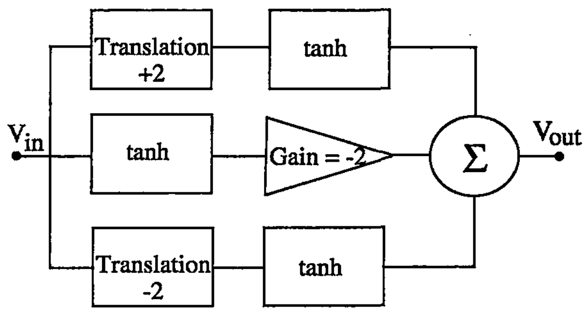

Figure 5.2: The block diagram of sigmoidal wavelet function

The output voltage of the wavelet block is

$$V_{out} = A_0\,\Psi(V_{in}(t)) \tag{5.4}$$

where A_0 is the overall voltage gain of the wavelet block. Simulation result of the wavelet circuit in Spice is shown in Figure 5.3.

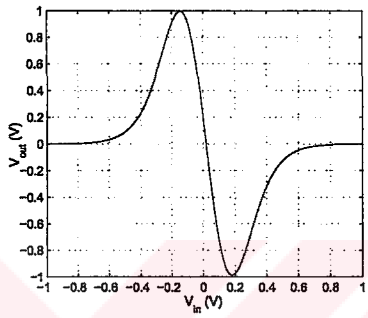

Figure 5.3: The input-output voltage pair of sigmoidal wavelet circuit

The circuit implementation of the tensor product wavelets defined in Equation 4.19 is obtained as the analog multiplication of the 1-dimensional wavelets. This operation has been implemented by the wavelet blocks and the analog multiplier macro-model AD633 of Analog Devices. The block diagram of one d-dimensional wavelon is shown in Figure 5.4.

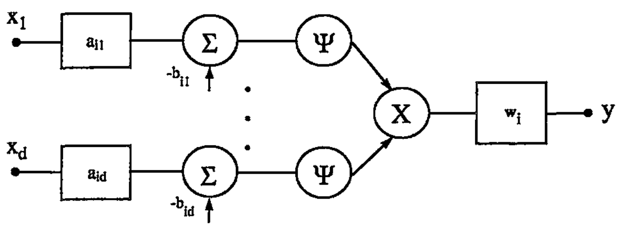

Figure 5.4: The block diagram of d-dimensional wavelon.

5.1.1 Applications

The circuits of the wavelet network modelling examples given in Section 4.3.1 have been implemented in Spice and the simulation results have been introduced below:

Example 5.1 *The wavelet network circuit of Example 4.1 has been simulated in Spice. The target function and the approximation result with sigmoidal mother wavelet are shown in Figure 5.5.*

Example 5.2 *The output of the approximation circuit of Example 4.2 and the target function are shown in Figure 5.6.*

Example 5.3 *The wavelet network circuit of Example 4.3 containing five* 2 – *dimensional wavelons have been simulated in Spice. The output of the wavelet network circuit has been shown in Figure 5.7.*

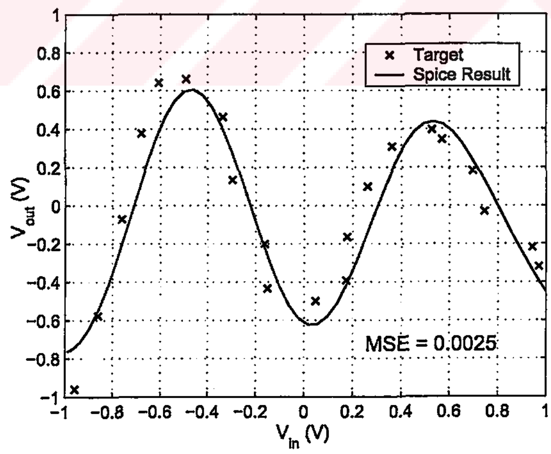

Figure 5.5: Result of approximation for Example 5.1 with sigmoidal wavelet network circuit.

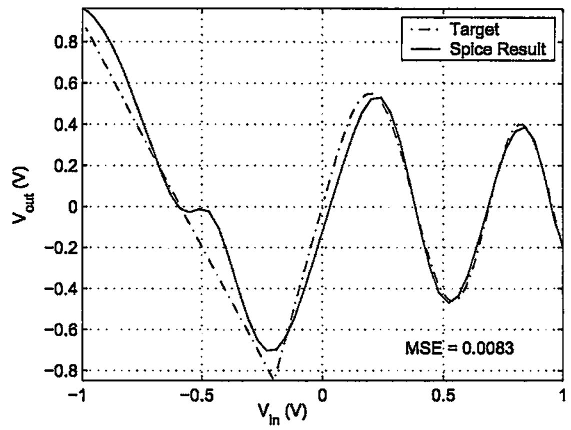

Figure 5.6: Result of approximation for Example 5.2 with sigmoidal wavelet network circuit.

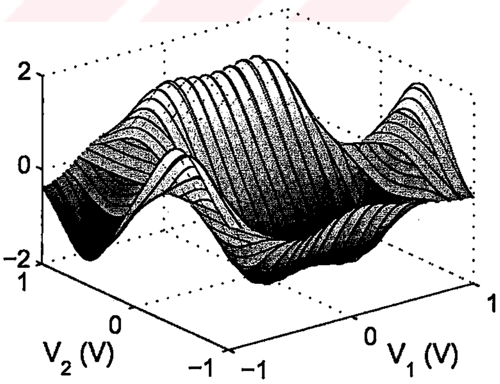

Figure 5.7: The result of approximation of 2-D function with sigmoidal wavelet network circuit.

5.2 The Circuit Implementation of Mexican Hat Mother Wavelet

The Mexican Hat mother wavelet is one of the commonly used real mother wavelet because of its good approximation ability. The mother wavelet defined as

$$\Psi(x) = (d - \|x\|^2)\, exp\,(-\frac{\|x\|^2}{2}) \quad \Psi(\cdot) : \mathbb{R}^d \to \mathbb{R}. \tag{5.5}$$

where $\|x\|^2 = x^T x$.

The block diagram of the $d-dimensional$ Mexican Hat mother wavelet circuit is shown in Figure 5.8. The adders and amplifiers have been implemented with operational amplifiers. The four channel four quadrant analog multiplier MLT04 of Analog Devices has been used for multiplication. The exponential function has been implemented with an antilog amplifier which is contained in the real time analog computational unit AD538 IC of Analog Devices. The antilog amplifier is shown in Figure 5.9.

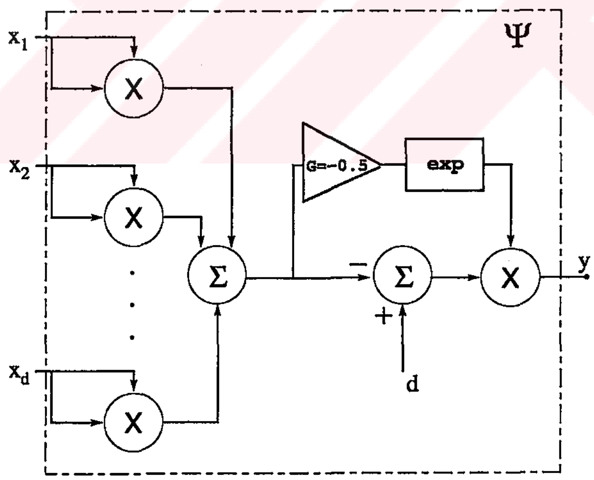

Figure 5.8: The block diagram of Mexican hat mother wavelet circuit

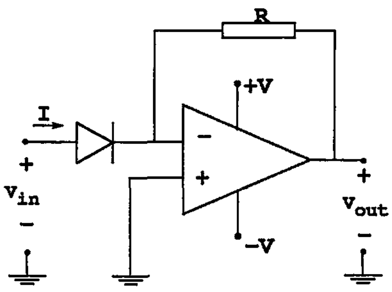

Figure 5.9: The antilog amplifier

Assuming that the current of the diode connected to the input of the operational amplifier is

$$I = I_s \, exp \, (\frac{V_{in}}{V_t}) \tag{5.6}$$

where I_s, V_{in}, V_t are reverse saturation current, the input voltage and threshold voltage respectively where $V_t = \frac{kT}{q}$ where k is the Boltzman constant, T is temperature and q is the electron charge. The output voltage is obtained as

$$V_{out} = -R \, I_s \, exp \, (\frac{V_{in}}{V_t}). \tag{5.7}$$

The measured input-output voltage pair of the Mexican Hat mother wavelet circuit is shown in Figure 5.10.

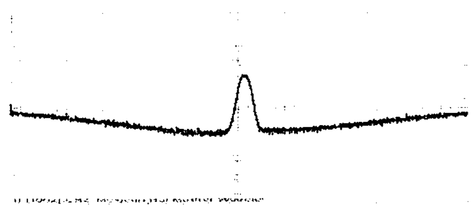

Figure 5.10: The Mexican hat mother wavelet

5.2.1 Applications

The circuit implementations of the sample wavelet networks with Mexican Hat mother wavelet have been introduced in this section.

Example 5.4 *The wavelet network circuit of Example 4.4 including* 3 *wavelons have been implemented in Spice. The target function and the simulation results have been shown in Figure 5.11.*

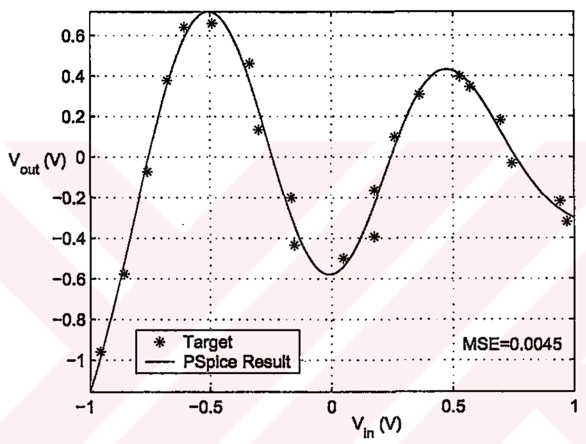

Figure 5.11: Result of approximation for Example 5.4 with Mexican Hat wavelet network circuit.

Example 5.5 *The wavelet network approximation circuit of Example 4.5 has been simulated in Spice. The target function and the simulation results have been shown in Figure 5.12.*

Example 5.6 *The circuit of* $2 - D$ *wavelet network with Mexican Hat trained for the approximation to the function given in Equation 4.21 has been simulated in Spice. The simulation result is shown in Figure 5.13.*

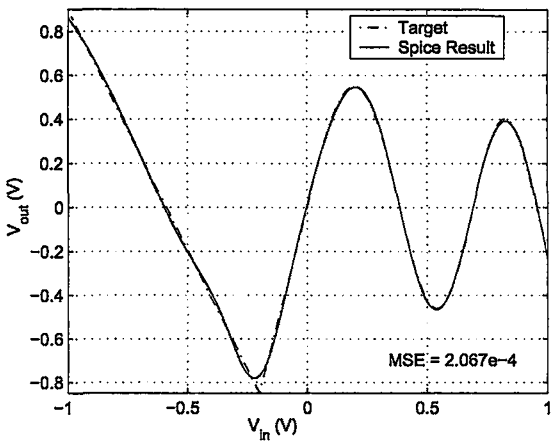

Figure 5.12: Result of approximation for Example 5.5 with Mexican Hat wavelet network circuit.

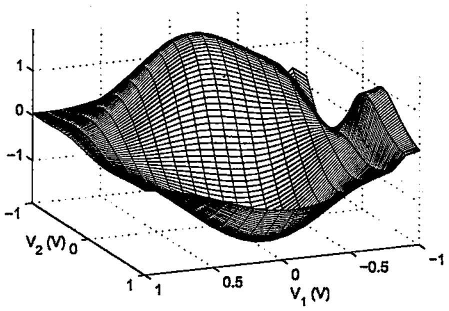

Figure 5.13: The result of approximation for Example 5.6 with Mexican Hat wavelet network circuit.

5.3 The Circuit Implementation of Dynamical Wavelet Network

The wavelet network can be used for modelling the nonlinear dynamical systems as explained in the Chapter IV. The circuit of the dynamical wavelet network shown in Figure 4.2 has been implemented using the static wavelet network with Mexican hat mother wavelet as the main block (Özkurt et al., 2003a) and also using the delay blocks which have been realized by voltage controlled switches and capacitors as shown in Figure 5.14-a (Özkurt et al., 2003b)

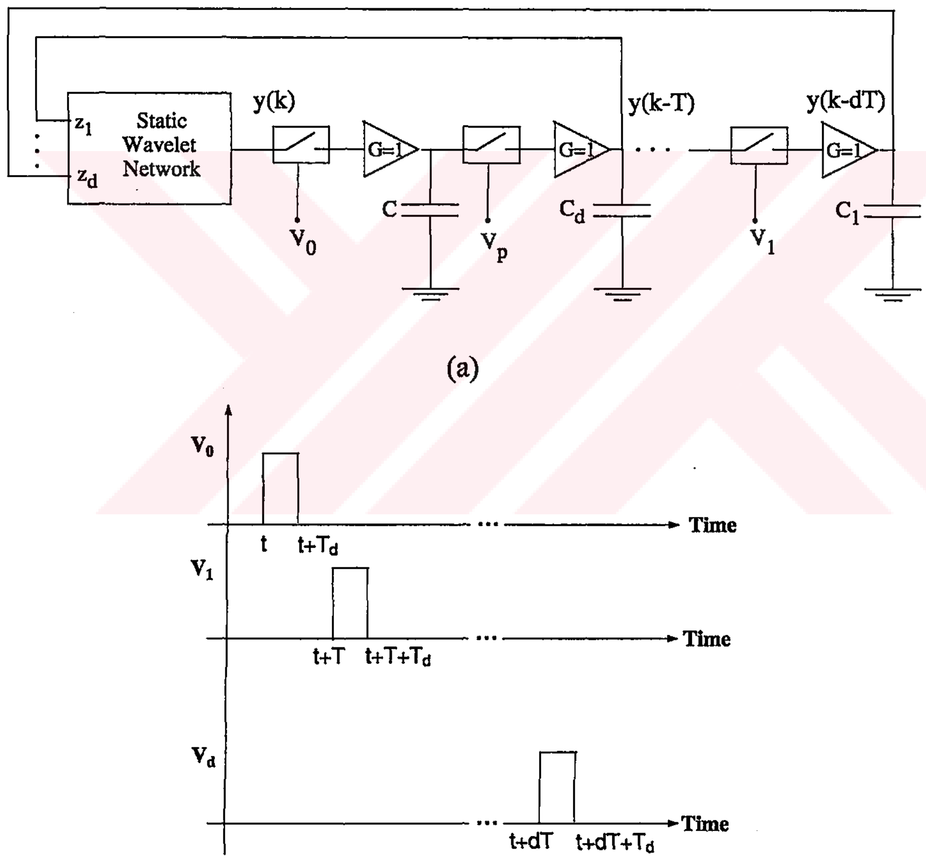

(a)

(b)

Figure 5.14: (a) Dynamical wavelet network circuit and (b) triggering pulses for voltage controlled switches.

The capacitors are used as the memory elements which store the delayed versions of the output of the wavelet network. The voltage controlled switches are controlled by the external pulse generators which are triggered sequentially as shown in Figure 5.14-b where the duration of the pulses satisfies $T_d < T$. The inputs of static wavelet network consist of the voltages on the capacitors.

5.3.1 Period-1 Limit Cycle of Chua's Circuit

The wavelet network trained for the Period-1 Limit Cycle of Chua's circuit has been implemented in Spice by using the structure given in Figure 5.14. The output of the circuit is shown in Figure 5.15. The circuit also have the same basin of attraction with the wavelet network simulated in MATLAB.

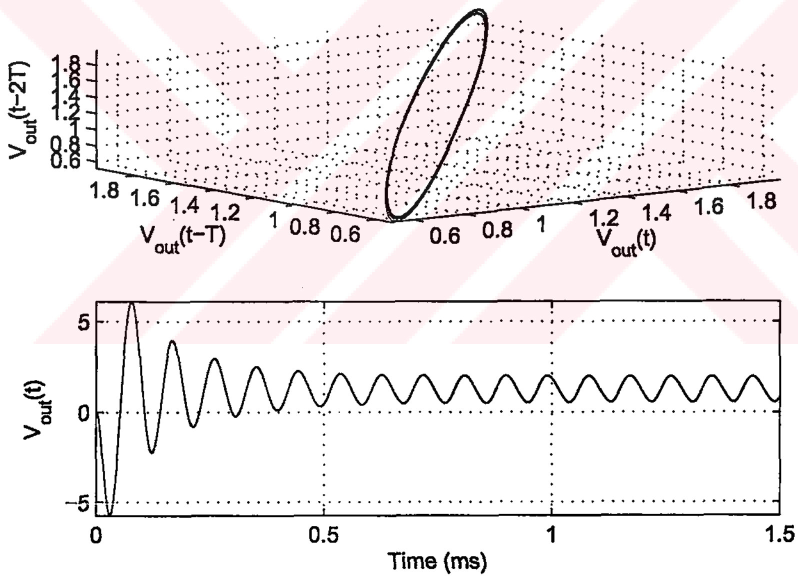

Figure 5.15: The output of dynamical wavelet network circuit for Period-1 limit cycle.

5.3.2 Spiral Attractor of Chua's Circuit

The dynamic wavelet network has been trained for spiral attractor of the Chua's circuit in Chapter IV. The circuit simulation of the wavelet network has been implemented and the result of simulation has been given in Figure 5.16.

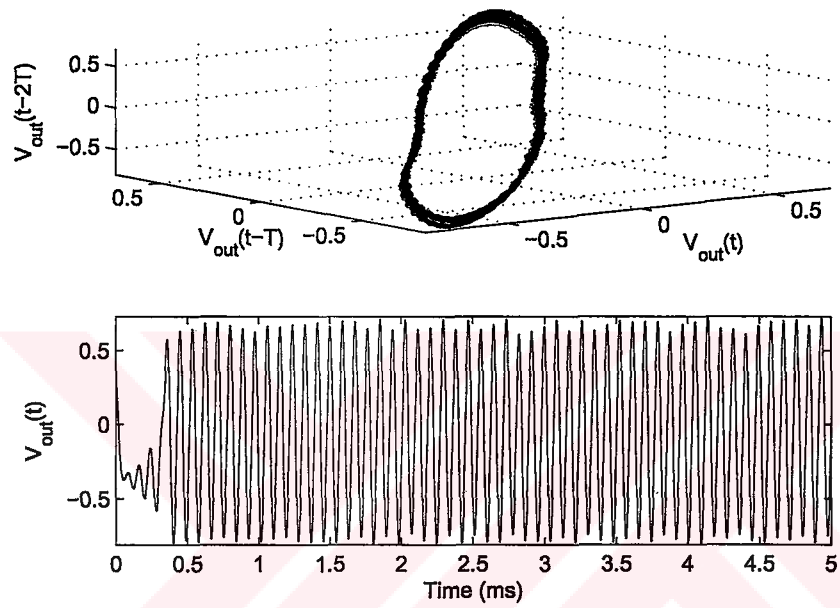

Figure 5.16: The output of dynamical wavelet network circuit for spiral attractor

CHAPTER SIX

ACCURACY OF THE SYNTHESIS

In the proposed system the circuit has been designed according to the specifications of the output signal given in the time-frequency domain. When the design process has been completed, the output of the system must be tested to determine whether the output signal satisfies the given conditions. Therefore, the wavelet ridges of the obtained signal should be determined. As it was explained in Chapter 3, there are several ridge determination algorithms. The methods proposed in (Carmona & Hwang, 1997) for noisy monocomponent signals and in (Carmona et al., 1999) for noisy multicomponent signals are successful in determination of the actual ridges. The proposed method based on the singular value decomposition (SVD) of the scalogram matrix (Özkurt & Savacı, 2003c, 2003b) is computationally more faster than both methods. The proposed algorithm is different than the ones given in (Carmona et al., 1995; Pilgram & Schappacher, 1998) which apply SVD directly to the data matrix, but it is similar to the algorithms which apply the SVD method to the wavelet transform coefficient matrix (Venkatachalam & Aravena, 1999; Casey, 1998). In (Venkatachalam & Aravena, 1999), the first left singular vector called as pseudo-power signature is used in the classification of the seismic signals. The left and right singular vectors are used to characterize the speech signals in (Casey, 1998). In the following section the SVD-based method has been introduced.

6.1 SVD Based Ridge Determination

Before introducing the new method related definitions will be given in the sequel:

Definition 6.1 *A singular value decomposition of* $A \in \mathbb{R}^{m \times n}$ *is any factorization of the form:*

$$\mathbf{A} \triangleq \mathbf{U\Sigma V^T} \tag{6.1}$$

where $U \in \mathbb{R}^{m \times m}$ *and* $V \in \mathbb{R}^{n \times n}$ *are orthogonal matrices and* $\Sigma \in \mathbb{R}^{m \times n}$ *is a diagonal matrix of singular values with components* $\sigma_{i,j} = 0$ *if* $i \neq j$ *and* $\sigma_{i,i} > 0$ $(\sigma_i \triangleq \sigma_{i,i})$*. Furthermore, there exist non-unique orthogonal matrices U and V such that* $\sigma_1 \geq \sigma_2 \geq \ldots \geq \sigma_K > \sigma_{K+1} = \ldots = \sigma_{min(m,n)} = 0$ *where* $rank(A) = K$*. The columns of the matrices U and V are called the left and right singular vectors, respectively (Golub & Loan, 1996)*

There is a relationship between the singular values of a matrix and the total energy which can be stated with the following lemma.

Lemma 6.1 *The Frobenius norm of an* $M \times N$ *matrix A of rank K*

$$E_A = \|A\|_F^2 = \sum_{i=1}^{M}\sum_{j=1}^{N}|a_{ij}|^2 = \sum_{k=1}^{K}\sigma_k^2 \tag{6.2}$$

where σ_k *are the singular values of A (de Moor, 1988; Golub & Loan, 1996).*

When the SVD of the scalogram matrix has been calculated, the energy of the signal in wavelet domain is related with the magnitudes of the singular values. Since the singular values are in decreasing order, the most of the energy is contained in the components associated with the greater singular values.

According to Equation 6.1, the scalogram matrix with rank K can be decomposed into its singular values as

$$P = U\,\Sigma\,V^T. \tag{6.3}$$

The singular value matrix Σ and the orthogonal matrices U and V can be decomposed into two parts

$$\Sigma = \begin{bmatrix} \Sigma_s & \theta \\ \theta & \Sigma_n \end{bmatrix} \quad U = [U_s\,U_n], \quad V = [V_s\,V_n] \tag{6.4}$$

where the $\mathbf{U_s} \in \mathbb{R}^{M\times S}$, $\mathbf{\Sigma_s} \in \mathbb{R}^{S\times S}$ and $\mathbf{V_s} \in \mathbb{R}^{N\times S}$ where $S \leq K$ representing the dominant components associated with the original signal, and the less significant components and the noise are included in $\mathbf{\Sigma_n} \in \mathbb{R}^{M-S\times N-S}$, $\mathbf{U_n} \in \mathbb{R}^{M\times M-S}$ and $\mathbf{V_n} \in \mathbb{R}^{N\times N-S}$.

The effects of the Additive White Gaussian Noise (AWGN) is higher on the smaller singular values which correspond to the components of the signal with lower energy levels. Therefore, the effect of the noise is reduced by truncating the lower singular values.

The approximated scalogram matrix $\tilde{P}$ with rank S is obtained as

$$\tilde{P} = U_s\,\Sigma_s\,V_s^T \tag{6.5}$$

by using only the signal components where $U_s \in \mathbb{R}^{M\times S}$, $\Sigma_s \in \mathbb{R}^{S\times S}$ and $V_s \in \mathbb{R}^{S\times N}$ where $S \leq K$.

The number of the singular values included in the approximation Σ_s has been defined by considering the ratio of the energy associated with the singular values to the total energy

$$r_k \triangleq \frac{\sigma_k^2}{E_T} \tag{6.6}$$

where E_T is the total energy of the scalogram matrix. For the given noise threshold ε $(0 < \varepsilon \leq 1)$, the singular values with $r_1 \geq r_2 \geq \ldots \geq r_S \geq \varepsilon$ have been included in Σ_s and the remaining $K - S$ singular values have been considered as the noise or the minor energy components. In the wavelet domain at the fixed time instant b_j the maximum energy occurs at the scale a_j^{main}, i.e.,

$$\tilde{p}_{a_j^{main},j} \triangleq \|\tilde{p}_j\|_\infty \tag{6.7}$$

where $\tilde{p}_j \in \mathbb{R}^M$ denotes the j^{th} column of the approximated scalogram matrix $\tilde{P}$ and

$$a_j^{main} \triangleq a^{main}(b_j) \qquad j = 1, \ldots, N \tag{6.8}$$

and $a^{main}(b)$ is the main ridge of the approximated scalogram. Therefore, the main ridge can be calculated by determining the global maximum (assuming it exists for most of the practical signals) of the approximated scalogram for each time instant $t = b_j$.

The ridges of the multi-component signal with sufficiently large amount of energy are also taken into account because the energy contribution of these components can not be neglected. The ridges are defined as

$$\begin{aligned} & a_j^l = a^l(b_j) \qquad j = 1, \ldots, N, \quad l = 1, \ldots, L \\ & \qquad \tilde{p}_{a_j^l,j} \geq \mu \, \tilde{p}_{a_j^{main},j} \qquad 0 < \mu < 1 \end{aligned} \tag{6.9}$$

where μ is the energy threshold and then the ridges are determined by finding the local maxima of the approximated scalogram for each time instant.

In the case of mono-component signal, since the signal has single instantaneous frequency at a given time instant, the main ridge will be sufficient to locate the energy concentrations.

6.2 Applications

The proposed method has been tested by applying to a chirp signal and a signal of the double-scroll attractor from Chua's circuit (Chua et al., 1999). The performance under Additive White Gaussian noise (AWGN) has been introduced by determining the ridges of a chirp signal composed of two hyperbolic chirps. Finally, the ridges of the periodic, quasiperiodic and chaotic attractors of Chua's circuit have been obtained and the degrees of chaoticity have been determined.

The center angular frequency of the mother wavelet has been chosen as $\omega_0 = 2\pi$ for the examples given below. Thus, the instantaneous angular frequency in Equation 3.23 for Morlet wavelet becomes

$$\omega_{inst}(t)|_{t=t_0} = \frac{\omega_0}{a(b)} = \frac{2\pi}{a(b)} \tag{6.10}$$

and the instantaneous frequency can be represented as

$$f_{inst}(t)|_{t=t_0} = \frac{1}{a(b)}. \tag{6.11}$$

Example 6.1 *The monocomponent chirp signal with compact support is given as follows*

$$x(t) = \begin{cases} w(t)\ \cos(2\pi f_0 t) & t \in [0,2] \cup (4,6] \\ w(t)\ \cos(2\pi 2 f_0 t) & t \in (2,4] \\ 0 & elsewhere \end{cases} \tag{6.12}$$

where $f_0 = 1Hz$ and $w(t)$ is the Hanning window which is defined as

$$w(t) = 0.5\left(1 - \cos\left(\frac{2\pi t}{N\Delta t}\right)\right) \tag{6.13}$$

where N is the number of samples and Δt is the sampling time which are chosen as 600 *and* 0.01, *respectively.*

For comparison of the methods, the chirp signal is embedded in AWGN with signal to noise ratio $SNR = -3dB$ *and the scalogram matrix has been calculated for* $M = 40$ *dilations which include the frequency range in which the energy of the signal is localized. The noise threshold coefficient has been chosen as* $\varepsilon = 0.15$*. Therefore, the approximate scalogram has been constructed by the first three singular values. Then, the ridge has been determined by finding the maxima of the approximated scalogram. The time-waveform of the noisy chirp signal is shown in Figure 6.1-a and its scalogram is illustrated in Figure 6.1-b. The actual ridge and the ridges calculated by Stationary Phase method are shown in Figure 6.1-c, while ridges calculated by Simple method and Carmona method are shown in Figure 6.1-d. The proposed method has been illustrated in both Figure 6.1-c and Figure 6.1-d for comparison purposes. Because of the noise, the actual ridge could not be found accurately with the stationary phase method. The simple method, Carmona method and SVD-based method produce acceptable results.*

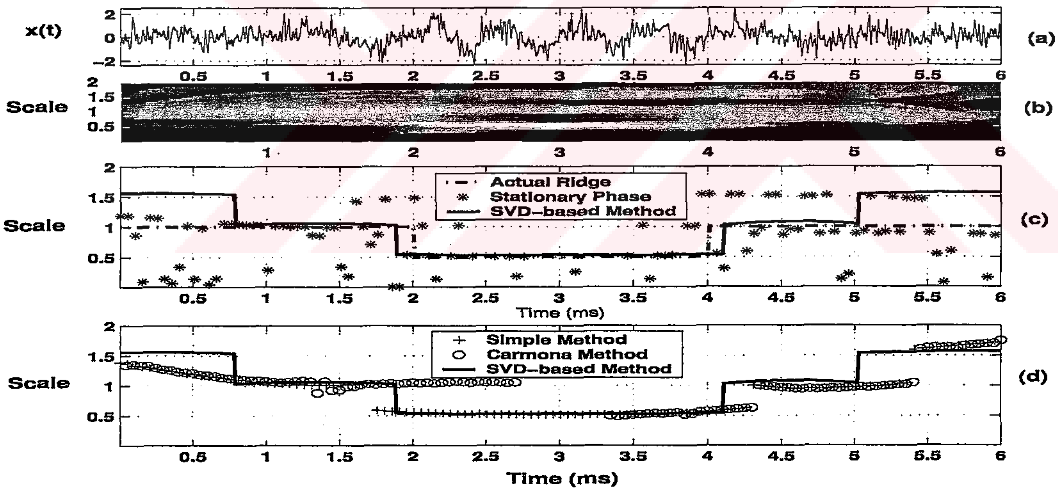

Figure 6.1: (a) Time-waveform, (b) scalogram, (c) actual ridge, ridges calculated by stationary phase and SVD-based method, (d)ridges calculated by Simple method, Carmona method and SVD-based method for Chirp Signal with Additive White Gaussian Noise

The ridge finding algorithms using the simple method, stationary phase method, Carmona method and SVD-based method have been implemented using MATLAB in a PC with 1.4*GHz CPU. The computation times of the algorithms are shown in Table 6.1.*

Table 6.1 The computation times of the ridge calculation algorithms for mono-component chirp signal

Method	Computation Time in Seconds
Stationary Phase Method	134.613
Simple Method	0.030
Multiridge Carmona Method	50.082
SVD-Based Method	3.715

Example 6.2 *The dynamics of the Chua's circuit (Chua et al., 1999) is described by the set of differential equations given in Equation 4.22. Using the measurements given in (Aguirre, Rodrigues, & Mendes, 1997), the scalogram matrix associated with the single state variable $x(t)$ has been obtained for $N = 2000$ samples and $M = 300$ dilations. Four singular values of which energy contribution is greater than $\%\ 10$ of the total energy have been included in the approximated scalogram $\tilde{P}$. Then, the local maxima of the approximate scalogram $\tilde{P}$ has been obtained and thresholded with $\mu = 0.1$. The ridges calculated by multi-ridge Carmona method and SVD-based method are shown in Figure 6.2. Both methods produce acceptable results showing the energy concentrations of the double-scroll attractor. Both algorithms have been implemented using MATLAB and the computation times are shown in Table 6.2. The computational cost of the Carmona method grows drastically when the size of the scalogram matrix becomes large, however the computations are faster when the ridges are calculated by SVD-based method.*

Table 6.2 The computation times of the ridge calculation algorithms for double-scroll attractor

Method	Computation Time in Sec
Carmona Method	1452.3
SVD-Based Method	22.12

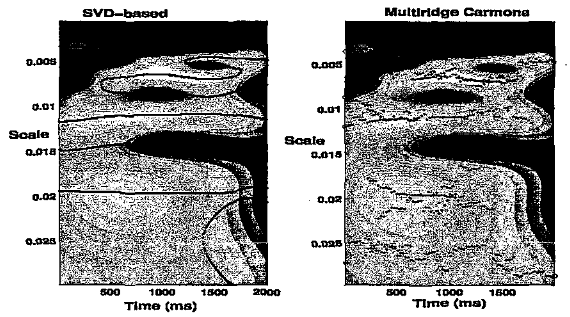

(a) (b)

Figure 6.2: The ridges found by (a) SVD-based method and (b) Multiridge Carmona method on the scalogram of double-scroll attractor

Example 6.3 *The signal containing two hyperbolic chirps is defined as*

$$s(t) = \begin{cases} sin(2\pi\frac{\alpha_1}{\beta-t}) + sin(2\pi\frac{\alpha_2}{\beta-t}) & 1 \leq t \leq 3 \\ 0 & elsewhere \end{cases} \tag{6.14}$$

where $\alpha_1 = 100, \alpha_2 = 25$ *and* $\beta = 7$. *The ridges of the given signal have been determined by using the SVD-based method for noise-free case and for two different signal to noise ratios. The scalogram of the noise-free signal and the computed ridges for three cases are shown in Figure 6.3.*

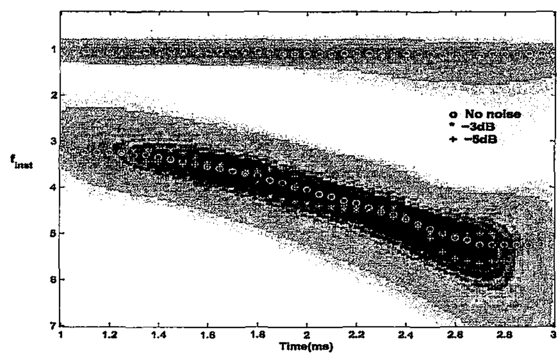

Figure 6.3: The scalogram and the ridges of the signal with two hyperbolic chirps

Example 6.4 *The wavelet ridges of the signals measured from the dynamical systems give information about the phase space structures of the system such as periodicity, quasiperiodicity, chaoticity. Also, the strength of chaos (i.e. the stronger chaos, the faster the divergence of the initially nearby trajectories and the larger the Lyapunov characteristic exponents (Kantz & Schreiber, 1999)) can be characterized by the geometry and number of the ridges: weak chaos is characterized by one main connected ridge whereas strong chaos is characterized by multiple short ridges distributed over the time-frequency plane without any order (Chandre et al., 2003). The trajectories and the instantaneous frequencies of the signals obtained from Chua's circuit are shown in Figure 6.4 and 6.5, respectively.*

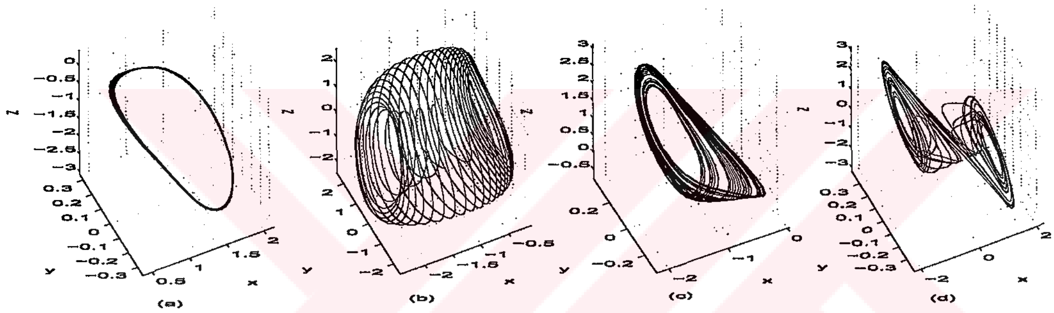

Figure 6.4: The trajectories of (a) period-1 limit cycle, (b) quasiperiodic attractor, (c) spiral attractor and (d) double scroll attractor.

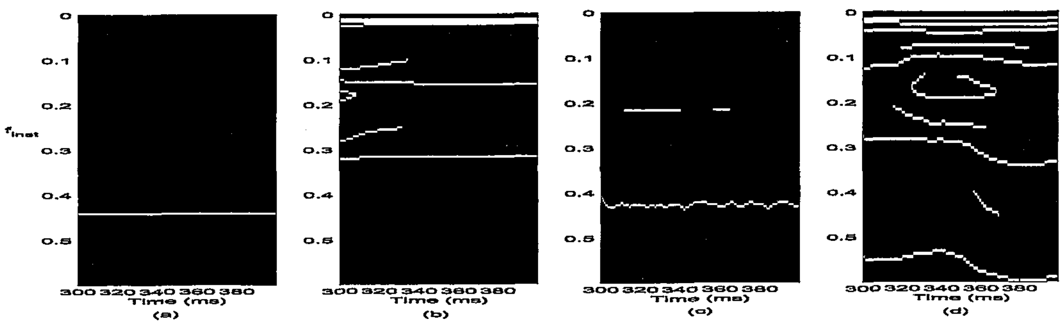

Figure 6.5: The instantaneous frequencies of (a) period-1 limit cycle, (b) quasiperiodic attractor, (c) spiral attractor and (d) double scroll attractor.

6.3 Reconstruction of Chaotic Attractors

The SVD-based ridge determination algorithm can also be used for the reconstruction of the nonstationary signals from the noisy measurements. The technique has been used for the reconstruction of the chaotic attractors of the Chua's circuit from the noisy measurements (Özkurt & Savacı, 2003d). For the reconstruction of the chaotic attractors, the wavelet ridges of the computed signal have been obtained. Then the approximated signal has been calculated by Equation 3.31 using the skeleton of the wavelet transform. Finally, the phase space has been reconstructed by time-delay embedding from the approximate discrete signal according to the Taken's Embedding theorem (Abarbanel, 1996).

The approximation can be accepted as accurate if the distance between the attractors of the original signal and the reconstructed signal is less than the distance between the attractors of the original signal and the noisy signal as

$$h(\mathcal{A}_O, \mathcal{A}_R) < h(\mathcal{A}_O, \mathcal{A}_N) \tag{6.15}$$

where $\mathcal{A}_O, \mathcal{A}_R$ and $\mathcal{A}_N$ are the attractors of the original, reconstructed and noisy signals, respectively, and $h(\mathbf{A}, \mathbf{B})$ is the Hausdorff distance which can be classified as the similarity measures (Veltkamp, 2001). The Hausdorff distance has been defined below.

Definition 6.2 *Let (X, d) is a complete metric space, and $\mathcal{H}(\mathbf{X})$ denotes the space whose points are the compact subsets of **X**, other than the empty set. Let $\mathbf{A}, \mathbf{B} \in \mathcal{H}(\mathbf{X})$, then the Hausdorff distance between two points $\mathbf{A}$ and $\mathbf{B}$ is defined by*

$$h(\mathbf{A}, \mathbf{B}) \triangleq max(d(\mathbf{A}, \mathbf{B}), d(\mathbf{B}, \mathbf{A})) \tag{6.16}$$

where $d(\mathbf{A}, \mathbf{B}) \triangleq \max_{a \in A}(\min_{b \in B}(d(a, b)))$ and $d(a, b)$ is the usual Euclidian distance between points $a \in \mathbf{A}$ and $b \in \mathbf{B}$ (Barnsley, 1993).

The approximation may be considered as successful if the original and reconstructed attractors are similar in the phase space, although the signals in the time-domain are quite different due to a shift in time and/or mean value, and/or a change in frequency. While the shift in time or a change in frequency cannot be observed in the phase space, the shift in the mean value has been seen as the translation of the attractor in the phase space. Therefore, instead of the usual Hausdorff distance, the Hausdorff distance under translations of the objects, $M_T(\cdot,\cdot)$ which is defined below, has been selected as the comparison measure.

Definition 6.3 *The minimum Hausdorff distance between all possible relative positions of the two sets is defined as*

$$M_T(\mathbf{A},\mathbf{B}) \triangleq \min_{t\in T} h(\mathbf{A}, t\mathbf{B}) \tag{6.17}$$

where T is the group of translations (Huttenlocher, Klanderman, & Rucklidge, 1993).

The Hausdorff distance is sensitive to the outlier points which can be caused by the noise and this can be the source of erroneous comparison results. In order to solve this problem the quantile-rank Hausdorff distance has been proposed in (Chmielewski, Gut, Kukolowicz, & Dabrowski, 1993) as follows

Definition 6.4 *The quantile rank Hausdorrf distance between the sets* $\mathbf{A}$, B *is defined as*

$$h^r(A,B) = Q^r_{a\in A} \min_{b\in B} d(a,b) \tag{6.18}$$

where $Q^r_{a\in A}$ is the quantile rank, i.e. the $h^r(A,B)$ is the set of the calculated distances ordered from maximum to the minimum.

Example 6.5 *The wavelet transform of the state variable $x(t)$ with additional Gaussian white noise of variance $\sigma^2 = 0.2$ is numerically computed for the spiral attractor which is* *observed for* $\alpha = 8.50000425$ *and* $\beta = 14.28$ *in Chua's circuit. The number of frequency bins is* $M = 120$ *and the time instants* $N = 500$. *The scalogram of the noisy state variable* $x(t)$ *of the spiral attractor is shown in Figure 6.6.*

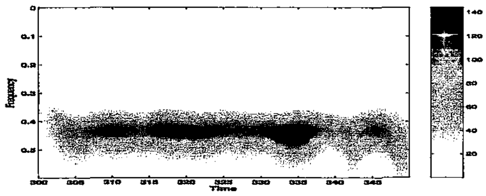

Figure 6.6: Normalized Scalogram of Spiral Attractor

The approximate scalogram $\tilde{P}$ *has been obtained for* $\varepsilon = 0.1$ *by removing the noise component. Then the wavelet ridges of the spiral attractor has been calculated by SVD-based method selecting energy threshold* $\mu = 0.2$.

The state variable $x(t)$ *has been reconstructed by using Equation 3.31 from the determined ridges and the phase space has been reconstructed using Taken's embedding theorem (Takens, 1985). The 2D projection of noisy attractor and the reconstructed attractor to the* $x - y$ *plane has been illustrated in Figure 6.7.*

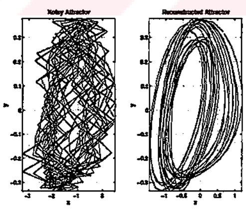

Figure 6.7: The Noisy and Reconstructed Attractors

The Hausdorff distance between the set of the points in the numerically computed noise-free and reconstructed spiral attractors has been calculated for scanning the phase space for all possible translations of the reconstructed attractor. The minimum distance in Equation 6.17 has been obtained as $M_T(\mathcal{A}_O, \mathcal{A}_R) = 0.2265$ *where* $\mathcal{A}_R$ *is the reconstructed and* $\mathcal{A}_O$ *is the original attractor. The Hausdorff distance between the original attractor and the noisy attractor* $\mathcal{A}_N$ *has been calculated as* $M_T(\mathcal{A}_O, \mathcal{A}_N) = 1.0364$.

Example 6.6 *The double-scroll attractor is observed for* $\alpha = 9$ *and* $\beta = 14.28$ *in Chua's circuit. The normalized scalogram has been obtained for the state variable* $x(t)$ *with additional Gaussian white noise with variance* $\sigma^2 = 0.2$*. The normalized scalogram matrix has been calculated for* $M = 120$ *scales and* $N = 1000$ *time instants. The scalogram matrix is shown in Figure 6.8.*

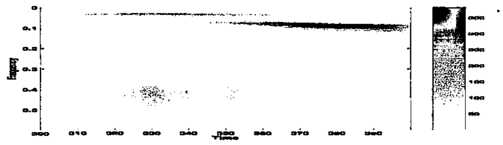

Figure 6.8: Normalized Scalogram of Double-Scroll Attractor

The approximate scalogram $\tilde{P}$ *has been obtained by choosing the noise threshold* $\varepsilon = 0.1$*. Then the wavelet ridges of the noisy double-scroll attractor has been calculated with energy threshold* $\mu = 0.2$*. The phase space has been reconstructed using Taken's embedding theorem (Takens, 1985). The embedding dimension* $d = 3$ *and the time delay* $\tau = 7T_s$*, where* T_s *is the sampling period, have been selected by Nonlinear Dynamics Toolbox (Reiss, 1996). The projection of the attractors to* $x - y$ *plane is shown in Figure 6.9. The minimum Hausdorf distance between the numerically computed noise-free attractor and the reconstructed attractor, and the distance between the noise-free and noisy attractor has been calculated as*

$$M_T(\mathcal{A}_O, \mathcal{A}_R) = 0.3862 < M_T(\mathcal{A}_O, \mathcal{A}_N) = 0.8366. \tag{6.19}$$

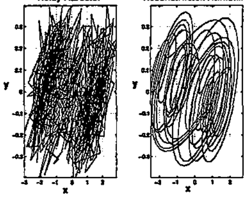

Figure 6.9: The Noisy and Reconstructed Attractors

CHAPTER SEVEN
APPLICATIONS

The proposed system contains four main blocks: The first block synthesizes the signal according to the given time-frequency domain specifications. The "System Modelling" block determines the parameters of the dynamical wavelet network which will produce the desired signal as the output. Finally, the wavelet network circuit is designed and simulated in Spice. In order to compare the obtained signal with the desired signal, the wavelet ridges of the wavelet network output is determined by the SVD-based ridge determination method. In the previous chapters, the theoretical foundations and applications of the blocks have been introduced in detail. The complete examples of the proposed system will be given in the following sections. The design of the circuit with monocomponent periodic output signal has been introduced in Example 1. The second example includes the synthesis of the circuit with multicomponent aperiodic output signal.

7.1 Example 1: Monocomponent Signal

The synthesis of the monocomponent signal with wavelet ridges method has been given in Example 3.4. The time series obtained from the "Signal Synthesis" block is then transferred to the second block in order to determine the wavelet network parameters. The time series has been embedded by time-delay embedding by choosing the embedding dimension as $d_e = 3$ and the embedding delay as $T = \tau_s$ where τ_s is the sampling period and chosen as $\tau_s = 0.001$ in the signal synthesis process. The suitable wavelons have been selected by the stepwise selection by orthogonalization algorithm. The number of wavelons has been selected as 3 and the algorithm has been implemented until the wavelet level 3. Then, the wavelet network has been trained by back-propagation training algorithm for 50 epochs. The time-delay embedded phase space and the output of the trained wavelet network are shown in Figure 7.1.

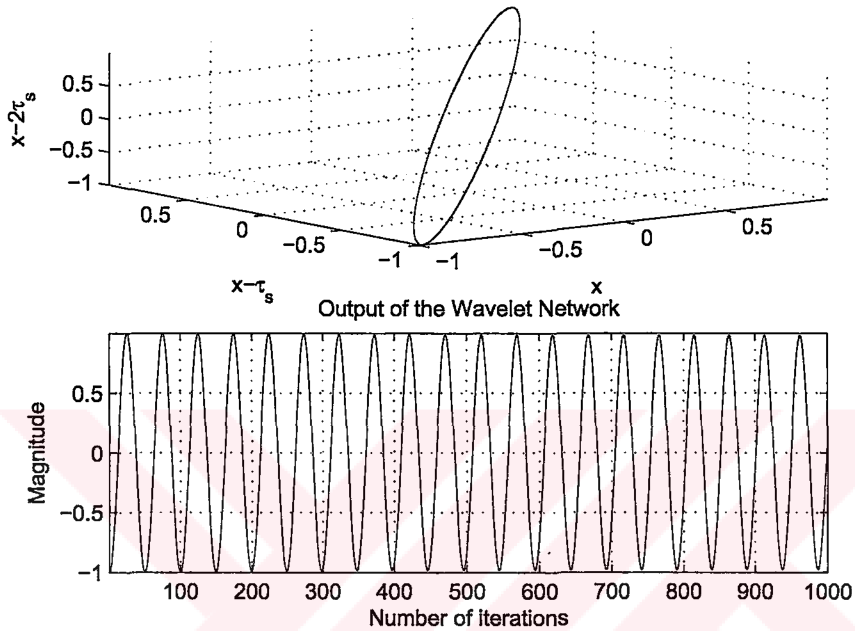

Figure 7.1: The embedded monocomponent signal in phase space and the output of the wavelet network.

After the determination of the wavelet network parameters, the wavelet network circuit has been designed by selecting the suitable wavelons and the adjusting the parameters of the wavelons and the amplifiers. The dynamical circuit structure has been given in Figure 5.14. The output of the circuit in time-domain and embedded phase space are shown in Figure 7.2. The circuit is not sensitive to the initial conditions, i.e. the sinusoidal output signal has been reached at the steady state after short transients.

The wavelet ridges of the output of the wavelet network has been determined by SVD-based method proposed in Chapter 6. The output of the wavelet network, the modulus and the phase of the wavelet transform and the instantaneous frequency of the signal are shown in Figure 7.3.

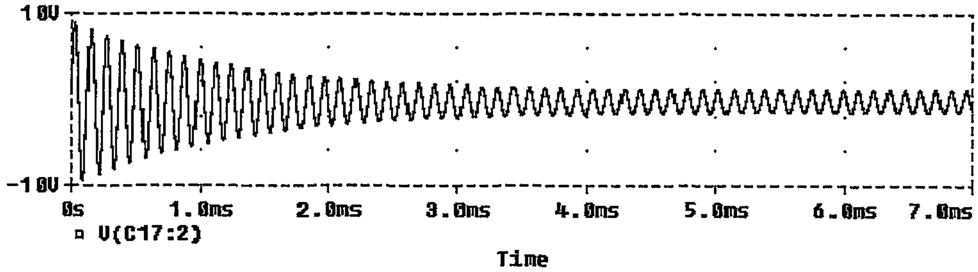

Figure 7.2: The output of the circuit for monocomponent signal.

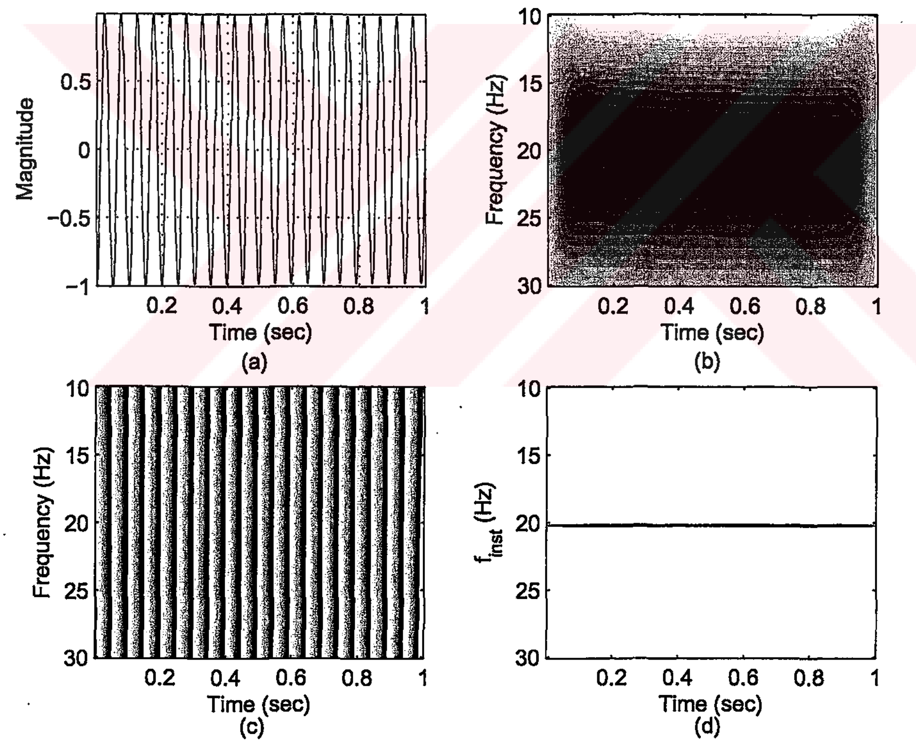

Figure 7.3: (a) The time waveform, (b) the modulus and (c) the phase of the wavelet transform and (d) the instantaneous frequency of the output of the wavelet network for monocomponent signal.

7.2 Example 2: Multicomponent Aperiodic Signal

The time-frequency domain specifications of the desired signal is as following

$$E(t,f) = \begin{cases} 0.2 & 0.2 \leq t < 0.8\,sec \quad and \quad f = 4Hz \\ 0.3 & 0.2 \leq t < 0.5\,sec \quad and \quad f = 7Hz \\ 0.2 & 0.4 \leq t < 0.7\,sec \quad and \quad f = 8Hz \\ 0.1 & 0.3 \leq t < 0.6\,sec \quad and \quad f = 11Hz \\ 0.2 & 0.5 \leq t < 0.8\,sec \quad and \quad f = 13Hz \\ 1 & 0.2 \leq t < 0.8\,sec \quad and \quad f = 15Hz \\ 0 & otherwise \end{cases} \tag{7.1}$$

and the desired signal, target time-frequency plane, the synthesized signal and the wavelet transform of the synthesized signal are shown in Figure 7.4.

In order to train the wavelet network the embedding delay has been chosen as $T = \tau_s$ where the sampling period is $\tau_s = 0.002sec$ and the embedding dimension of $d_e = 3$. The number of wavelons in the wavelet network is 7 and the network has been trained for 1000 epochs. The obtained mean squared error is $MSE = 0.000375857$. The output of the wavelet network in phase space and in time-domain are shown in Figure 7.5.

The wavelet network circuit has been simulated in Spice. The output signal of the circuit in time domain and the embedded phase space are shown in Figure 7.6.

The wavelet ridges of the output signal have been obtained by the SVD-based ridge determination algorithm. The results are shown in Figure 7.7.

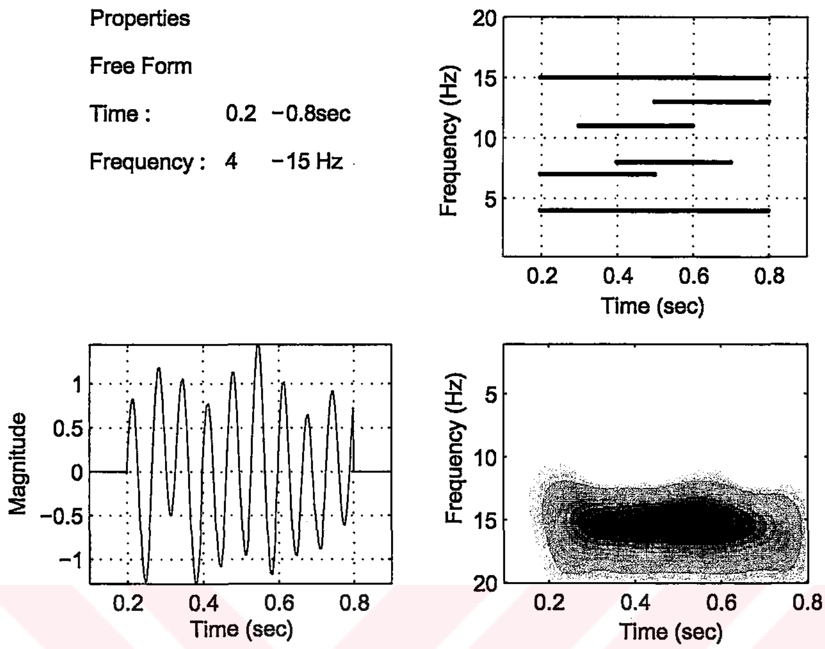

Figure 7.4: The synthesized multicomponent aperiodic signal by the wavelet ridges method.

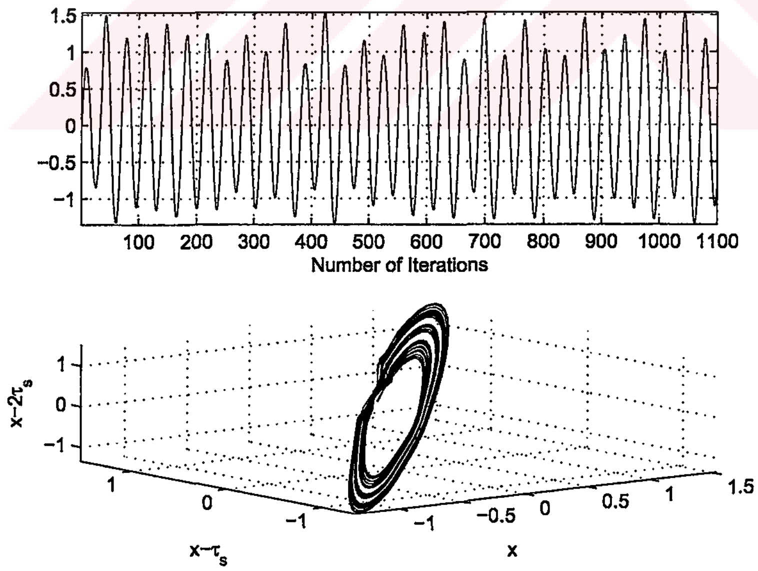

Figure 7.5: The embedded multicomponent aperiodic signal in the phase space and the output of the wavelet network.

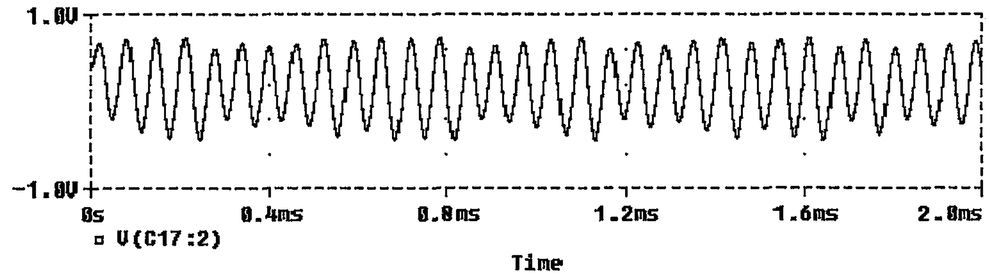

Figure 7.6: The output of the circuit for multicomponent aperiodic signal.

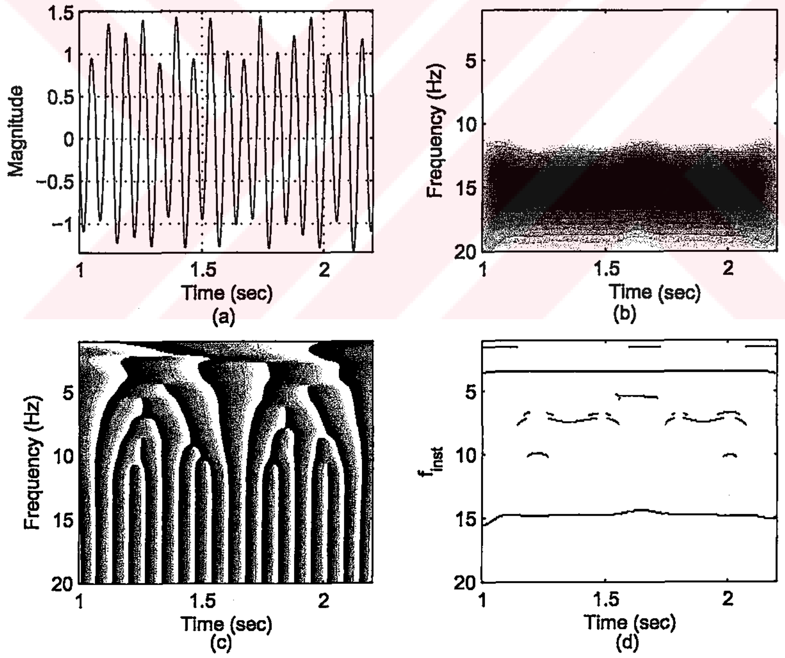

Figure 7.7: (a) The time waveform, (b) the modulus and (c) the phase of the wavelet transform and (d) the instantaneous frequency of the output of the wavelet network for multicomponent signal.

CHAPTER EIGHT

CONCLUSIONS

In this thesis, the modelling and the circuit implementation of the dynamical systems from time-frequency domain specifications have been accomplished. Given the specifications in the time-frequency domain, there are four steps in order to implement the nonlinear circuit: In the first step, the signal which has the desired time-frequency domain properties has been synthesized by using either wavelet atom method or the wavelet ridges method. Then, the wavelet network has been constructed from the time-series obtained in the signal synthesis stage. The dynamical wavelet network circuit has been implemented with the proposed wavelet network circuit using the sigmoidal or Mexican Hat wavelons. As the last step, the accuracy of the synthesis has been investigated by the verification block. The wavelet ridges of the output of the wavelet network have been calculated using the wavelet ridge determination based-SVD algorithm.

The nonlinear circuit with an output signal which has the desired time-frequency domain energy localizations can be synthesized by using the proposed method. Although the number of the components of the circuit may be large compared to the nonlinear dynamical systems exhibiting several nonlinear phenomena, the wavelet network circuit contains only operational amplifiers, diodes and passive circuit components and it is suitable for VLSI manufacturing because of the systematic procedure.

Since the ridges obtained from nonstationary signals can give the relevant information about the phase structures of the dynamical systems, the time-frequency domain may be the suitable domain for giving the specifications of the output of the nonlinear dynamical circuit.

The constructed phase spaces of the output of the designed circuits with the proposed method support this observation.

The energy distribution of the signal over time-frequency domain can be obtained by constructing the scalogram matrix since the wavelet transform conserves the total energy of the signal. The singular value decomposition of the scalogram matrix have been successfully used for the extraction of the dominant energy components because the singular values are related with the energy of the matrix. The greater singular values are associated with the higher energy components and hence the SVD-based ridge determination algorithm can be used for noise reduction by truncating the lower singular values. Also, the classifications of the natural signals can be made by locating the energy concentrations in time-frequency domain (i.e., the wavelet ridges). Hence, it can be possible to diagnose the patients from biomedical signals, for instance.

The wavelet network is a powerful tool for modelling the nonlinear dynamical systems since it combines both the wavelet decomposition and the neural networks with great approximation abilities. However, the selection of the mother wavelet plays a crucial role in the approximation. There is no systematic method in the selection of the mother wavelet; therefore the selection have been made heuristically according to the application.

The proposed method may be used in music synthesis applications to implement the musical compositions or in any sound synthesis applications.

By observing the wavelet transform characteristics of the signals from nature, the approximate characteristics can be implemented with the given method. Hence the prediction of the future behavior of the natural phenomena can be possible.

REFERENCES

Abarbanel, H. (1996). Analysis of observed chaotic data. New York: Springer.

Aguer, F., Flandrin, P., Goncalves, P., & Lemoine, O. (1996). Time-frequency toolbox for use with Matlab tutorial. Technical Report, CNRS, France: Rice University, USA.

Aguirre, L., Rodrigues, G., & Mendes, E. (1997). Nonlinear identification and cluster analysis of chaotic attractors from a real implementation of Chua's circuit. Int. Jour. of Bifurcation and Chaos, *7*, 1411–1423.

Akay, M. (1997). Time frequency and wavelets in biomedical signal processing. Boston: IEEE Press Series on Biomedical Engineering and John Wiley & Sons.

Allingham, D., West, M., & Mees, A. (1998). Wavelet reconstruction of nonlinear dynamics. Int. Jour. of Bifurcation and Chaos, *8*, 2191–2201.

Askar, A., Cetin, A., & Rabitz, H. (1996). Wavelet transform for the analysis of molecular dynamics. Jour. Phys. Chem., *100*, 19165–19173.

Barmada, S., & Raugi, M. (2000). Transient numerical solutions of nonuniform MTL equations with nonlinear loads by wavelet expansion in time or space domain. IEEE Trans. on Circuits and Systems I: Fundamental Theory and Applications, *47*, 1178–1190.

Barnsley, M. F. (1993). Fractals everywhere. California: Academic Press.

Bernard, C., Mallat, S., & Slotine, J. (1998). Wavelet interpolation networks. 6th European Symposium On Artificial Neural Networks ESANN'98, Bruges, Belgium.

Billings, S., & Coca, D. (1999). Discrete wavelet models for identification and qualitative analysis. Int. Jour. of Bifurcation and Chaos, *9*, 1263–1284.

Boashash, B. (1992). Estimating and interpreting the instantaneous frequency of a signal-Part 1: Fundamentals. Proc. of IEEE, *80*, 520–538.

Cao, L., Hong, Y., Fang, H., & He, G. (1995). Predicting chaotic time series with wavelet networks. Physica D, *85*, 225–238.

Carmona, R., & Hwang, W. (1997). Characterization of signals by the ridges of their wavelet transforms. IEEE Trans. on Signal Processing, *45*, 2586–2590.

Carmona, R., Hwang, W., & Frostig, R. (1995). Wavelet analysis for brain-function imaging. IEEE Trans. on Medical Imaging, *14*, 556–564.

Carmona, R., Hwang, W., & Torresani, B. (1999). Multiridge detection and time-frequency reconstruction. IEEE Trans. on Signal Processing, *47*, 480–492.

Casey, M. (1998). Auditory group theory with applications to statistical basis methods for structured audio. Ph.D. Dissertation: Massachusetts Institute of Technology Media Laboratory.

Chakrabarti, C., & Mumford, C. (1999). Efficient realizations of encoders and decoders based on the 2-D discrete wavelet transform. IEEE Trans. on Very Large Scale Integration (VLSI) Systems, *7*, 289–298.

Chakrabarti, C., Vishwanath, M., & Owens, R. (1996). Architectures for wavelet transforms: A survey. Journal of VLSI Signal Processing, *14*, 171–192.

Chandre, C., Wiggins, S., & Uzer, T. (2003). Time-frequency analysis of chaotic systems. Physica D, *181*, 171–196.

Chen, P. (1994). Study of chaotic dynamical systems via time-frequency analysis. Proc. of the IEEE-SP Int. Symp. on Time-Frequency and Time-Scale Analysis, *1*, 357–360.

Chmielewski, L., Gut, P., Kukolowicz, P., & Dabrowski, A. (1993). Robust feature-based image registration using modified Hausdorff distance measure with evolving quantile rank. IEEE Trans. on Pattern Analysis and Machine Intelligence, *15*, 850–863.

Chua, L., Komuro, M., & Matsumoto, T. (1999). The double-scroll family. IEEE Trans. on Circuits and Systems I: Fundamental Theory and Applications, *CAS-33*, 1073–1118.

Chui, C. (1992). An introduction to wavelets. Boston: Academic Press.

Clancy, D., & Ozguner, U. (1994). Wavelet neural networks: A design perpective. Proc. of IEEE Int. Symp. on Intelligent Control, Ohio, USA., 376–381.

Cohen, L. (1989). Time-frequency distributions-A review. Proc. of IEEE, *77*, 941–981.

Conti, M., & Turchetti, C. (1994). Approximate identity neural networks for analog synthesis of nonlinear dynamical systems. IEEE Trans. on Circuits and Systems I: Fundamental Theory and Applications, *41*, 841–858.

Cunningham, W. (1958). Introduction to nonlinear analysis. New York: Mc Graw Hill.

Cybenko, G. (1989). Approximation by superposition of a sigmoidal function. Mathematics of Control, Signals and Systems 2, *1*, 303–314.

de Moor, B. (1988). Mathematical concepts and techniques for modelling of static and dynamic systems. PhD Dissertation: Katholieke University, Leuven.

Delprat, N., Escudie, B., Guillemain, P., Kronland-Martinet, R., Tchamitchian, P., & Torresani, B. (1992). Asymptotic wavelet and Gabor analysis: Extraction of instantaneous frequencies. IEEE Trans. on Information Theory, *38*, 644–664.

Fedorova, A., & M.G.Zeitlin (1996). Wavelets in dynamics, optimal control and Galerkin approximations. Proc. of IEEE Digital Signal Processing Workshop, 409–412.

Foufoula-Georgiou, E., & Kumar, P. (1994). Wavelets in geophysics. San Diego, CA.: Academic Press.

Fridman, J., & Manolakos, E. (1997). Discrete wavelet transform: Data dependence analysis and synthesis of distributed memory and control array architectures. IEEE Trans. on Signal Processing, *45*, 1291–1308.

Galleani, L., Presti, L., & de Stefano, A. (1998). A method for nonlinear system classification in the time-frequency plane. Signal Processing, *65*, 147–153.

Genesio, R., & Tesi, A. (1992). Harmonic Balance methods for the analysis of chaotic dynamics in nonlinear systems. Automatica, *28*, 531–548.

Golub, G. H., & Loan, C. V. (1996). Matrix computations. Boston: The Johns Hopkins University Press.

Hess-Nielsen, N., & Wickerhauser, M. (1989). Wavelets and time-frequency analysis. Proc. of IEEE, *84*, 523–1996.

Hlawatsch, F., & Kozek, W. (1995). Second order time-frequency synthesis of nonstationary random processes. IEEE Trans. on Information Theory, *41*, 255–267.

Huttenlocher, D., Klanderman, G., & Rucklidge, W. (1993). Comparing images using the Hausdorff distance. IEEE Trans. on Pattern Analysis and Machine Intelligence, *15*, 850–863.

Judd, K., & Mees, A. (1995). On selecting models for nonlinear time series. Physica D, *82*, 426–444.

Judd, K., & Mees, A. (1996). Modelling chaotic motions of a string from experimental data. Physica D, *92*, 221–236.

Kantz, H., & Schreiber, T. (1999). Nonlinear time series analysis. London: Cambridge Univ. Press.

Kolmogorov, A. N. (1957). On the representation of continuous functions of many variables by superpositions of continuous functions of one variable and addition. Doklady Akademi Nauk USSR, *114*, 953–956.

L. Galleani, M. Biey, M. G., & Presti, L. (1999). Analysis of chaotic signals in the time-frequency plane. IEEE Int. Conf. on Nonlinear Signal and Image Processing NSIP99, *1*, 100–104.

Li, X., Ling, X., & Zheng, X. (2002). A wavelet balance approach for steady-state analysis of nonlinear circuits. IEEE Trans. on Circuits and Systems I: Fundamental Theory and Applications, *49*, 689 –694.

Liang, Y., & Page, E. (1997). Multiresolution learning paradigm and signal prediction. IEEE Trans. on Signal Processing, *45*, 2858–2864.

Lin, J., Pati, Y., Edwards, T., & Shamma, S. (1996). Analog VLSI implementations of auditory wavelet transforms using switched-capacitor circuits. Technical Report, Systems Research Center: University of Maryland.

Mallat, S. (1999). A wavelet tour of signal processing. San Diego, CA: Academic Press.

Mallet, Y., Coomans, D., & de Vel, J. K. O. (1997). Classification using adaptive wavelets for feature extraction. IEEE Trans. on Pattern Analysis and Machine Intelligence, *19*, 1058–1066.

Mead, C. (1989). Analog VLSI and neural systems. NewYork: Addison-Wesley.

Meyer, Y. (1992). Wavelets and operators. Cambridge: Cambridge University Press.

Minorsky, N. (1962). Nonlinear oscillations. New Jersey: Van Nostrand.

Newland, D. (1993). Random vibrations, spectral and wavelet analysis. New York: Longman Scientific and Technical.

Ogata, K. (1970). Modern control engineering. New Jersey: Prentice Hall.

Oussar, Y., Rivals, I., Personnaz, L., & Dreyfus, G. (1998). Training wavelet networks for nonlinear dynamic input-output modelling. Neurocomputing, *20*, 173–188.

Özkurt, N., Gündüzalp, M., & Savacı, F. (2001). Zaman-frekans düzleminden işaret sentezi. SIU'2001 Kurultayı, *KKTC*, 773–778.

Özkurt, N., & Savacı, F. (2001). Wavelet analysis of the generalized Chua's circuit. Proc. of 9th Workshop on Nonlinear Dynamics of Electronic Sytems, *1*, 100–104.

Özkurt, N., & Savacı, F. (2003a). Chaotic signal reconstruction using wavelet ridges. Int. Jour. of Bifurcation and Chaos, *To be submitted.*

Özkurt, N., & Savacı, F. (2003b). Determination of wavelet ridges of nonstationary signals by singular value decomposition. IEEE Trans. on Circuits and Systems I: Fundamental Theory and Applications, *Submitted.*

Özkurt, N., & Savacı, F. (2003c). Determination of wavelet ridges of nonstationary signals by singular value decomposition method. European Conference on Circuit Theory and Design, ECCTD 2003, *1*, 137–140.

Özkurt, N., & Savacı, F. (2003d). Reconstruction of nonstationary signals in wavelet domain based on singular value decomposition. Proc. of 11th Workshop on Nonlinear Dynamics of Electronic Sytems NDES'2003,Scuol, Switzerland, *1*, 181–184.

Özkurt, N., Savacı, F., & Gündüzalp, M. (2002a). Bir dalgacık işlev yaklaşım devresi gerçekleme önerisi. SIU'2002 Kurultayı, *Pamukkale, Denizli*, 1301–1306.

Özkurt, N., Savacı, F., & Gündüzalp, M. (2002b). The circuit implementation of a wavelet approximator. Int. Jour. on Analog Integrated Circuits and Signal Processing, *32*, 171–175.

Özkurt, N., Savacı, F., & Gündüzalp, M. (2002c). A wavelet function approximator circuit. Proc. of 11th Workshop on Nonlinear Dynamics of Electronic Sytems NDES'2002, *Izmir, Turkey*.

Özkurt, N., Savacı, F., & Gündüzalp, M. (2003a). The circuit realization of Mexican hat wavelet function. AEU Int. Jour. Electronics and Communications, *Submitted*.

Özkurt, N., Savacı, F., & Gündüzalp, M. (2003b). The circuit realization of wavelet network for modelling nonlinear dynamical systems. Int. Jour. on Analog Integrated Circuits and Signal Processing, *To be submitted*.

Pati, Y., & Krishnaprasad, P. (1994). Analysis and synthesis of feedforward neural networks using discrete affine wavelet transformations. Proc. of the IV. IEEE Neural Networks for Signal Processing Workshop, 195–203.

Pilgram, B., & Schappacher, W. (1998). Estimation of the dominant singular values for SVD based noise reduction method. Int. Jour. of Bifurcation and Chaos, *8*, 571–580.

Pittner, S., & Kamarthi, S. (1999). Feature extraction from wavelet coefficients for pattern recognition tasks. IEEE Trans. on Pattern Analysis and Machine Intelligence, *21*, 83–88.

Poggio, T., & Girosi, F. (1990). Networks for approximation and learning. Proc. of IEEE, *78*, 1481–1497.

Quatieri, T. (2001). Discrete-time speech signal processing: Principles and practice. Upper Saddle River, NJ: Prentice Hall PTR.

Rasband, S. (1990). Chaotic dynamics of nonlinear systems. New York: Wiley.

Reiss, J. (1996). Nonlinear Dynamics Toolbox. http://www.physics.gatech.edu/: Technical University of Georgia, USA.

Rosso, O., Blanco, S., Yordanova, J., Kolev, V., Figliola, A., Schürmann, M., & Basar, E. (2001). Wavelet entropy: a new tool for analysis of short duration brain electrical signals. Jour. Neurosci. Methods, *105*, 65–75.

Sastry, S. (1999). Nonlinear systems: Analysis, stability and control. New York: Springer.

Savacı, F., Günel, S., Özkurt, N., & Yapalı, I. (2001). Harmonic balance analysis of generalizad Chua's circuit. Int. Conf. on Progress in Nonlinear Science, Nizhny Novgorod, Russia.

Savacı, F., & Özkurt, N. (2003). The system modelling and circuit implementation from time-frequency domain signal specifications. Int. Jour. of Bifurcation and Chaos, *To be submitted.*

Shah, S., El-Jaroudi, A., Loughlin, P., & Chaparro, L. (2000). Signal synthesis and positive time-frequency distributions. Jour. of Franklin Institute, *337*, 317–328.

Soveiko, N., & Nakhla, M. (2000). Efficient capacitance extraction computations in wavelet domain. IEEE Trans. on Circuits and Systems I: Fundamental Theory and Applications, *47*, 684–701.

Staszewski, W., & Worden, K. (1999). Wavelet analysis of time series: Coherent structures, chaos and noise. Int. Jour. of Bifurcation and Chaos, *9*, 455–471.

Sureshbabu, N., & Farrel, J. (1999). Wavelet-based system identification for nonlinear control. IEEE Trans. on Automatic Control, *44*, 412–417.

Suykens, J., Huang, A., & Chua, L. (1997). Family of n-scroll attractors from a generalized Chua's circuit. AEU Int. Jour. Electronics and Communications, *51*, 131–138.

Suykens, J., & Vandewalle, J. (1993). Generation of n-double scrolls (n=1,2,3,4,...). IEEE Trans. on Circuits and Systems I: Fundamental Theory and Applications, *40*, 861–867.

Takens, F. (1985). On the numerical determination of the dimension of an attractor. Lecture Notes in Mathematics, *1125*, 99–106.

Todorovska, M. (2001). Estimation of instantaneous frequency of signals using the continuous wavelet transform. Technical Report, CE 01-07: Univ. of Southern California.

Veltkamp, R. (2001). Shape matching: Similarity measures and algorithms. Technical Report: Utrecht University, The Netherlands.

Venkatachalam, V., & Aravena, J. (1999). Nonstationary signal classification using pseudo power signatures: The matrix SVD approach. IEEE Trans. on Circuits and Systems II: Analog and Digital Signal Processing, *46*, 1497–1505.

Vetterli, M., & Herley, C. (1992). Wavelets and filter banks: Theory and design. IEEE Trans. on Signal Processing, *40*, 2207–2232.

Vetterli, M., & Kovacevic, J. (1995). Wavelets and subband coding. Upper Saddle River, NJ: Prentice Hall PTR.

Wong, L., & Chen, J. C. (2001). Nonlinear and chaotic behavior of structural system investigated by wavelet transform techniques. Int. Jour. of Non-Linear Mechanics, *36*, 221–235.

Yalçın, M., & Savacı, F. (1996). New realization of Chua's circuit and verifcation of chaos by Harmonic Balance Analysis. ARI, *51*, 169–174.

Yalçın, M., Suykens, J., & Vandewalle, J. (2000). Experimental confirmation of 3- and 5-scroll attractors from a generalized Chua's circuit. IEEE Trans. on Circuits and Systems I: Fundamental Theory and Applications, *47*, 425–429.

Yu, Y., Tan, S., Vandewalle, J., & Deprettere, E. (1996). Near optimal construction of wavelet networks for nonlinear system modelling. Proc. of IEEE Int. Symp. on Circuits and Systems, 1996. ISCAS '96, *3*, 48–51.

Zhang, Q. (1997). Using wavelet network in nonparametric estimation. IEEE Trans. on Neural Networks, *8*, 227–236.

Zhang, Q., & Benveniste, A. (1992). Wavelet networks. IEEE Trans. on Neural Networks, *3*, 889–898.

Zhou, D., Cai, W., & Zhang, W. (1999). An adaptive wavelet method for nonlinear circuit simulation. IEEE Trans. on Circuits and Systems I: Fundamental Theory and Applications, *46*, 931–938.